DISSERTATION

EPILEPTOGENESIS FOLLOWING HYPOXIC-ISCHEMIC (HI) ENCEPHALOPATHY IN THE NEOCORTEX OF A RAT MODEL FOR PERINATAL HI.

Submitted by
Shilpa D. Kadam
Department of Biomedical Sciences

In partial fulfillments of the requirements
For the Degree of Doctor of Philosophy
Colorado State University
Fort Collins, Colorado
Fall - 2006

COLORADO STATE UNIVERSITY

DATE 10.27.2006

WE HEREBY RECOMMEND THAT THE DISSERTATION PREPARED UNDER OUR SUPERVISION BY SHILPA KADAM ENTITILED "EPILEPTOGENESIS FOLLOWING HYPOXIC-ISCHEMIC (HI) ENCEPHALOPATHY IN THE NEOCORTEX OF A RAT MODEL FOR PERINATAL HI" BE ACCEPTED AS FULLFILLING IN PART REQUIREMENTS FOR THE DEGREE OF DOCTOR OF PHILOSOPHY.

Committee on Graduate Work

Dr. Kathryn M. Partin

Dr. James E. Madl

Dr. James Bamburg

Dr. F. Edward Dudek
ADVISOR

Dr. Barbara M. Sanborn
DEPARTMENT HEAD/DIRECTOR

ABSTRACT OF DISSERTATION

EPILEPTOGENESIS FOLLOWING HYPOXIC-ISCHEMIC (HI) ENCEPHALOPATHY IN THE NEOCORTEX OF A RAT MODEL FOR PERINATAL HI.

Little is known of the long-term changes that occur after perinatal hypoxic-ischemic insults that lead to epilepsy. Using rats with unilateral carotid occlusion followed by hypoxia at postnatal day 7 (Rice-Vannucci model), this study provides an initial analysis of the epilepsy caused by a perinatal HI insult with chronic and continuous behavioral monitoring, radio-telemetric recording of cortical electroencephalograms (EEG) and in vitro slice electrophysiology. The cortical and hippocampal histopathology were investigated at postnatal day 30 and later at ≥6 months of age using cresyl violet, Timm and rapid Golgi staining and immunocytochemistry. The resultant epilepsy showed an increase in seizure frequency and severity over time with a preponderance for seizure clusters and behavioral features of an ipsilateral cerebral syndrome. The in vitro recording of evoked field potentials (EFPs) in the somatosensory cortices was done at an early and late time point after the initial HI insult. They revealed the progressive nature of the epileptiform activity in the ipsi-lateral spared neocortex that over time spread to involve contralateral mirror cortices. In addition to parasagittal infarcts and porencephalic cysts in severe lesions, columnar neuronal death was found with cytomegaly in isolated groups of dysmorphic cortical neurons. Cortical dysgenesis was seen in the form of deep laminar gliosis, microgyri, white matter hypercellularity, and blurring of the white and grey matter junction. Mossy fiber sprouting was not only detected in the atrophied

ipsilateral dorsal hippocampus of HI rats with chronic epilepsy, but was also found in comparable grades in spared ipsi- and contralateral ventral hippocampi. The cortical lesions in this animal model show histological similarities with those found in human perinatal HI. The occurrence of cortical abnormalities that are associated with epilepsy in humans correlates with the subsequent detection of spontaneous recurrent seizures. The accompanying hippocampal reorganization may represent "dual pathology" for the model.

Shilpa D. Kadam
Department of Biomedical Sciences
Colorado State University
Fort Collins, CO 80523
Fall 2006

ACKNOWLEDGEMENTS

I would like to thank Drs. F. E. Dudek, P.A. Williams, A.M. White, Li-Rong Shao, Ping Dou and Suzanne Clarke for their valuable input, guidance and support.

TABLE OF CONTENTS

LIST OF TABLES

LIST OF FIGURES

CHAPTER 1

INTRODUCTION

1.1 Hypoxic ischemic (HI) encephalopathy

Encephalopathies affecting the neonatal brain are a heterogeneous group of disorders that are congenital and/or acquired forms of neonatal brain affections of variable known and unknown etiologies. The neuropathologies associated with neonatal encephalopathies vary widely in their distribution, histological morphologies, severity and clinical outcomes. Hypoxia ischemia (HI) induced cerebral encephalopathy is the major cause of epilepsy in infants and children (Volpe, 2001). HI encephalopathy induced cortical lesions are often associated with mutifactorial causative factors ranging from prematurity, low birth weight, traumatic/prolonged labor, asphyxia, severe systemic cardiovascular hypotension, respiratory disorders and maternal and fetal infections (see table1.1, Courville, 1959; Cowan et al., 2003; Golomb et al., 2001; Nelson and Lynch, 2004; Scher et al., 2002).

HI encephalopathy is associated with a high incidence of acute mortality and chronic neurologic morbidity, such as epilepsy (Aso et al., 1990; Bergamasco et al., 1984; Lanska et al., 1991; Ramaswamy et al., 2004). Refractory epilepsy is a common sequela (~30%) in children who survive such insults (Marin-Padilla, 2000b). Although there is a plethora of clinical data on perinatal HI resulting from intensive bedside,

Antepartum	Antepartum and Intrapartum	Intrapartum	Postnatal
Maternal Hypotension	Maternal Diabetes	Abruptio Placentae	Congenital heart disease
Uterine Haemorrhage	Preeclampsia	Uterine Rupture	Postnatal cardiac arrest
Maternal Hypoxia	Intrauterine Growth Retardation	Cord Prolapse	Severe pulmonary disease
Maternal Chorioamnionitis	Dysmorphic Syndromes	Velamentous insertion of the cord and Vasa Previa	Nonspecific term asphyxia
Vascular embolism of Placental vessels		Traumatic delivery	Vascular spasm from subarachnoid hemorrhage
Hereditary Coagulopathies			Disseminated intravascular coagulation
			Venous thrombosis.

Table 1.1 Mutifactorial etiology of HI encephalopathy as related to time of insult.

pathological and radiological studies, the chronic impact of the insult on the developing brain and its maturation in the surviving infants is poorly understood. Pathogenesis of neurologic sequelae like epilepsy in relation to the acquired cortical dysplasias detected in these infants is poorly studied. These cortical dysplasias result from the post-injury reorganization of the injured as well as adjacent and associated spared cortex. Autopsy and surgically resected neocortical tissues have revealed a variety of dysplasias and abnormal neuronal morphologies, which are thought to underlie the abnormal electrophysiological properties recorded during intraoperative and in vitro slice studies (Avoli et al., 1999; Burneo et al., 2004; Calcagnotto et al., 2005; Matsumoto et al., 2005; Najm et al., 2004; Palmini et al., 1994). Recent investigations have found a strong association between disorders of cortical development and medically refractory epilepsy in children (Mischel et al., 1995; Spreafico et al., 1998). Animal models of HI provide a means to study the impact of a perinatal HI insult on the maturation of the brain and

understand the underlying mechanisms of HI-related pathogenesis of the subsequent neurologic morbidities (Kelly, 2002). Perinatal injury based animal models of methylazoxymethanol acetate (MAM), MAM + hyperthermia, freeze lesion induced microgyri and irradiation, have demonstrated functional changes from increased neocortical hyperexcitability to electrographic spike wave discharge activity on chronic electroencephalograms (EEG's) associated with behaviors of freeze posturing and interictal and ictal EEG activity (Chevassus-Au-Louis N. et al., 1999; Kondo S et al., 2001; Scantlebury et al., 2004; Schwartzkroin et al., 2004; Smith BN et.al, 1999). Valuable data have been contributed to the understanding of the molecular mechanistic and functional threshold changes in the central nervous systems of these rodent models with the above mentioned insults related to their cortical histopathological findings. Studies of their respective dysplastic cortical lesions have attempted to correlate their possible direct and indirect (diachisis) causal effects to epileptogenicity.

Understanding how HI-induced plasticity can lead to chronic recurrent seizures after a latent period is an important question in epilepsy research. Clinically, perinatal insults leading to parasagittal infarcts, ulegyri, polymicrogyri or massive porencephalic cysts are generally associated with progressive alterations that have been proposed to be the underlying pathognomic reason for the ensuing epilepsy (Marin-Padilla; 2000b). Changes in seizure semiology over time probably represent continuing reorganizational changes in the surviving neocortex and the recruitment of additional pathways. Epileptiform activity in para-lesioned tissue following massive loss of neuronal inputs to and from the infarcted cortex has been shown to result from hyperinnervation of spared cortical neurons (Jacobs and Prince, 2005; Neumann-Haefelin and Witte, 2000) and

represents at least one form of the plasticity of cortical structures. These clinical and experimental findings suggest that an appropriate animal model with a comparable perinatal insult would show development of seizures and a progressive form of epilepsy with characteristic histopathology in the cortex and hippocampi. This study attempts to report the possible epileptogenic histopathological features of the cortex and hippocampus (dual pathology) detected in a rat model for perinatal hypoxia ischemia which is a modified Levine's technique (Levine, 1960; Rice JE et al., 1981) intended to mimic a term perinatal insult similar to findings in human lesional epilepsies as described by Cendes et al., 1995.

The P7 rat has been chosen because at that age, the stage of development of the animal's brain is comparable to that of a 32-36 week gestation human fetus (Vannucci RC, Vannucci SJ, 2005). This insult therefore represents a more peri-term injury rather than the very pre-term kind of insult that has been shown to have a distinctive histopathology of its own in the form of peri-ventricular leucomalacia highlighting the role of developmental stages in the vulnerability of specific brain areas to similar insults (Back et al., 2002; du Plessis and Volpe, 2002; Sizonenko et al., 2003). Clinically the epilepsy that follows a perinatal insult leading to parasagittal infarcts, ulegyri, polymicrogyri or massive porencephalic cysts is generally associated with progressive increase in seizure frequency and changes in seizures semiology. Experiments exposing P7 rats to an HI insult have demonstrated induction of mossy fiber sprouting in the inner molecular layer of the dentate gyrus (Williams PA et al., 2004). Similar sprouting is seen after kainate-induced status epilepticus, a standard animal model for temporal lobe epilepsy (Nadler JV et.al, 1980). The HI-related infarct in this model of right common

carotid artery ligations followed by 8% O_2 hypoxia in the neocortex closely mimics the parasagittal HI infarct commonly seen in newborns with HI-induced encephalopathy (Volpe, 2001). A sub-threshold reduction in cerebral blood flow with subsequent hypoxia ischemia is presumed to underlie the basic neurological injury associated with HI encephalopathy. During the intrapartum period, this is invariably secondary to asphyxia.

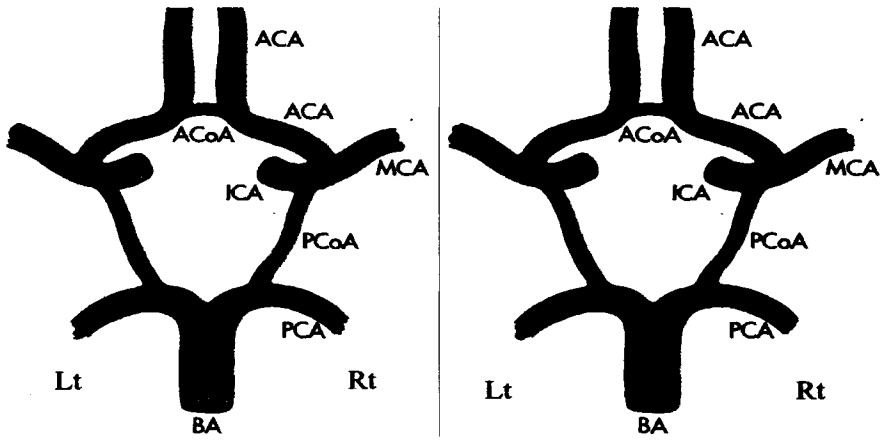

Fig. 1.1 Schematics of altered haemodynamics within the Circle of Willis with unilateral common carotid ligation and superadded hypoxia. ICA internal carotid artery, ACA anterior cerebral artery, ACoA anterior communicating artery, MCA middle cerebral artery, PCA posterior cerebral artery, PCoA posterior communicating artery, BA basilar artery. (left) Normal circulation (right) Compensation to unilateral common carotid ligation.

The subsequent cellular mechanisms of brain damage involve energy failure, intracellular acidosis, cytosolic calcium overload, free radical formation, nitric oxide, excitatory amino acid and cytokine release (Inder et al., 2000). Experimental hypoxic ischemic brain injury is characterized by two phases: an initial phase that begins during hypoxia ischemia and a secondary phase of injury that evolves following restoration of the circulation (Pulsinelli WA et al., 1982). The term reperfusion injury has been used to describe the damage caused by return of oxygenated blood to previously ischemic tissue.

It involves injury to the microvasculature and is mediated in large part by free radicals, endothelial cell derived factors, neutrophils and coagulation factors (Palmer C, 1995). There is an increasing interest to study possible interventional methods at this clinically relevant phase which allows a small window for the actual diagnosis of HI encephalopathy. Cerebral blood flow (CBF) studies in this model show that ligation by itself does not drastically drop cerebral perfusion below critical levels so as to cause ischemia (Fig. 1.1). Superadded hypoxia causes the pathogenic ischemia (Vannucci RC, Vannucci SJ, 2005). This means that once the rat pups are taken out the hypoxia chamber CBF returns to pre-hypoxia levels representing the reperfusion stage in this model (Silverstein F et al. 1984; Lynch JK et.al, 2002). This particular animal model therefore seems highly appropriate for chronic analysis of the histopathology and development of seizures in terms of the relevance to an equivalent human insult.

1.2 HI susceptibility in neonates

The immature brain is highly susceptible to perinatal HI injury. Irrespective of age HI causes neurotoxic damage to both grey and white matter structures due to accumulation of glutamate. The HI insults result in energy failure with a shift towards increased cerebral glucose influx, glycogenolysis and anaerobic energy production from glucose that results in lactate production and tissue acidosis (Fig. 1.2).

Energy depletion leads to failure of energy dependent glutamate reuptake pumps which increase the extracellular concentration of this excitatory amino acid (EAA). Glutamate in turn acts on metabotropic and non-metabotropic receptors such as N-methyl-D-aspartate (NMDA) and kainate-alpha-amino-3-hydroxy-5-methyl-4-isoxazole

Aerobic energy production

$$Glucose + 38ADP + 38Pi + 6O_2 \rightarrow 6CO_2 + 44H_2O + \underline{38ATP}$$

VS

Anaerobic energy production

$$Glucose + 2ADP + 2Pi \rightarrow 2\ Lactate^- + 2H^+ + \underline{2ATP}$$

Fig. 1.2 Energy production from glucose under *aerobic* and *anaerobic* conditions. Note contrast in ATP production for every glucose molecule utilized. ADP – Adenosine diphosphate; ATP – adenosine triphosphate; Pi – inorganic phosphate.

propionic acid (KA–AMPA) to depolarize cell membranes. Sustained membrane depolarization due to excess glutamate causes massive calcium influx that leads to degradation of cellular lipids by activation of phospholipases; of proteins by activation of proteases and of DNA by activation of nucleases.

The increased susceptibility to injury in the immature brain arises from the fact that developmentally excitatory signals act as trophic factors in the guidance and stabilization of circuit formation. It has been shown that during distinct time intervals of development EAA heteromeric receptors such as AMPA are deficient in the GLUR2 subunit expression (Talos et al., 2006). Since the GLUR2 subunit has been shown to confer Ca^{2+} impermeability to the receptor, decreased GLUR2 expression leads to increase in Ca^{2+} influx with every depolarizing signal that developmentally helps strengthen synapses and circuits. During a HI insult this expression profile acts against cell survival by allowing accumulation toxic levels of intracellular Ca^{2+}. Another feature of the immature brain is the normally inhibitory actions of gamma-aminobutyric acid (GABA) are depolarizing during the specific developmental window periods. This occurs due to the developmentally controlled expression of the Na^+, K^+, $2Cl^-$ cotransporter

(NKCC1). This cotransporter is expressed in the cortex of rat pups for up to 12 days after birth and up to 1-2 months in human term neonates (Dzhala et al., 2005). The electroneutral activity of this cotransporter uses the transmembrane sodium gradient to import two chloride ions, along with one sodium and one potassium ion and thus results in accumulation of cytoplasmic chloride. Chloride is the principle ion that flows through channels activated by the $GABA_A$ receptor. Normally there is very little cytoplasmic choride (~4mM) compared to extracellular concentrations (~110mM). This gradient causes an influx of negatively charged Cl^- ions into the cell after GABA opens the $GABA_A$ channel. Influx of this extra negative charge hyperpolarizes the cell taking it away from its threshold potential for firing an action potential and therefore causes inhibition. However the Cl^- accumulation in the immature neurons reverses the flow of chloride ions and depolarizes the cell, thus GABA helps the cell to fire action potentials at that stage. This feature however works against the immature brain under conditions of stress where excessive and sustained depolarization's associated with the energy failure seen in HI insults results in massive neuronal death.

1.3 Pediatric epilepsy and clinical management.

Epilepsy is prevalent at the two extremes of the human life span, namely in the pediatric and geriatric age groups. Although the pediatric population is susceptible to epilepsy, there is no FDA-approved antiepileptic drug (AED) that has been specifically developed for this population. This is true inspite of the fact that recent research has shown currently used pediatric AED therapies to have a substantial incidence of unwanted side effects, possible interference with normal brain development and most

importantly lack of efficacy in seizure control at non-toxic doses. The poor response of seizures during the neonatal period to medication has been rigorously investigated at the bedside and the bench. Clinically enhancing the effects of GABA mediated inhibition has proven to be an effective anticonvulsant therapy in adults. AEDs like barbiturates, benzodiazepines, tiagabine, vigabatrin and valproate have all been shown to have enhancing effects on $GABA_A$ channels. The developmentally regulated expression of NKCC1 as described earlier negates the inhibitory effect of open $GABA_A$ channels by reversing the chloride gradient in the immature brain. Additionally the electroneutral chloride exporting transporter KCC2 that helps maintain the low cytoplasmic chloride concentration in adult neurons developmentally has a rostro-caudal format of expression (Stein et al., 2004). This means that the transporter that gives the $GABA_A$ channels their inhibitory property is developmentally expressed first in the spinal cord and brain stem and finally in the cortex. This then probably accounts for the "electroclinical dissociation" reported in 85% neonates where the anticonvusant blocks the behavioral features of a seizure but fails to block the EEG response (Connell et al., 1989). Considering that developmentally GABA is excitatory in the central nervous system due to the expression of NKCC1 transporter and lack of expression of the KCC2 transporter, we understand why the AED that is a GABA agonist fails to block seizure activity. When we add to that the phasic expression of KCC2 in the spinal cord first which renders GABA inhibitory in that part of the central nervous system, we begin to understand why then the GABA agonist anticonvulsant is successful in suppressing the transmission of the seizure activity through the spinal cord thus blocking the behavioral manifestation of the seizure but not the seizure itself.

The relationship of brain development and epilepsy has recently become an important focus of both animal and clinical research. Data from animal models have helped prove the irrationality of current AED therapies in pediatric epilepsy. Chronic effects of perinatal insults and acute neonatal seizures that lead to learning disabilities and epilepsy in a large population of infants and children still remains an area that needs to be explored in animal models. For better age-specific therapies to be designed we need to have a clearer picture of the chronic human condition and the chronic picture that develops in the relevant animal models to generate and test future hypotheses. Without understanding animal model research with regard to its relevance to the human condition we are delaying our goal of understanding underlying mechanisms of the human diseases and therefore possible preventative and interventional therapies.

1.4 Research aims and hypotheses

Perinatal insult to the brain results in plasticity that allows the brain to adapt or compensate for the injury and holds the potential for recovery of function. In a normal developing brain such plasticity accounts for enhancing a skill with practice (Johnston, 2004). On the other hand excessive plasticity may lead to maladaptive circuitry that can result in neurological disorders. This may be especially true for an immature brain with an enhanced ability for plasticity. In investigating neurological disorders associated with adaptive plasticity and the associated pathological attributes, it is important to understand the temporal relationship of the process with the severity of ensuing disorders. The goal of the study conducted and presented here was to better understand the chronic histological and electrophysiological features of an animal model for perinatal HI insults

specifically in relation to the resultant epilepsy. The hypothesis was that the post-injury plasticity in this model for perinatal HI is progressive as a function of time in relation to the neuropathology of the lesion, the severity of the epilepsy and the cortical epileptiform activity. The first aim was to determine the susceptibility of rats exposed to HI at postnatal day 7 to then later develop epilepsy as adults. Epileptic status and seizure semiology were determined by chronic and continuous behavioral video-monitoring. The second aim was to examine the histopathological features of the cortex and hippocampus (i.e. dual pathology) in this model. The possibility that there may be progressive changes in the histology of the cortical infarct over time was addressed by studying the infarct lesion and the spared cortices at an early and late time point after the perinatal insult. Histological, immunocytochemical and stereological reconstructive techniques were used to determine the extent and nature of the injury and adaptive reorganization that had occurred over time, at post natal day 30 and at $\geq$ 6 months of age. The third aim was to study if there was progression in the severity of the neurological disorder of epilepsy in the model by analyzing cortical EEG's and their behavioral correlates for months following a perinatal insult. This is the first study to report chronic telemetric monitoring of EEG for this model. Use of radio-telemetry for intermittent and chronic continuous recording has been described recently in rats with kainate induced epilepsy (Bastlund et al., 2004 and 2005, Williams et al., 2006) it has also been used previously in patients for epilepsy monitoring (Stevens et al., 1971). We used implantable telemetry units which transmitted three bipolar channels of EEG data to record chronically for periods of up to 5 months in perinatally HI-treated rats. We first sought to determine the apparent latency-to-onset and temporal progression of the epilepsy. The fourth and final aim was to

examine post-injury plasticity in the sensorimotor cortices in this model. In vitro slice studies were conducted in the spared sensorimotor cortices at time points similar to the ones used for the second aim, to investigate neocortical epileptogenesis over time in isolation from its numerous afferent and efferent circuits, both ipsi- and contralateral to the HI-induced infarct. The combined behavioral and EEG seizure data and histopathological observations indicate that this is a good model to help understand the process of epileptogenesis following perinatal HI insults in term neonates.

CHAPTER 2

METHODS

2.1 Surgical procedure for HI model (Rice and Vannucci 1981)

Sprague-Dawley dams with dated postnatal day 4 litters were obtained from Harlan Laboratories; single-cage housed, and allowed to acclimate for 2 days before carotid ligation surgeries were conducted at postnatal day 7. Cerebral hypoxia was induced using the procedure described by Levine (1960), and modified by Rice et al. (1981). Sprague-Dawley male and female litter mates were anesthetized using a 2% isoflurane/oxygen mixture. The ventral midline of the neck was surgically prepared and infused with bupivicane (0.5%, 0.2 ml). A 0.5-cm ventral midline incision was made, and the right common carotid artery was exposed and double-ligated unilaterally with 4-0

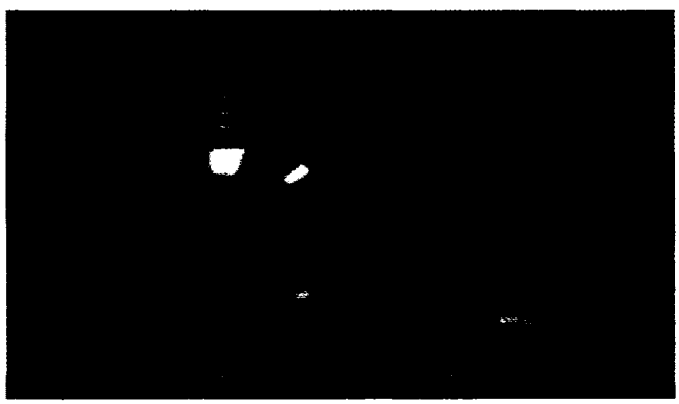

Fig. 2.1 Hypoxia chamber with flow meter. The flow meter on the right maintained a 6 lit/min flow of 8% oxygen into the hypoxia chamber (left).

surgisilk (Vicryl-polyglactin/braided). The skin was closed with 4-0 surgisilk. Age-matched sham controls had the carotid artery exposed under the same anesthesia but not ligated. After a 2-h recovery period, the rat pups with the ligated carotid artery were placed in a hypoxia chamber (i.e. a chicken incubator from Lyon's Electronics, CA) where the temperature and humidity was maintained at 37°C and 90%, respectively. The hypoxic insult was achieved by a high flow rate (6 liters/min) of 8%-oxygen balanced with nitrogen through the chamber, adjusted with a flow meter. An oxymeter placed in the chamber recorded consistent 8% oxygen levels in the chamber, which dropped to a minimum of 7.7% in the late phase of the hypoxia when most of the rat pups were hyperventilating. The rat pups were exposed to 8%-oxygen for 2 h, then allowed to recover in room air and placed with their mother and littermates. Rectal temperatures taken before pups were placed in the chamber averaged 32-33°C and just after hypoxia averaged 33-34°C. These temperatures were recorded to rule out hyperthermia as a variable during the acute insult.

2.2 Histological studies

Histological studies were done on the brains of HI and control rats at post-natal day 30 (n=36) and at ≥6 months of age. Animals that were ≥6 months in age were either from the behavioral monitoring study described below (n=12) or a chronic video-EEG study (n=28). Animals were anesthetized with halothane and then decapitated.

i Cresyl violet at postnatal day 30. This stain (also known as Nissl stain) has a strong affinity for ribosomes, initially called Nissl bodies. All cells have ribosomes, but neuron cell bodies have more thus stain much more darkly. This stain is commonly used

to count cell bodies in an area. For this study the whole brain was rapidly removed and stored in ice-cold physiological solution (composition in mM: 124 NaCl, 3 KCl, 1.3 $CaCl_2$, 26 $NaHCO_3$, 1.3 $MgSO_4$, 1.25 NaH_2PO_4, 10 glucose equilibrated with 95% O_2, 5% CO_2, pH 7.2-7.4) before being rapidly transferred into a fixative (4% paraformaldehyde). The fixed brain was then quick-frozen to cut 40-μm coronal sections on a sliding microtome in serial order starting at the genu of the corpus callosum anteriorly to the caudal end of the dorsal hippocampus posteriorly, and every third section was mounted serially (16 control, 20 HI-treated). All sections were examined and images obtained with a Zeiss microscope and Microfire software in Neurolucida (Microbrightfield, Inc VT).

ii Cresyl violet and Timm staining at ≥6 months of age. A modified Timm histological procedure was used to label the zinc-containing axons of the granule cells. The cerebrum was dissected out and prefixed in phosphate-buffered 0.37% Na_2S to precipitate the zinc in the mossy fibers. This was followed by immersion-fixation in phosphate-buffered 4% paraformaldehyde (pH 7.2). The tissue was then saturated with 30% sucrose and 40-μm coronal sections were cut on a sliding microtome in serial order starting at the genu of the corpus callosum anteriorly to the brain stem caudally. Every third section was serially mounted and processed for cresyl violet staining and a similar batch of consecutive sections starting from the rostral tip of the dorsal hippocampus to the caudal end of the ventral hippocampus was serially mounted and processed for Timm and cresyl violet counter staining (n = 40; behavioral study, 10 HI: 2 control; chronic video-EEG study, 18 HI: 10 control). All slides with the relevant sections were coded, and the intensity of the Timm stain in the dentate inner molecular layer was graded. True

blinding of slides with respect to treatment (i.e., HI versus control) was not possible due to the obvious lesion, but blinding achieved removal of bias when grading epileptic (n=11) rats with variable seizure severities vs. non-epileptic HI rats (n=16). Timm stain was graded according to the rating scale of Tauck and Nadler (1985). The data were then grouped according to treatment, ipsilateral versus contralateral and dorsal versus ventral hippocampus; and then, average grades with standard errors were obtained. A multiple comparisons (i.e., Bonferroni's) test was used to assess differences between groups and anatomical locations. Serial reconstruction and solid modeling of lesioned brains was done with Virtual Slice software (Microbrightfield, Inc VT) to create three dimensional closed and open contours of the ipsilateral lesion and non-lesioned contralateral hemisphere.

iii Immunocytochemistry. NeuN (Neuronal Nuclei) immunocytochemistry was done at postnatal day 30. NeuN antibody specifically recognizes the DNA binding, neuron-specific protein NeuN, which is present in most central and peripheral nervous system neuronal cell types. The protein is restricted to neuronal nuclei, perikarya and some proximal neuronal processes. Coronal sections (40 μm) were cut on a cryostat and stored in cryoprotectant solution. Sections were then incubated in NeuN mouse monoclonal (MAB377, Chemicon: 1:1000 dilution) as primary in blocking solution overnight, followed by secondary incubation with Alexaflour 594 goat anti-mouse (Molecular Probes). Sections were mounted serially and coverslipped with Vectashield.

iv Rapid Golgi staining. Golgi stain impregnates a limited number of neurons at random (for reasons that are still not understood), and permits the clear visualization of a nerve cell body with all its processes in its entirety by staining them black. HI-treated and

control rats (n=8; ≥6 months of age) were anesthetized with halothane and then decapitated. The whole brain was rapidly removed and rinsed in ice-cold phosphate-buffered saline and then immediately submerged into rapid Golgi stain kit solutions (FD Neurotechnologies, MD 21041 USA). After 2 weeks, brains were quick frozen and 200-μm coronal sections were cut on a cryostat at -22° C. Sections were mounted on slides and cover slipped with mounting medium from kit.

2.3 Behavioral monitoring for seizures in post HI rats

The rat pups that underwent the HI insult at postnatal day 7 were videotaped 24 h per day for 1 week every month (i.e. 25% of the time) using a Panasonic WV-BP330 B/W camera connected to three Panasonic videocassette recorders, each with 8-h videotapes. The rats were housed in a 12-hour light /dark cycle from 6 am to 6 pm. Night recordings were performed with a Kodak 1A filter over a safelight, and day recordings were accomplished with diffuse fluorescent light. The recording started immediately after the rats were weaned at age postnatal day 30. Before this age, they were housed with the mother (dam) in a single cage and tended to sleep and feed huddled together at most times under the dam, which made it difficult to detect any possible seizures with a video camera, especially with litter sizes around 10-15. Once they were weaned, the rats were same-sex housed 2 per cage. Seizures were scored using the Racine scale (grade 1-5) to determine the severity of motor seizure activity (Racine, 1972; Ben Ari, 1985): P1 – Frozen (immobility with open eyes) and or "wet dog shakes" associated with facial convulsions (vibrissae twitching, jaw clonus, blepharospasms); P2 – Same behaviors as P1 with head bobbing; P3 - Forelimb clonus with a lordotic posture; P4 - Forelimb clonus

continued along with rearing; P5 – Same behaviors as a P3 and 4 stage seizure, but the rats also fall over. Some rats fell to one side first, and then showed evidence of forelimb clonus. Ictal events lasted from 20 sec to 3 min. The video analysis was conducted initially in fast forward-mode to detect behavioral postures (i.e., lordosis, straight tail, jumping/running, forelimb clonus, and/or rearing). Once a behavioral posture was observed the tape was re-examined at real-time speed and the seizure scored. After an ictal event was confirmed on real-time video, rat behaviors for a few minutes preceding and following the event were noted. The animal was scored as 'inactive' if there was 30 sec of little to no volitional movement (i.e. animals were considered inactive even if they displayed slight head movement), or following 30 sec of apparent sleep (i.e. lying still with head down and eyes apparently closed). Spontaneous motor seizures that occurred within 30 sec after arousal were also considered to be seizures during inactivity. These behaviors were combined into one group based on similar methods described by Hellier and Dudek, 1999. Motor seizures were considered to be during activity when the animal had spent more than 30 sec in apparent volitional movement (e.g. grooming, walking and eating). Although this definition required that the animal show a specific behavior for more than 30 sec preceding a seizure, post hoc analysis revealed that most rats were in a particular behavioral state (i.e. inactive or active) for several minutes prior to the onset of a seizure. This group of rats was monitored for a total of 7 months. With the 1-week-per-month protocol, this amounted to 49 days of 24-h video-monitoring.

2.4 Radio-telemetry

The radio-telemetry setup has been previously described (see Williams et al., 2006). Briefly male and female Sprague-Dawley rats that underwent surgery for

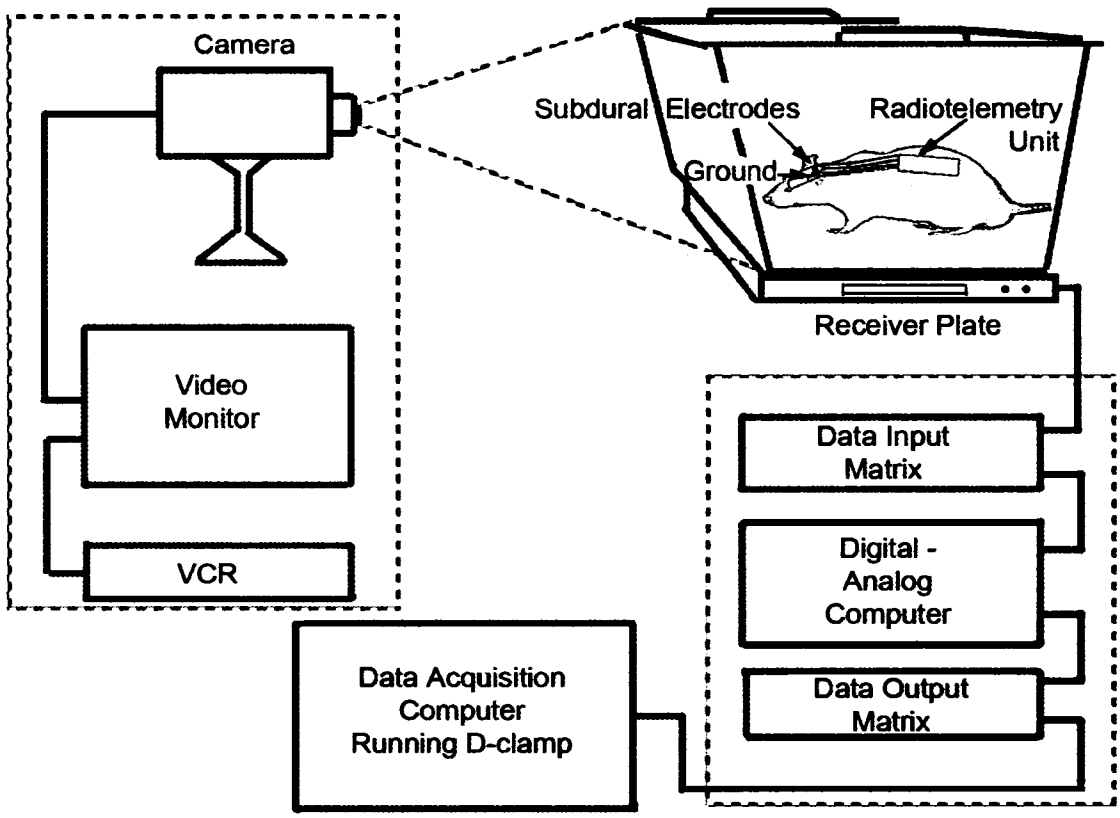

Fig. 2.2 Schematic representation of the video–EEG system for chronic monitoring. Single housed freely behaving HI-treated/control rats implanted with telemetry units with three bio-potential electrodes were positioned on a receiver plate that collected and sent EEG signals from the telemetry unit to the data input matrix. The digital data were converted to an analog signal by the DSI A.R.T. computer. This analog signal was reconverted into digital data and stored on another computer with the D-clamp software (written by Dr. Kevin Staley) that created a new file for each animal every 24 h. All of the rats in the telemetry system were also simultaneously video- monitored 24 h per day throughout the duration of EEG recordings.

continuous recording of electrocortigrams were individually housed in cages under a 12-h light/dark cycle (lights on at 6 am). Singly housed freely behaving HI-treated or control rats implanted with telemetry units (DSI model TL10M3-F50-EEE magnetic activated transmitters – Transoma Medical , Arden Hills, MN) that had three bipolar electrographic channels were positioned on a receiver plate (RPC-1, Transoma Medical)

that collected and sent EEG signals from the telemetry unit to the data exchange matrices (Data Sciences International, USA). The digital data were converted to an analog signal by the DSI A.R.T. analog software (Transoma Medical) with an OS/2 operating system (IBM corp., White Plains, NY). This analog signal was reconverted into digital data to be recorded and stored on a PC with the D-clamp software (Dr. Kevin Staley, UCHSC) written in Visual Basic 6.0 (Microsoft, Seattle ,WA) that created a new file for each animal every 24 h beginning at 12am (Fig.2.2).

2.5 Video-monitoring

Every rat in the telemetry setup was also simultaneously video monitored 24 h per day throughout the duration of the EEG recordings with focus surveillance black and white cameras (Fig. 2.2). Two Color Quad Observation Systems SOD14C4LN (Samsung, Korea), allowed for the video recording of 8 animals simultaneously. The time stamps for these systems were synchronized to the digitizing computer. The individual cameras were placed 50 cm from each rat cage; the outputs from four cameras were connected to the four-channel video system, and the output from the video system was connected to three Panasonic VCRs. Each VCR was programmed to record consecutive periods on 8-h VHS tapes in EP mode. Night recordings were performed with a Kodak (Eastman Kodak, Rochester, NY) 1A filter over a safelight and daytime recordings with a diffuse fluorescent light. The behavioral data were used in this study for visualization of seizure semiology, grading individual ictal events, differentiating EEG seizure activity from electrical noise generated by jaw movement artifact and grooming.

2.6 Surgical procedure for implanting telemetry units and sub-dural electrodes

Surgery was performed using stereotaxic equipment and sterilized instruments. The stereotaxic unit was sprayed with 95% alcohol. All surgical tools were autoclaved and maintained sterile intraoperatively with a glass-bead sterilizer. The 2-month-old and 6-month-old Sprague-Dawley rats were given prophylactic antibiotic penicillin (300,000 I.U.) subcutaneously 15 min prior to surgery along with dexamethasone (4.0 mg/kg) and atropine (2 mg/kg SC) and anaesthetized with 2% isoflurane. The surgical site was clipped and prepped with betadine scrub and lotion. The head of the rat was placed in the stereotaxic apparatus. The incision site was isolated with sterile surgical towels. Bupivicaine (0.5 ml, 0.5%) was injected at the incision site for local anesthesia prior to making the incision. A 2-cm longitudinal midline incision was made through the scalp. The periosteum was removed and haemostasis achieved with gentle pressure application with sterile cotton tips or a cautery pen. Small holes were bored through the skull with a Dremel and #105 drill bit for electrode implantation. Recording electrodes were placed in the three locations using coordinates marked by using the bregma for reference. The electrodes were fastened with dental acrylic, which was also used to cover and seal all exposed skull surfaces. Extending the incision caudally 1 cm, a subcutaneous pocket 5-cm long and 2-cm wide was created with blunt dissection, 2 cm caudal to the shoulder blades. The unit was then inserted into this pocket deep enough such that the leads wires lay flat against the deep fascia once the recording leads were placed in their final positions. Absorbable 4-0 Vicryl (polyglactin braided) sutures were used to close down the any dead space between the subcutaneous tissue and muscle fascia along the rostral end of the tunnel to prevent any potential serum pockets forming around the unit itself

and invading the area of electrode implantation over under the scalp . The scalp incision was closed with 3-0 Dermalon (non-absorbable monofilament nylon suture) achieving close approximation and primary healing of incision. Animals were allowed to recover from surgery for 2 days prior to being programmed into the video-telemetry system during which time they received adequate antibiotic and analgesic cover.

2.7 Three bio-potential transmitter placements

The leads on the three channel transmitters were cut to appropriate lengths and the silicone covering peeled back to expose 2-3 mm of the helical steel leads. The exposed ends of the leads were then curved into tight "C" shaped loops such that the distal end of the loop slid into the holes bored into the skull with the blunt end of the "C" facing the pial surface of the brain to avoid any implantation related trauma to the neocortex either during surgery or over time. Continuous EEG recordings were obtained with implanted sub-dural recording electrodes in bilateral hemispheres. Ch1 and Ch3 recording electrodes were placed 0.5 mm caudal to the bregma and 3.5 mm lateral to midline over the forelimb area of the sensorimotor cortex bilaterally. Ch2 recording electrode was placed over the parainfarct spared cortex (paracingulate cortex) of the ipsilateral (right) hemisphere 0.5 mm caudal to the bregma and 1 mm lateral to sagittal suture (Fig. 2.3). The reference electrodes for the three channels were placed at similar lateral coordinates to their respective recording electrodes but more caudally over the parietal cortex. The ground was placed caudal to the lambda suture over the right cerebellar hemisphere and one self-tapping screw was paced over the opposite cerebellar hemisphere to strengthen the adhesion between the dental acrylic holding all the leads in position and the skull.

These implantation surgeries were carried out at 2 months of age in one group of animals and at 6 months of age in another. Using these radio-telemetric implants, interictal spikes and electrographic seizures were recorded continuously.

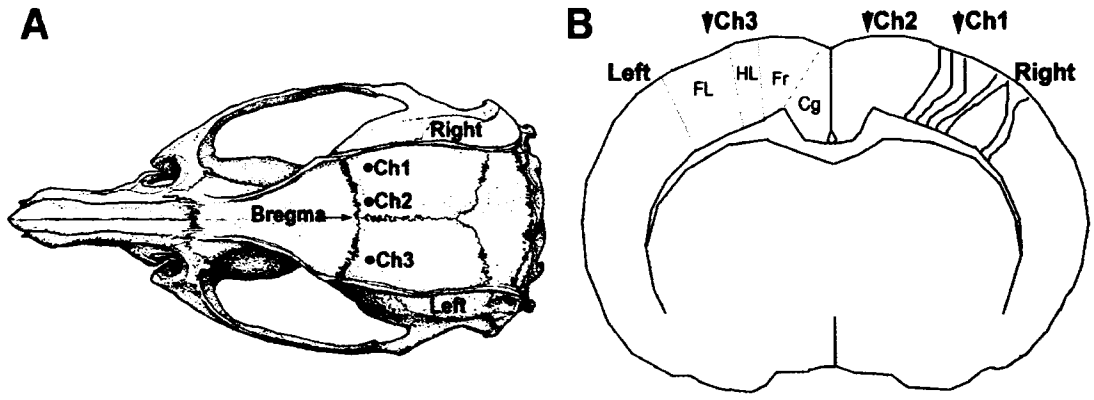

Fig. 2.3 A. Dorsal skull surface of rat showing locations of the three sub-dural bipolar electrodes over bilateral hemispheres (modified from Paxinos & Watson 1998); B. Schematic of coronal view of cortical surface locations for the three sub-dural electrodes over the bilateral forelimb motor and paracingulate cortex and their respective channel numbers for the recorded EEG data. Ch1: Core of the ipsilateral infarct, Ch2: Ipsilateral paracingulate neocortex (para-lesion cortex), Ch3: Contralateral motor cortex. Cg - cingulate cortex, Fr - frontal cortex, HL - hindlimb area of cortex, FL - forelimb area of cortex.

2.8 Grading of seizures

Synchronized EEG-video recording made it convenient to view specific time slots on the VHS tape and note behaviors associated with the EEG activity. The epileptic behaviors associated with epileptiform activity on EEG's were classified based on the modified Racine scale (Racine, 1972; Ben Ari, 1985) to determine the severity of motor seizure activity: P1 - Frozen (immobility with open eyes) and or "Wet dog shakes" associated with facial convulsions (vibrissae twitching, jaw clonus , blepharospasms); P2 - P1 and head bobbing; P3 - Rats display forelimb clonus with a lordotic posture; P4 -

Forelimb clonus continues along with rearing; P5 - Animals have a P3/4 stage seizure and fall over. Some rats fell to one side first and then show evidence of forelimb clonus.

2.9 Experimental design for telemetry study

Both male and female rats underwent telemetric monitoring (n=28, 14 male/14 female). Eighteen rats were implanted at 2 months age (12 HI-treated and 6 controls) and 10 rats at >6 months of age (6 HI-treated and 4 controls). This protocol was designed to account for the low frequency of seizures of the resultant epilepsy as determined by the behavioral monitoring protocol conducted in this model (Chapter 3). Ideally we would have liked to implant at an earlier time point than 2 months after the HI insult but were surgically restricted by the size and weight of the three bio-potential units (Fig. 2.4; volume – 5.5 cc, weight 11.5 gm, recommended minimum animal weight =175 gm).

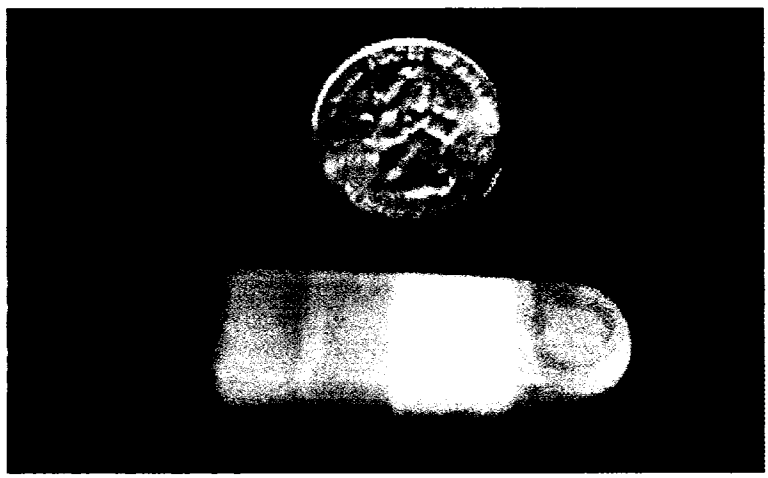

Fig. 2.4 Three biopotential telemetry unit with three recording leads (red) paired with three reference leads (grey) and a ground lead (1st lead at bottom of picture). Compare size to that of a quarter.

2.10 Slice preparation and in vitro electrophysiological studies

Coronal brain slices were prepared from rats that had undergone an HI insult or sham surgery for controls at P7. Briefly rats were deeply anesthetized (halothane) and euthanized by decapitation. The brain was rapidly dissected out and placed in ice-cold oxygenated (95% O_2 – 5% CO_2) physiological solution (composition in mM: 124 NaCl, 3KCl, 1.3 $CaCl_2$, 26 $NaHCO_3$, 1.3 $MgSO_4$, 1.25 NaH_2PO_4, 10 glucose equilibrated with 95% O_2, 5% CO_2, pH 7.2-7.4). The cerebellum and anterior forebrain was then dissected out with coronal cuts and the brain block then glued to the chuck of a vibroslicer (Lancer vibrotome) in order to cut 450-μm thick coronal slices from bregma +0.7 mm to -2.3 mm. The slices were transferred to a storage chamber where they were immersed in ACSF (32-35° C) for at least 1 h prior to placement in an interface type recording chamber. In some experiments the $GABA_A$ antagonist bicuculline (30μM) was added to the ACSF. Field potential recordings were obtained from coronal slices of the sensorimotor neocortex in an interface recording chamber that allowed the placement of both stimulating and recording electrodes. Bipolar stimulating electrodes were made of two tightly wound, Teflon-insulated platinum-iridium wires (75 μm diameter) and placed at the junction of layer VI and white matter. Patch pipettes were pulled from borosilicate glass capillaries (1.65 mm outer diameter and 0.45 mm wall thickness) to a tip diameter of 1-2 μm. They were filled with perfusion fluid (ACSF) and had open resistances of 2-5 MΩ. Evoked and spontaneous field potentials were recorded with an Axoprobe – 1A amplifier (Axon instruments). Data was recorded and analyzed with the Clampex 8 software. Evoked field potentials were recorded bilaterally from superficial layers of

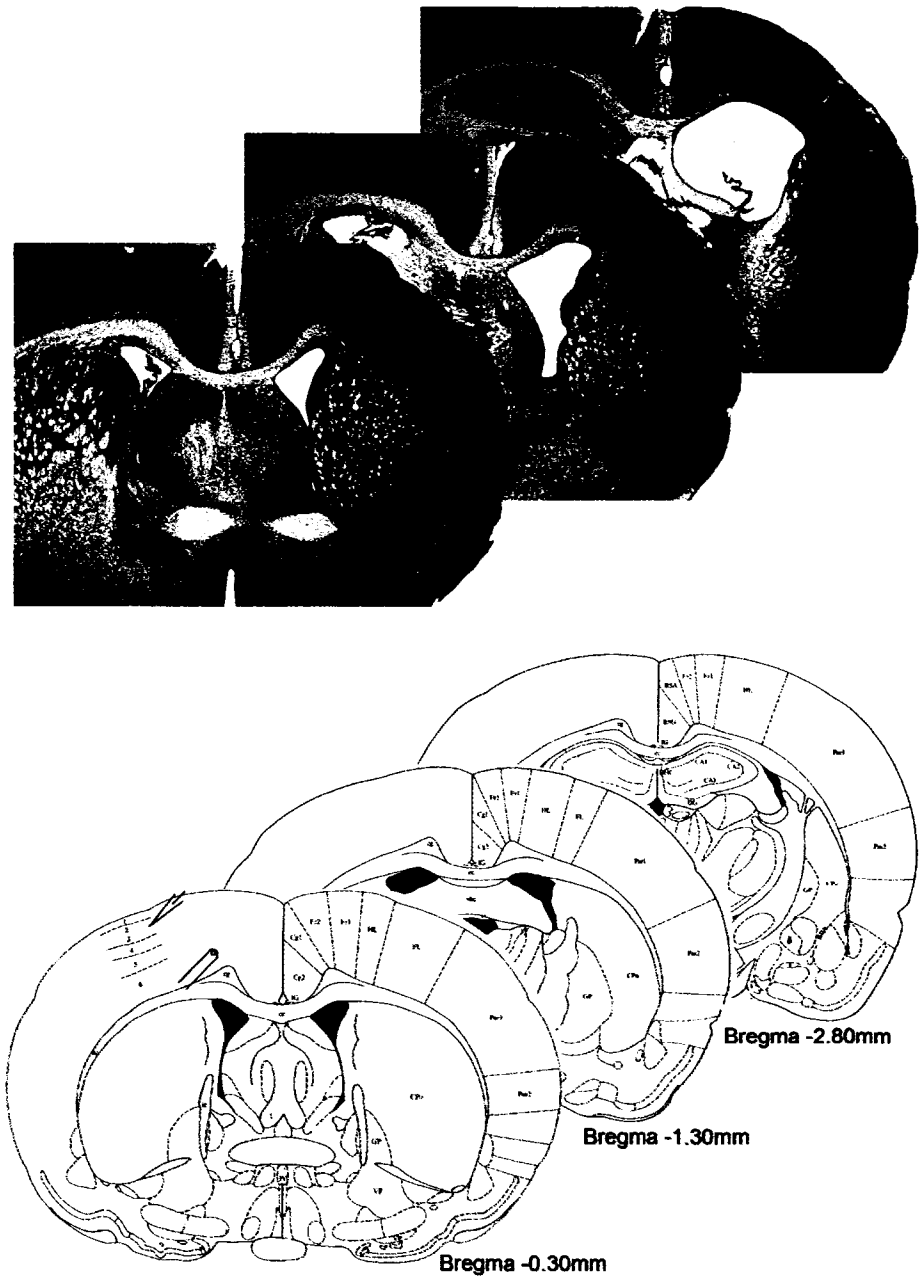

Fig. 2.5 Protocol for recording evoked field potentials (EFPs) in the somatosensory cortex from bilateral hemispheres in HI-treated and control rats at early and late time points. A. Cresyl violet stained coronal sections from the HI model with the cortical lesion in the right hemisphere representing the parasagittal infarct. B. Schematic representation of coronal slices with somatosensory cortex at different distances from bregma and location of stimulating (junction of white matter and layer VI) and recording electrode (layer II/III) placement for recording evoked field potentials in this study (modified from Paxinos and Watson, 1998).

the somatosensory cortex (Fig.2.5) starting at threshold (T, i.e., negatively going field potential distinct from baseline; 0.3 ± 0.04 mV for this study) and increasing stimulus intensities in standard gradients of this threshold stimulus intensity (i.e., T to 6T). Exact placement of the recording electrode was determined by the highest amplitude negative population response elicited by stimulation in normal medium. Evoked field responses were recorded by stimulation at every 10 sec interval for 200μ sec duration. After conducting this protocol in normal medium, the $GABA_A$ receptors were blocked using high dose BMI (30μM) added to the ACSF. Next, 10 min of wash-in time with the new perfusing solution was allowed during which spontaneous activity was recorded continuously. After that time, a similar stimulating protocol to that conducted previously in normal medium was carried out after strongly blocking $GABA_A$ receptor mediated inhibition. If a slice demonstrated an episode of slow spreading depression, it was allowed to recover for 5 minutes without stimulation and then the experimental protocol was resumed. If slow spreading depression occurred more than twice or recovery was not seen after 5 minutes the data from that slice was discarded. This phenomenon although often seen in slices from young rats (P21-P32) was rarely seen in adult brain slices (≥6 month old). Although histology was not performed on slices that the data was recorded from, a comprehensive description of the histological abnormalities produced in this model and their significance in epileptogenesis is reported in chapter 4.

2.11 Statistical analysis

All values are expressed as means ± SEM. Statistical analysis for multiple comparisons was done using Bonferroni's test. All paired and independent observations

were tested for significance using Students *t* tests. P values of <0.05 were considered significant.

CHAPTER 3

CHRONIC CONTINUOUS BEHAVIORAL VIDEO-MONITORING OF HI-TREATED RATS TO DETERMINE LATENCY TO ONSET, SEIZURE SEMIOLOGY AND PROGRESSION

This study was conducted to estimate the susceptibility of HI-treated rats to develop epilepsy as adults. Epilepsy in humans is known to be progressive in its severity. Our hypothesis was that we would find a similar progression in HI-treated rats that were detected to be epileptic. A previous study conducted in the model using a protocol of random 6h per week of behavioral monitoring (Williams, 2004) failed to detect progression in severity. We hypothesized that increasing the monitoring time would increase the probability of detecting such a progression if it occurred as a function of time.

3.1 Animal behavior

Routine observation and handling the HI-treated rats did not elicit any abnormal behaviors or disturbances in eating and grooming that differentiated them from their sham-control littermates. Continuous video-behavioral monitoring demonstrated these rats to be equally active as their control counterparts. Although specific tests to examine contralateral limb power were not done, there was no apparent contralateral loss of power associated with the unilateral infarct. Ipsilateral torticollis was noted for 2 rats that may

be attributed to the ipsilateral trauma to neck muscles during the carotid ligation surgery (also reported by Levine, 1960).

3.2 Behavioral monitoring for motor seizures in post-HI rats

Latency to detection of first behavioral seizure with the behavioral monitoring protocol was ~2 months (Fig. 3.1), which is much lower than the latent period reported in a previous study (~200 days; William et al. 2004). No behavioral seizures were detected in the first month of video monitoring. Out of 10 HI rats, 3 were detected to manifest spontaneous behavioral seizures (≥ P3) in the second month of monitoring, which was substantially shorter than the previously reported latency to epilepsy after HI insult at postnatal day 7 (i.e. 194 ± 43 days to 68.3 ± 0.3 days). Overall total counts of ≥ P3 seizures in this group of rats showed an increase in seizure frequency over time (Fig. 3.1).

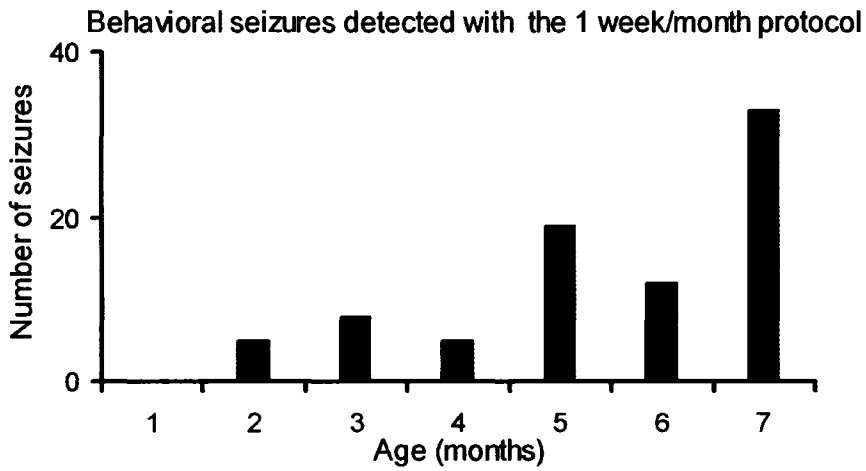

Fig. 3.1 Progression of post-HI epilepsy with increasing seizure frequency. **A.** Total number of P3, P4 and P5 seizures detected with the 1-week-per-month video-monitoring protocol. Histogram shows total counts for 10 HI-treated rats, 3 of which showed an increase in recurrent spontaneous seizures over the 7 consecutive months of video-monitoring.

The seizure rate for the 3 HI rats with spontaneous recurrent seizures increased from 0.43 ± 0.08 seizures per day at 2 months of age to 1.62 ± 1.09 seizures per day at 7 months of age. The mean seizure rate for the total number of seizures observed over the 7 months of monitoring with the 1 week per month monitoring protocol was 0.66 ± 0.35 seizures per day. Even with the 7-day continuous monitoring period, clusters of seizures were detected. As seen in figure 3.2, the ictal events were detected to cluster within 24-h periods inspite of low seizure frequencies. The preponderance for seizures to occur in

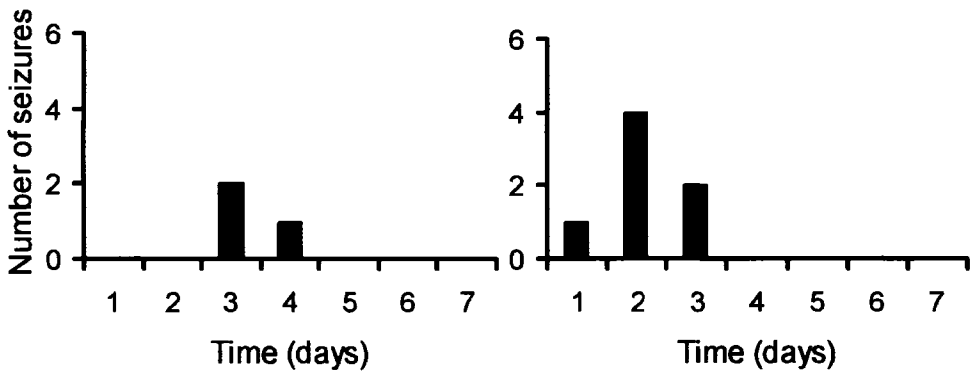

Fig. 3.2 Seizures occurred in clusters. Data from the second and third month (left and right histograms, respectively) of monitoring for an individual epileptic HI-treated rat showed clustering of seizures within 24-h periods in the 7-day monitoring protocol. The data from the third month shows an increase in the number of seizures within the detected cluster compared to the cluster detected in the second month, consistent with the increase in seizure frequency over time for this animal.

clusters was evident when 83.5% of the seizures occurred in clusters of ≥2 and 62.9% occurred in clusters of ≥ 3 seizures within 24h time bins (Fig. 3.3). The total number of clusters detected per month showed a gradual increase as a function of time (Fig. 3.4) with an associated increase in mean number of seizures with each cluster (Fig. 3.5).

Fig. 3.3 The percent of total detected seizures occurring as clusters (within a 24-h period) as a function of the minimum number of seizures in the cluster over the 7-month period. The histogram shows about 84% of the seizures were associated with at least 1 other seizure in a 24-h period and about 54% of the seizures were part of a cluster of 4 or more seizures.

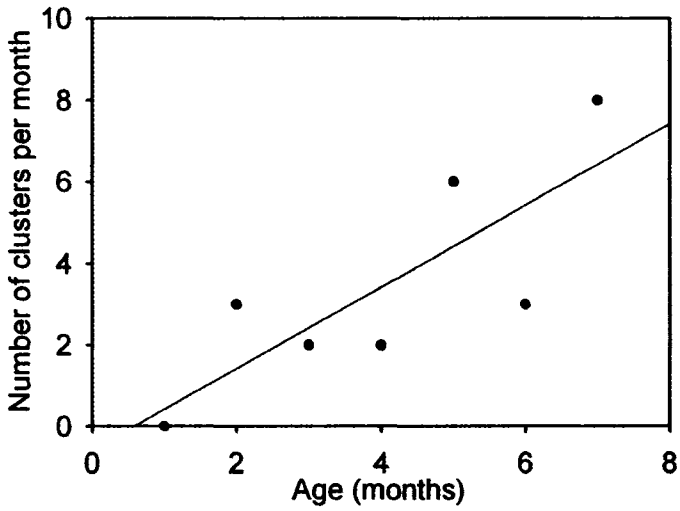

Fig 3.4 A gradual increase in the total number of clusters (≥2 seizures in 24 h) was observed as a function of time.

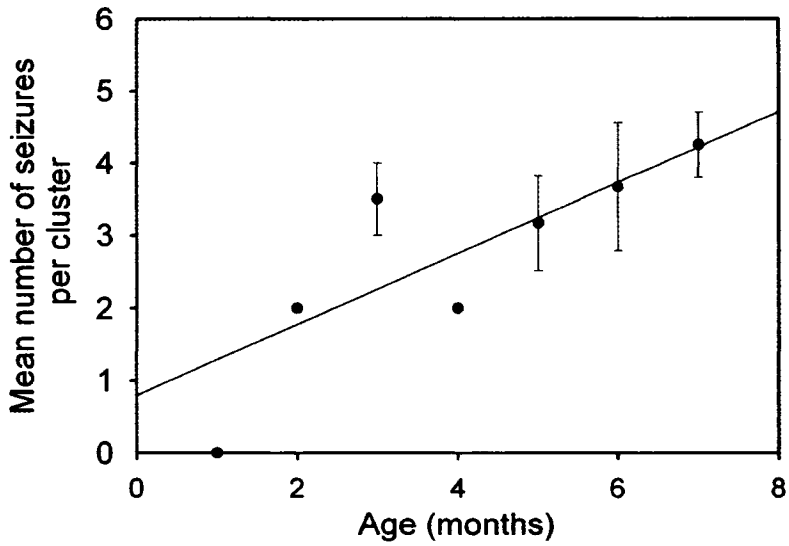

FIG. 3.5 A gradual increase in the number of seizures within a cluster (normalized to number of clusters) was observed as a function of time.

In addition to the 3 epileptic rats, episodes of class 1 and 2 behaviors (see methods) were noted in 3 more HI-treated rats. On histological analysis their ipsilateral cerebral hemispheres were later found to have lesions and Timm staining comparable to the HI-treated epileptic rats. These class 1 and 2 behaviors were not included in this data set because of lack of concurrent EEG data for verification of these episodes as ictal events. Since this protocol did monitor the rats for 25% of the time, and given the propensity of the HI-treated rat to seize in clusters separated by days of seizure-free periods (Fig. 3.2) it is possible that the 1 week/month protocol failed to detect seizures in some of the epileptic rats with a low seizure frequency.

3.3 Diurnal variation of seizures

The time-of-day of ictal events (≥P3) was noted for the HI epileptic rats over the 7-month period of monitoring. The average ratio of the light-phase seizures (6 am to 6 pm)

to the dark-phase seizures was 1.7:1 (Fig. 1C, 63.4% vs. 36.6%). Although this variation may have been influenced by the vivarial handling of the animals by personnel for cage changes during the light cycle, no seizures were noted during (as reported by the personnel, off camera) or immediately after a cage change (on camera) in this protocol. Thus, handing and noise were not variables that detectably exacerbated seizures. Although overall more seizures occurred during the light-phase versus the dark-phase, the difference was not significant (P>0.1). Fifty-five of the total 82 seizures (67.1%) occurred while the rats were inactive or in a sleeping posture versus active. Most of the light-phase seizures (80.8%) occurred at arousal from sleep compared to 46.7% of the dark-phase seizures (Fig. 3.6). This is not surprising considering that rats are nocturnal, so the light-phase would be when most of the inactive states would be expected to occur. Therefore, the occurrence of spontaneous motor seizures depended significantly on the activity state, during the light-phase but not for the dark-phase (P=0.001). Similar observations have been noted in the kainate model for temporal lobe epilepsy by Hellier and Dudek, 1999.

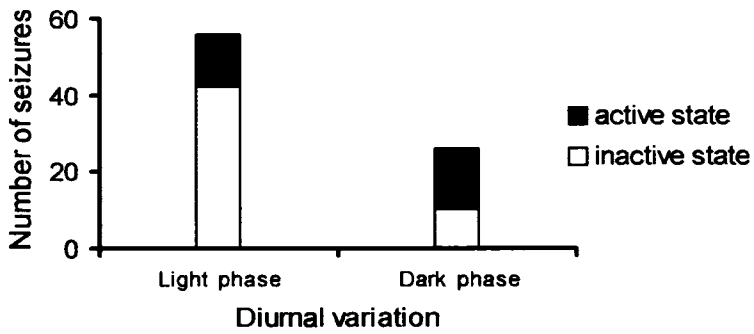

Fig. 3.6 Diurnal distribution of seizure occurrence and dependence on activity state. A stacked histogram shows the diurnal distribution of total ictal events (≥P3) detected, presented as seizures occurring during the light phase (n=52) versus the dark phase (n=30). The data are further differentiated by seizures that occurred when the animal was active or inactive within the respective phase of the diurnal cycle.

3.4 Seizure semiology of resultant epilepsy in post HI-treated rats

Seizure semiology consisted of a cerebral syndrome wherein most seizure onsets were associated with pre-ictal versive head movements, predominantly ipsiversive and/or start of tonic-clonic activity first in the left forelimb and post-ictal circular swaying movements. Among other observed behaviors were pre-ictal arousals from sleep, followed by counterclockwise turning (towards side of lesion). Most ictal events were initiated by a subtle contraversion of the head followed by an exaggerated ipsiversion of the head and torso, and a tonic-clonic seizure. Most seizures that were classified as P3 on the Racine scale (1972, i.e., bilateral forelimb clonus) were actually unilateral left-forelimb tonic-clonic seizures. Most P5 seizures started as partial seizures (i.e., left forelimb clonus) and then became generalized in nature. Early seizures in the 2-month-old rats were partial seizures. These motor ictal events had an average duration of 71.7 ± 2.9 sec. Seizure durations for the motor seizures ranged from 10 sec to 2 min. Every episode was followed by variable periods (sec to min) of a group of behaviors that included volitional walking around the cage with head bobbing, freeze posturing with eyes open and inactivity with eyes closed. These periods were not included in the quantification of the duration involved in the actual convulsive motor seizure itself.

CHAPTER 4

NEUROPATHOGICAL FEATURES OF A RAT MODEL FOR PERINATAL HYPOXIC-ISCHEMIC ENCEPHALOPATHY WITH ASSOCIATED EPILEPSY

After having determined that a postnatal day 7 HI-insult results in a progressive form of epilepsy in the HI-treated rats as adults, the associated neuropathogy was examined. The aim was to determine the histopathology of infarcted and spared cortical and hippocampal structures bilaterally. Our hypothesis was that for this animal model of perinatal HI to be a good model of the human condition, there needed to be a good correlation between the lesions seen in patients and those occurring in epileptic HI-treated rats. A corollary to the above hypotheses was that since the first aim had shown evidence for progression in severity, the histopathology would also show progressive changes in lesion morphology.

4.1 Cortical histopathology

This study found significant correlation between the histological features of the neocortical lesion in the animal model and the corresponding clinical findings of the human condition. Histological studies were done with cresyl violet and immunocytochemistry on postnatal day 30 in HI-treated and sham-control rats. The modified Levine's method (1960) in postnatal day 7 rat pups mimicked the infarct defined

by the region lying between perfusion territories of the major cerebral arteries ("watershed zone") seen in human neonates after HI encephalopathy (Fig. 4.1). The core of the infarct was parasagittal in location with variability in its dimensions of middle cerebral artery territory involvement between animals. The paracingulate cortex supplied by the anterior cerebral artery was spared, possibly because it retained collateral circulation during the unilateral ischemic insult through the anterior communicating artery. This presented the paracingulate cortex as a consistent para-infarct zone to the core of the infarct for both moderate as well as severe lesions. In figure 4.1A, the representative coronal slices from an HI-treated rat with a cystic infarct are shown according to their rostral-to-caudal position in relation to the bregma (Paxinos and Watson, 1998). Note that the border between the unaffected cortex of the paracingulate cortex and the core of the infarct formed a distinct border marking the perfusion territories of the anterior and middle cerebral arteries. In contrast, at the ventral border of the infarct, broad-spectrum involvement of the middle cerebral artery and possibly poor collateral circulation of the posterior cerebral artery blurred the margin of their respective perfusion territories. Marked atrophy of the ipsilateral hemisphere was seen and the lateral ventricles were enlarged ipsilaterally, at the more caudal coordinates (compare A2 & 3 to A1 in Fig. 4.1). Enlarged ipsilateral ventricles eventually fused with the infarct cavity to form the porencephalic cyst in severely lesioned rats. The dilatation represented lost brain tissue compensated by cerebrospinal fluid filling rather than a non-obstructive hydrocephaly, because the contralateral ventricle remained unchanged and the aqueducts and the third and fourth ventricles were undilated and similar to controls. The three dimensional reconstruction of the HI lesion (Fig. 4.1, B1 and 2) in one of the rats with a

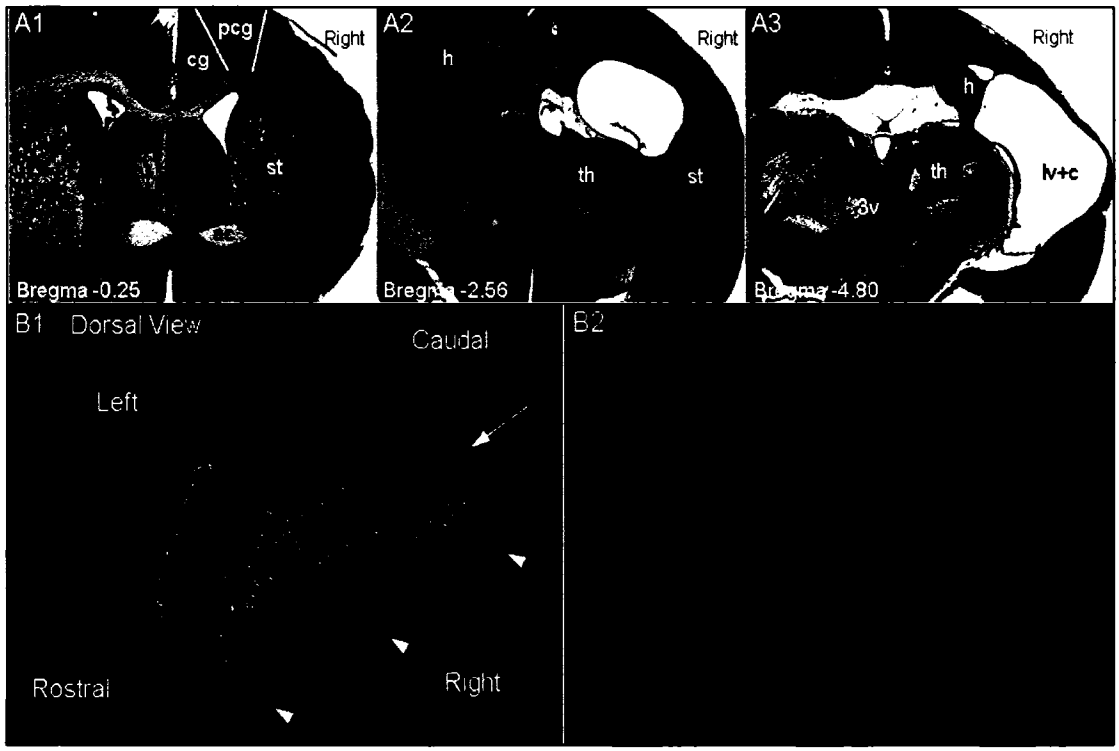

Fig. 4.1. Location and dimensions of cystic infarct. **A**. Cresyl violet-stained coronal sections from a postnatal day 30 rat following the HI insult at postnatal day 7. A1, 2 and 3 are images of 40-μm coronal sections shown in reference to bregma and demonstrate the core of the infarct in the parasagittal zone of the right hemisphere. In the section through the anterior commissure (ac) at -0.25 Bregma (**A1**), the lateral ventricles (lv) are seen bilaterally and are comparable in size. Striatal (st) atrophy is evident in right (ispsilateral) hemisphere. Columnar bands of cell death are seen predominantly in the parasagittal zone with a relatively preserved cingulate (cg) and paracingulate cortex (pcg). In the section through dorsal hippocampus (h) at -2.56 Bregma (**A2**), right thalamic (th) atrophy was especially marked in the dorsolateral nuclei. The right dorsal hippocampus is conspicuously absent in this section, and replaced by an enlarged lateral ventricle lined by an ependymal layer and a visible choroid plexus. The section through the posterior thalamus at -4.80 Bregma (**A3**) shows mineralized lesions in the region of the ventral posteromedial thalamic nucleus (asterisk); the cystic infarct (c) has coalesced with the lateral ventricle to form a porencephalic cyst and the third ventricle is undilated. **B**. Serial reconstruction using Virtual Slice software in Neurolucida representing the rostro-caudal dimensions of the cystic infarct. The three dimensional dorsal view of the wireframe generated by serial reconstruction is shown in **B1**. The cystic infarct is seen in right cerebral hemisphere predominantly in the middle and posterior cerebral artery vascular territory (arrow). Arrow heads represent sections the sections shown in A1, A2 and A3 along the rostro-caudal axis respectively. A solid model of the reconstructed lesioned brain in the same orientation as in B1 is shown in **B2.** A baso-frontal view allows better visualization of the asymmetry of the lateral ventricles (yellow), with the ipsilateral lateral ventricle coalescing with the infarct cyst to form the porencephalic cyst. The severely atrophied dorsal hippocampus (green) in the ipsilateral hemisphere is seen

in comparison to the contralateral hippocampus. Color code: white - section contour; pink - corpus callosum; yellow - porencephalic cyst merged with lateral ventricle; green - hippocampus; purple – third and fourth ventricles.

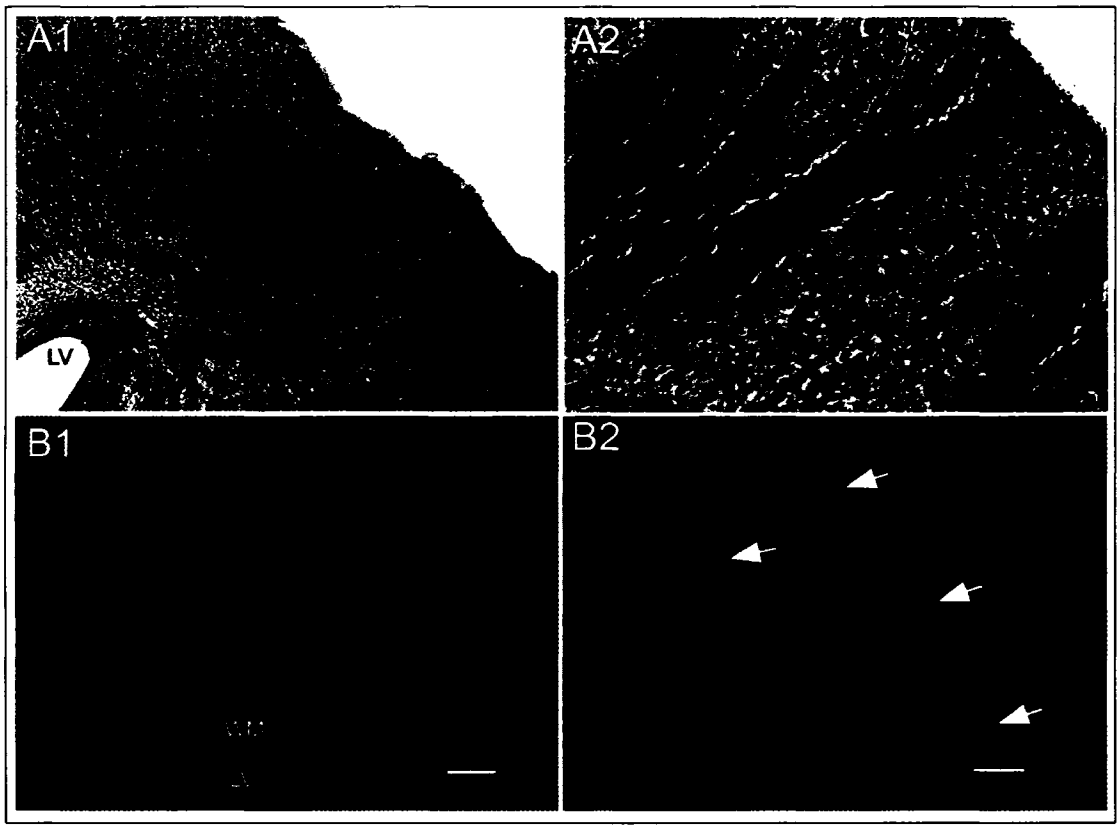

Fig. 4.2 Columnar cell death visualized with cresyl violet and NeuN immunocytochemistry at postnatal day 30. Coronal section of sensorimotor cortex shows the core of the infarct with columnar cell death at lower magnification (**A1**). At higher magnification, columns of surviving gray matter separate bands of gliotic neocortex (arrows, **A2**). NeuN-stained 40-μm coronal sections demonstrate the marked dorsal border of the infarct that lies between the spared paracingulate cortex (anterior cerebral artery perfusion) and the "watershed zone" delineated by a massive loss of neurons in the parasagittal neocortex (**B1**). Magnified view (**B2**) shows columns of NeuN-positive surviving neurons (arrows) separated by bands of tissue devoid of any stained cells (gliotic bands). WM – white matter, LV – lateral ventricle; Scale bars = 250 μm in A1 and B1; 100 μm in A2 and B2.

cystic lesion was performed with "virtual slice" software (Neurolucida) and revealed shrinkage of the ipsilateral hippocampus such that its anterior septal anatomical

coordinates were pushed back to a more caudal location and replaced by the porencephalic cyst (infarct cavitation coalescing with the lateral ventricle to form a large cystic lesion lined by ependymal layer and inclusive of the choroid plexus).This was evident by comparing the rostro-caudal location and dimensions of the ipsi- and contralateral hippocampal tracings (green) in the three dimensional wireframe and solid model reconstructions (Fig. 4.1, B1 and 2). The porencephalic cyst involved the posterior cerebrum predominantly, representing the watershed territory of all of the three major cerebral arteries. Sparing of the more rostral and temporal border zones may be explained by perfusion of those regions by larger proximal cerebral vessels. The neocortical neuronal cell death was predominantly columnar, due to immaturity of penetrating cerebral vasculature at the age of postnatal day 7 (Rorke, 1992), which were seen as bands of spared neuronal populations separated by columns devoid of neurons (Fig. 4.2, A1 & A2). NeuN immunocytochemistry allowed better visualization of these columns of surviving neurons in the core of the infarct (Fig. 4.2, B1 & 2). As the infarct increased in severity, it affected the neocortex supplied by the middle cerebral artery in addition to the watershed zone between the middle and anterior cerebral artery territories thus extending over the parietal cortical convexities. Sometimes, the ipsilateral grey matter was reduced to a thin membrane comprised of gliotic tissue and the piamater, coalesced to form the outer wall of the porencephalic cyst. The deep gray matter showed moderate-to-severe striatal and thalamic atrophy in the ipsilateral hemisphere in the HI-treated epileptic rats. Mineralization was commonly seen within the deep gray matter as chalky spots in the posterior lateral thalamic nuclei in unprocessed sections from HI-treated epileptic rats. After cresyl violet staining, these spots became a dark violet hue (asterisk in A3 in Fig

4.1). Calcifications of ischemic lesions in brains of children are well documented (Ansari et al., 1990). Therefore the model mimicked a term perinatal insult similar to findings in human lesional epilepsies as described by Cendes et al. (1995), where dual pathologies have been shown to be prevalent.

4.2 Acquired microgyri

Cortical dysplasias occurred in the form of deep laminar gliosis (Fig. 4.3, A & B), microgyri (Fig. 4.3, C & D), and cortical layering abnormalities in the affected neocortex of all epileptic HI-treated rats (Fig. 4.3, F). They were detected in the frontal and sensorimotor neocortex of HI-treated epileptic rats. In the more severe forms of infarcts, these cortical malformations overlay the porencephalic cysts. These findings correlate with the concomitant human neuropathogy (Levine et al., 1974; Courville, 1958). Histology performed at age of postnatal day 30 in HI-treated rats showed the presence of deep-laminar gliosis and possible signs of a microgyrus in its early stages of formation (Fig. 4.3, A & B). Acquired microgyri were detected in 45% of the epileptic HI-treated rats (≥6 month's age) in the ipsilateral neocortex (Fig. 4.3, C & D). These microgyri were characterized by marked disruption of cortical cytoarchitecture and deep-laminar gliosis, flanked by clusters of misaligned hypertrophic neurons representing areas of surviving grey matter that seemed isolated within bands of gliotic scar tissue (Fig. 4.3, E). Comparing the histological sections from the early and late time points in HI-treated rats suggested that there was progressive post-injury evolution of the microgyric formation in this model, which along with the increasing dysplastic features may have also involved

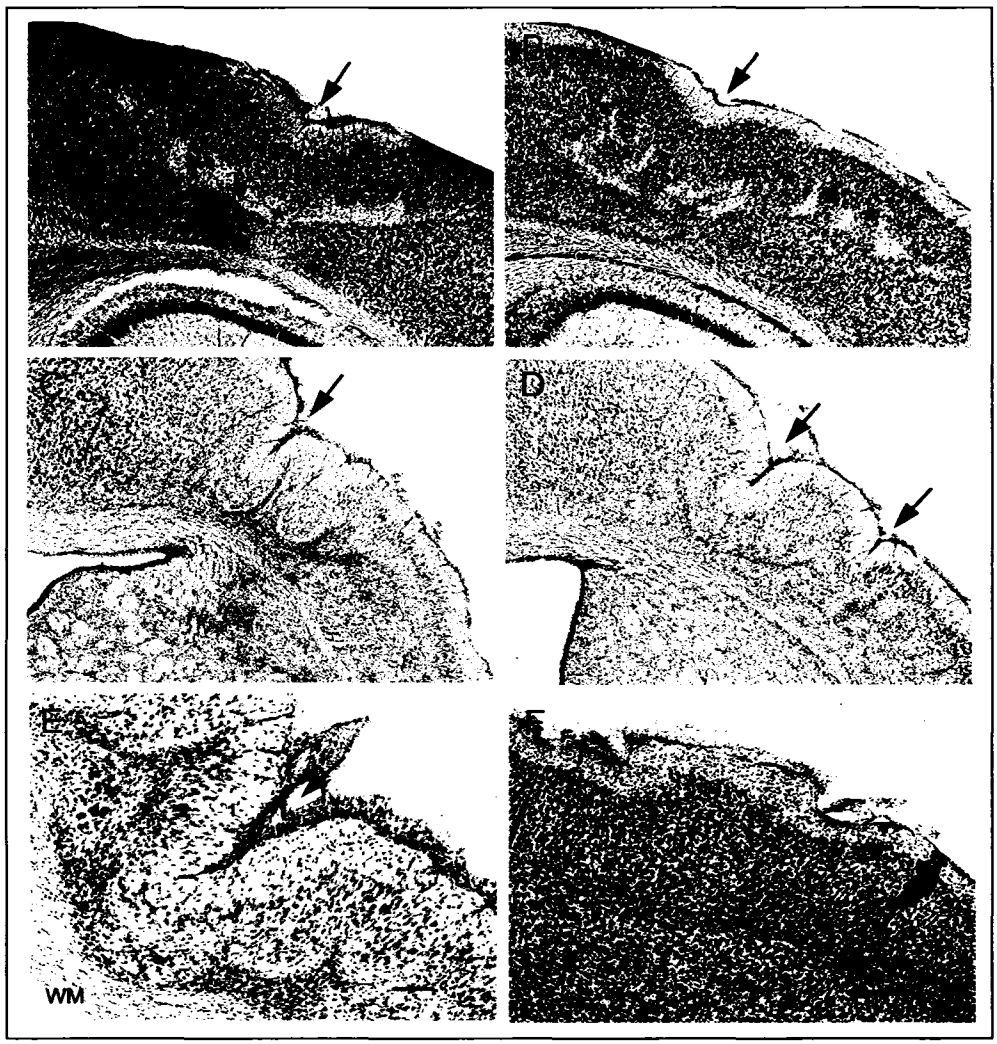

Fig. 4.3 Dislamination of parasagittal cortex. Coronal cresyl-violet-stained sections showing deep laminar cell loss at postnatal day 30 (**A, B**) and microgyri in the chronic (≥ 6 month age) group of HI-treated rats (**C-E**). **A.** Early stages of the possible progressive collapse (arrow) of the neocortex to a microgyrus at the cortical surface overlying the deep laminar gliosis (asterisk). The pattern of patchy deep laminar gliosis coincides with the columnar predilection to cell death that was commonly observed (**B**), which is likely linked to immaturity of the cerebral vasculature (3 asterisks) at the time of the HI. **C.** The presence of acquired microgyral like structures (arrows) in tissue fixed from a chronically epileptic rat (age > 6 months); **D.** Two such microgyri are seen, compared to the one microgyrus seen in C. The rat that generated the tissue in D also had twice as many seizures as rat with tissue in C, as noted in a 24/7 chronic EEG monitoring protocol using video-telemetry (Kadam et.al, in preparation); **E.** A microgyrus from an epileptic rat is shown at higher magnification to demonstrate the collapse of the neocortex into a four-layered structure; **F.** Cortical surface irregularities were accompanied by underlying cell death, and could be compared to cortical warts where layer II/III neurons protrude along with the molecular layer above a normally lissencephalic brain. WM – white matter; Scale bars = 250 μm in F (applies to A, B, C and D); 100 μm in E.

increased epileptogenesis. In addition to the presence of the microgyri, other forms of dyplasia included cortical warts (Fig. 4.3, E) and obliteration or marked thinning of molecular layer I overlying the affected neocortex. The propensity of such structural alterations in the cortex of HI-treated rats that became epileptic, suggests that massive laminar and focal cell loss within the infarcted tissue led to adaptive reorganization in the surviving neurons that had lost their intra- and inter-laminar connections. This may have led to reorganization of the circuitry in the parainfarct cortex, where axon collaterals and maloriented dendrites established novel contacts. The spared ipsilateral sensorimotor cortex in most HI-treated epileptic rats showed cortical dysplastic features (Fig. 4.4, compare B to control A) in the form of cytomegalic neurons. Cytomegally was seen in two groups of cells, one group was darkly stained cells with larger cell bodies that retained their pyramidal structure, and the other group contained lightly stained cells with large rounded or misshapen cell bodies. Similar dysplastic cells were also seen in the contralateral sensorimotor cortex (Fig. 4.4, C). Comparable findings have been described in cortical tissue resected from patients diagnosed with intractable epilepsy secondary to cortical dysplasia (Alonso-Nanclares et al., 2004; Ferrer et al., 1992). Cytomegalic neurons and large cells with atypical morphology have been suggested to play an important role in the generation of epileptic activity due to their abnormal electrophysiological properties (Cepeda et al., 2003; Kerfoot et al., 1999).

4.3 White matter-layer VI junction

In the control sections, the corpus callosal white matter tract formed a distinct border with the layer VI of the sensorimotor cortex (Fig. 4.5, A). This junction of white

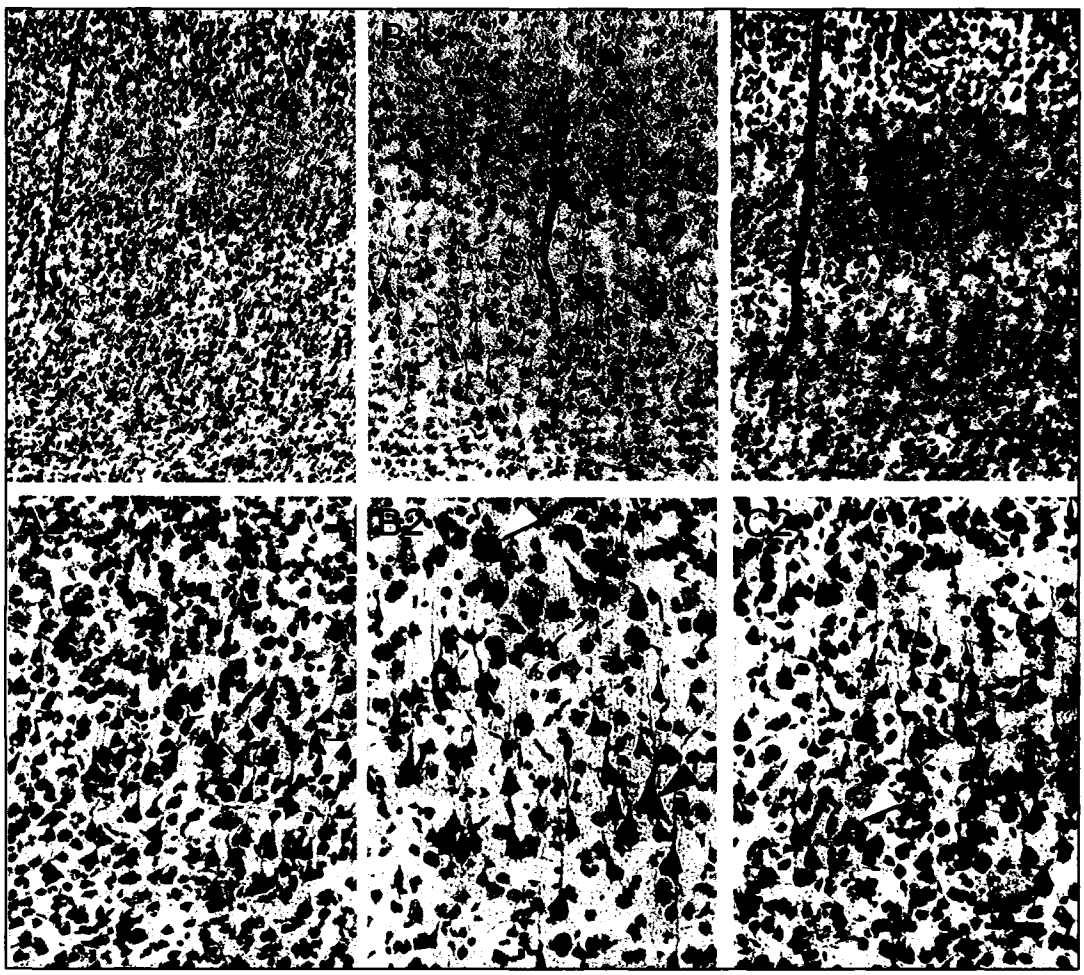

Fig. 4.4 Cresyl-violet-stained coronal sections showing cytomegalic neurons in deep laminar layers of paracingulate neocortex. All panels show paracingulate neocortex with layer II/III at the top of the panel and layer VI at the base with the lower panels showing the deeper layers at higher magnification. Compared to control (**A**), ipsi- (**B**) and contralateral (**C**) neocortex showed presence cortical dysplasia (ipsilateral more than contralateral) in the form of hypertrophic, strongly Nissl-stained pyramidal neurons and lightly stained misshapen cytomegalic neurons in the deep laminar layers (lower half of panels in A1, B1 and C1) . Black arrowheads point to one of many hypertrophic strongly stained layer 5 pyramidal neurons and white arrow heads point to lightly stained cytomegalic neurons in B2 and C2 (compare with control A2). Scale bars = 100 μm in C1 (applies to top row); 50 μm in C2 (applies to bottom row).

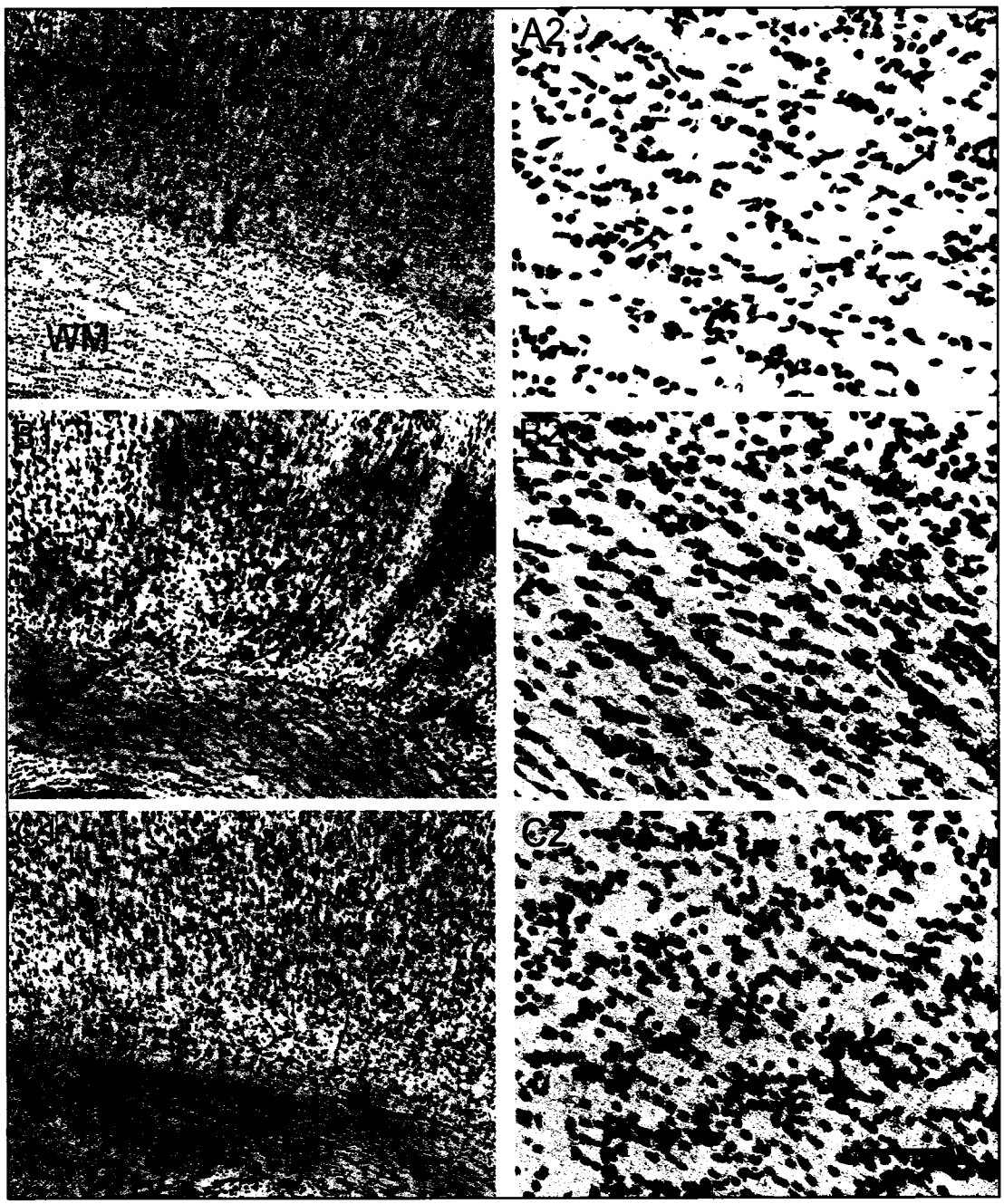

Fig. 4.5 Layer VI /white matter (WM) junction dysplasia and WM hypercellularity. The left panels show the layer VI/WM junction of the parasagittal sensorimotor neocortices and the right panels are magnified views of the WM underlying the sensorimotor cortices at the corresponding locations of the left panels. The normal distinct layer VI/WM junction (arrows) is seen in a control rat (**A1**), while blurring of this junction was noted in the ipsilateral (**B1**) and contralateral (**C1**) sensorimotor neocortex of an HI-treated epileptic rat. Note the hypercellularity of the WM underlying the HI-treated ipsi- and contralateral cortex compared to control. Scale bars = 100 μm in C1 (applies to A1 and B1); 25 μm in C2 (applies to A2 and B2).

matter and layer VI underlying the lesion in the HI-treated epileptic rat was blurred and hypercellularity was observed in the white matter underlying the injured cortex not only in the ipsilateral cortex but the contralateral as well (compare Fig. 4.5,B & C to 4.5,A) in all the HI-treated epileptic rats. Similar histological findings have been noted in resected human samples of cortical dysplasia (Andres et al., 2004; Armstrong, 1997; Meencke, 1985). Closer microscopic examination showed the blurring of the white matter and layer VI junction to result from isolation of clumps of neurons by tracts of glial tissue. This patchy glial infiltration caused the loss of definition of the overlying neocortex from the hypercellular white matter.

4.4 Rapid Golgi stain

Golgi staining of HI-treated rat brains using the Rapid-Golgi technique revealed marked loss of laminarity leading to neuronal disorganization in the sensorimotor and entorhinal spared cortices. Dysmorphic features dominated these sections (Fig. 4.6 & 4.7). The spared paracingulate cortex that appeared laminar in cresyl violet stained sections revealed dysmorphisms in the form of maloriented clumps of neurons forming dense dendritic networks (Fig. 4.6, B), similar to the types reported by Marin-Padilla (2003) in the irradiation-induced cortical dysplasia model. Some of these cytomegalic (25-30 μm) neurons had dysmorphic dendritic branching and a multitude of pedunculate spines on their dendrites (compare Fig. 4.6, B1 to A1). Neurolucida tracings of neurons in and around a microgyrus revealed pyramidal neurons with transformed morphologies (Fig. 4.7, compare B3 to A3).

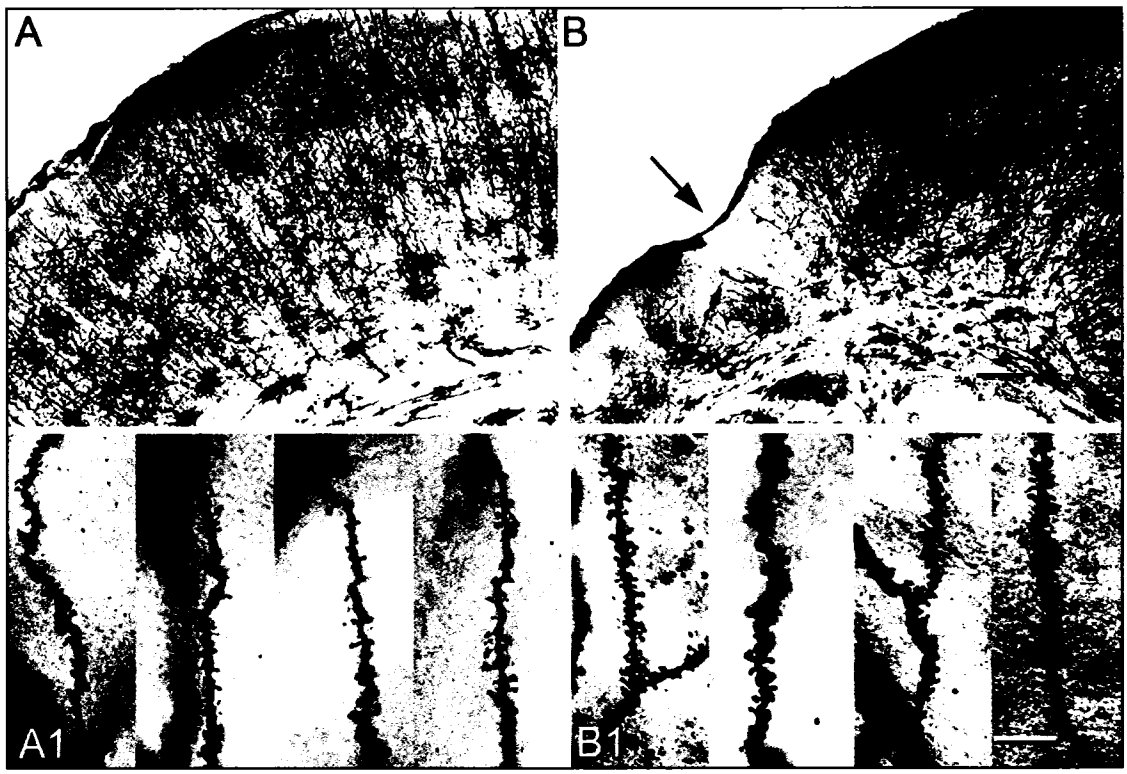

Fig. 4.6 Dislamination of spared paracingulate cortex as revealed by the rapid-Golgi stain. The upper panels show low-magnification images of control (**A**) and HI-treated neocortex (**B**), and the lower panels are high magnification images showing the corresponding apical dendrites and spines. **A.** Golgi-stained paracingulate neocortex from a control rat shows isocortical cytoarchitecture, starting outside with the molecular layer I, followed by the outer granular and pyramidal layer (II/III), the inner granular layer IV, the inner pyramidal layer V and mutiforme layer VI followed by corpus callosal white matter tract. **B**. The ipsilateral Golgi-stained section from an HI-treated brain with a parasagittal microgyrus (arrow). Note the lack of Golgi staining in the gliotic bands around the microgyrus and the loss of laminar cytoarchitecture in the spared paracingulate cortex, which looked comparatively laminar in cresyl-violet-stained sections. Pedunculate spines were seen on apical dendrites reaching the molecular layer from pyramidal neurons in layer II in control (**A1**) and lesioned (**B1**) sensorimotor neocortices. The distal apical dendrites from HI-treated rats showed an abundance of pedunculate spines compared to control. Scale bars = 250 μm in B (applies to A); 10 μm in B1 (applies to A1).

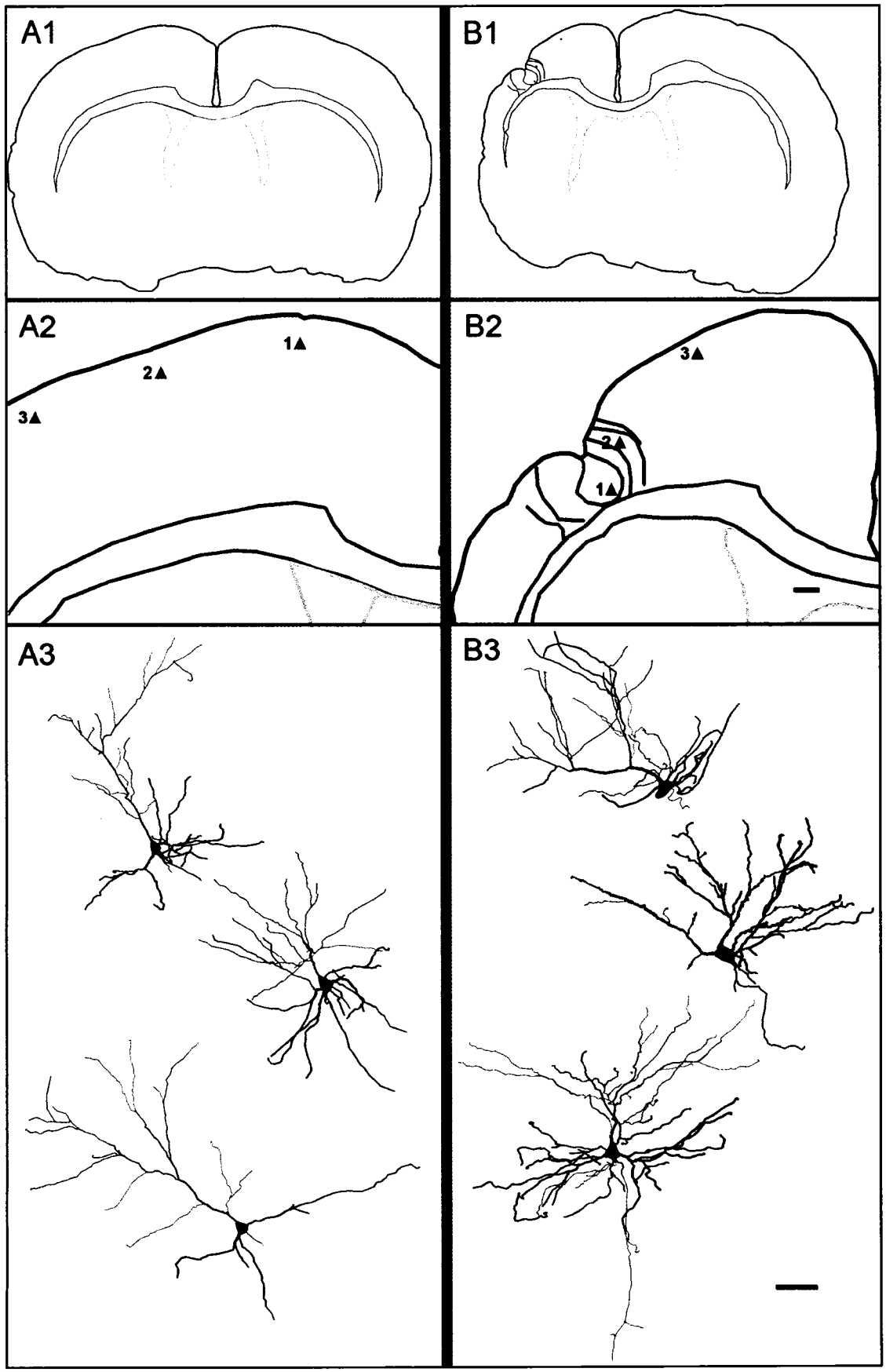

Fig. 4.7 Cortical neuronal morphologies revealed by neuronal reconstructions from rapid-Golgi-stained sections. Top panels show low magnification traces of sections from control (**A**) and HI-treated rats (**B**). Middle panels show higher magnification of the traces in the top panels from the corresponding right parasagittal neocortices. Bottom panel shows the dysmorphic features of reconstructed layer II/III pyramidal neurons from HI-treated sections compared to corresponding neurons from control sections. The tracing of a Golgi-stained 200-μm coronal section from control and HI-treated rats shows bilateral symmetry in control (**A1**) and an atrophied ipsilateral hemisphere with a microgyrus in the sensorimotor cortex (red) in a lesioned rat (**B1**). In contrast to control (**A2**) the presence of a parasagittal microgyrus and the surrounding gliotic bands are traced (red contours) in **B2** to give reference to the location of the reconstructed pyramidal neurons (i.e., solid blue triangles 1, 2 & 3). The reconstructed pyramidal neurons are depicted in the exact dorso-ventral orientation they were found in the coronal sections and are shown in a numerically ascending order from top to bottom (**A3 and B3**). Neuron 1 from HI-treated rat (**B3**) is a displaced layer II/III neuron showing a dominant apical dendritic tree (grey) with basal dendrites (black) running along the curvature formed by the pit of the microgyrus. Neuron 2 is a layer II/III neuron lying abut the microgyrus and a gliotic band. It shows a sparsely branched apical dendrite running along the gliotic band towards the molecular layer and a unilateral tree of basal dendrites directed away from the gliotic band and towards the parainfarct cortex. Neuron 3 is a layer II/III layer pyramidal neuron in the parainfarct sensorimotor cortex with a well formed apical and basal dendritic tree and axon collaterals (red); cell body – blue, apical dendrite – grey, basal dendrite – black, axon – red; scale bars = 250 μm in B2 (applies to A2); 50 μm in B3 (applies to A3).

4.5 Hippocampal lesion and mossy fiber sprouting

The hippocampus showed massive loss of neurons in the ipsilateral CA3 region (Fig. 4.8, A & B) of all HI-treated epileptic rats. Examination of the entorhinal cortex revealed marked laminar neuronal cell death ipsilaterally (Fig. 4.8, C & D); similar findings have also been reported in the pilocarpine-treated rat model of epilepsy (Kobayashi et al 2003). Hippocampal ipsi- and contralateral lesion scores and conclusions as described by Williams et al.,(2004) were found to be similar for this study, where ipsilateral hippocampi from HI-treated rats had higher lesion scores compared to hippocampi from sham-control rats and contralateral hippocampi from HI-treated rats.

Timm stain was seen bilaterally in the inner molecular layer of the dentate gyrus in the HI-treated epileptic rat (Fig. 4.9 & 4.10), both in the dorsal (Fig. 4.9, B2 & C2) and ventral (Fig. 4.10, B2 & C2) hippocampus. The average grades of Timm stain product were compared between sides (ipsi- and contralateral) and the three groups of animals (HI-treated epileptic rats, HI-treated non-epileptic rats and sham control rats, Fig. 4.11). In HI-treated epileptic rats, significantly higher average grades were found in the ipsilateral dorsal (septal) hippocampus compared to the contralateral dorsal hippocampus ($P<0.0001$). In comparison, a similar difference was not found to be significant in HI-treated non-epileptic rats ($P=0.02$). Both the above-mentioned grades in HI-treated epileptic rats were significantly different from average grades for controls ($P<0.0001$ and $P <0.0001$ respectively) but for HI-treated non-epileptic rats they were only significantly different from control ipsilaterally but not contralaterally ($P<0.0001$ and $P=0.07$ respectively). On the other hand, the ventral hippocampi of HI-treated epileptic rats showed significantly higher grades of stain product compared to both the HI-treated

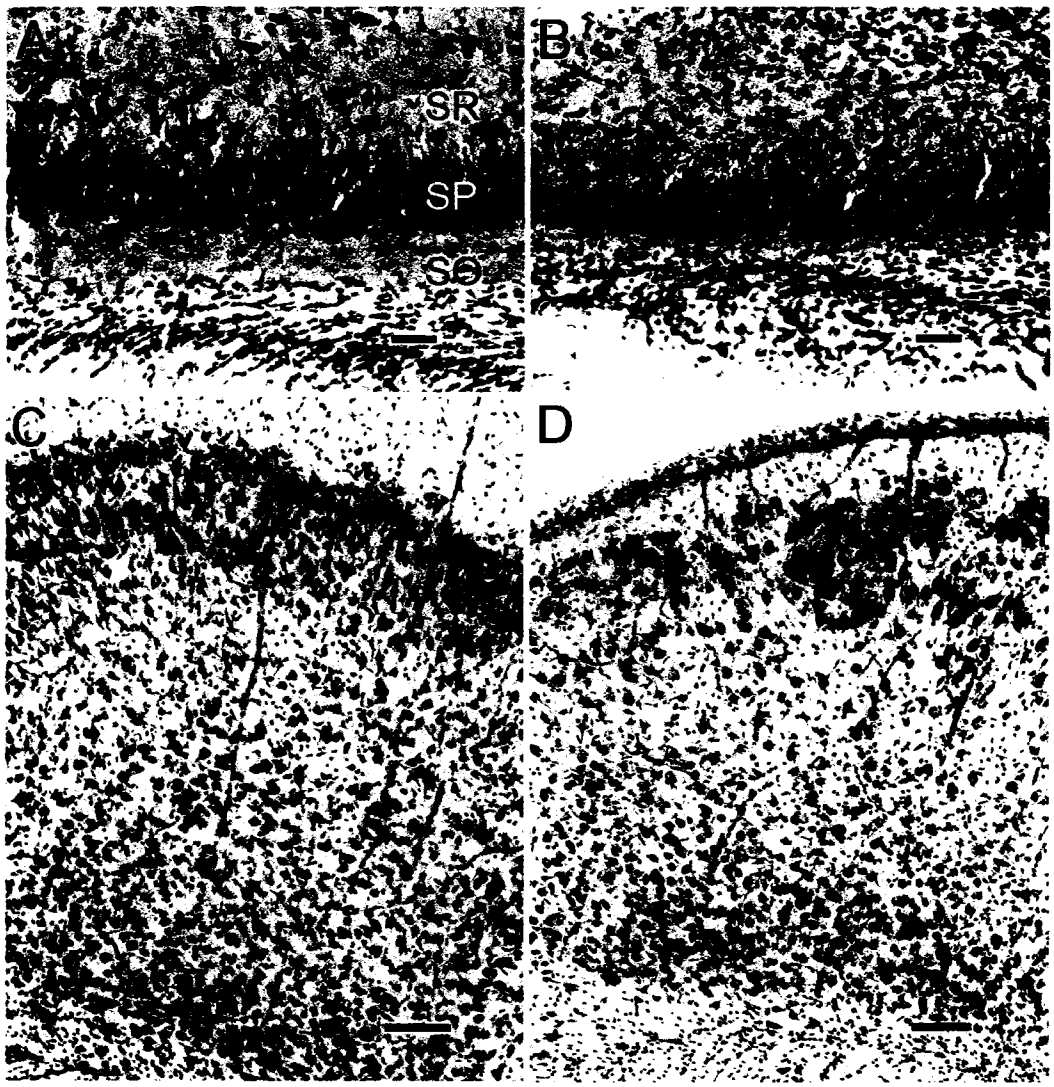

Fig. 4.8 Cell loss in the dorsal hippocampus and the entorhinal cortex. Cresyl-violet-stained coronal sections of the ipsilateral dorsal hippocampus (A and B) and entorhinal cortex (C and D) with the molecular layer I, at the top of the panels are shown. Neurons in the stratum pyramidale (SP) are seen populating the CA3 region of the right hippocampus in a control rat (**A**). Massive loss of neurons is shown in the corresponding CA3 region in an HI-treated rat (**B**). Note the reactive gliosis in the stratum oriens (SO) and stratum radiatum (SR) in the HI lesioned section. Compared to control (**C**) the entorhinal cortex shows laminar loss of neurons marked by the superficial presence of large neurons normally located in the deeper layers in the section from an HI-treated epileptic rat (**D**). Note the thinning/obliteration of the molecular layer I in D. Scale bars = 50 μm in A & B; 100 μm in C & D.

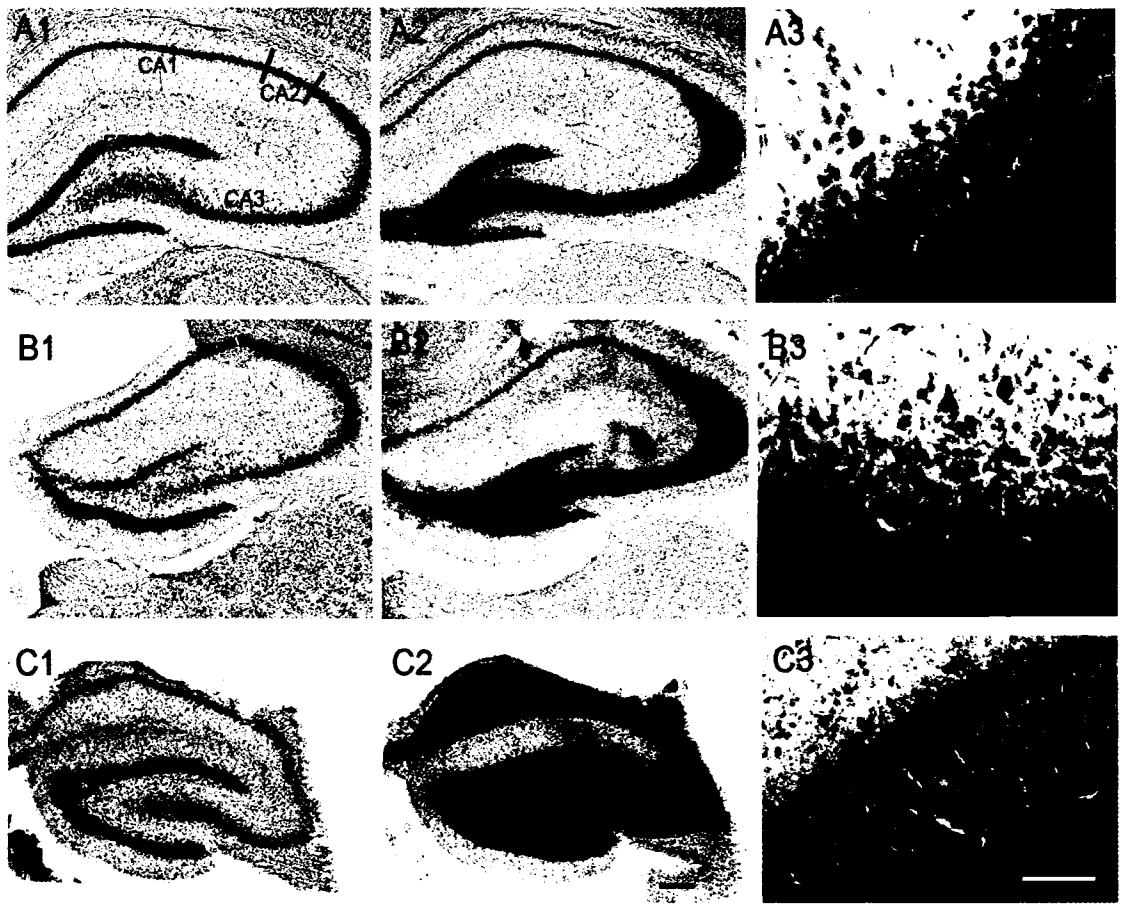

Fig. 4.9 Representative coronal cresyl-violet and Timm-stained-sections focusing on the ipsi- and contralateral dorsal hippocampi. Top and bottom panels show ipsilateral cresyl-violet (A1 and C1), Timm stained sections (A2 and C2) and magnified views of the inner molecular layer of the dentate gyrus (A3 and C3) from a control and HI-treated epileptic rat respectively. Middle panel shows the corresponding contralateral sections from the same HI-treated epileptic rat as shown in panel C (B1, B2 and B3). The dorsal hippocampus from a control rat (**A1**) shows fascia dentata (FD) and the Ammon's horn (CA3, CA2 and CA1). The Timm stained section shows dark brown precipitate in the region of mossy fiber innervation (**A2**). Grade 0 Timm stain product is seen in dentate inner molecular layer (**A3**). The contralateral dorsal hippocampus (B1) shows no apparent cell loss of CA3 neurons. Timm stain shows a more robust distribution compared to control (**B2**) and minimal (grade 1) stain product is seen in dentate inner molecular layer (**B3**). Massive loss of lateral CA3 neurons causing a distinct demarcation between the CA3 and CA2 (relatively spared) junction is seen in the ipsilateral region of the epileptic rat (**C3**); note the relative preservation of the fascia dentata (FD) medial CA3 and hilar neurons. Robust innervation of the CA3 region till the CA3/CA2 junction by mossy fibers masks presence of the few surviving neurons in the region by cresyl violet counter stain (**C2**). The dentate inner molecular layer shows grade 3 stain product (**C3**); note atrophy of ipsilateral dorsal hippocampus in ipsilateral compared to the contralateral and control sections. Scale bars = 250 μm in C2 (applies to A, B & C (1 &2); 50 μm in C3 (applies to A3 and B3).

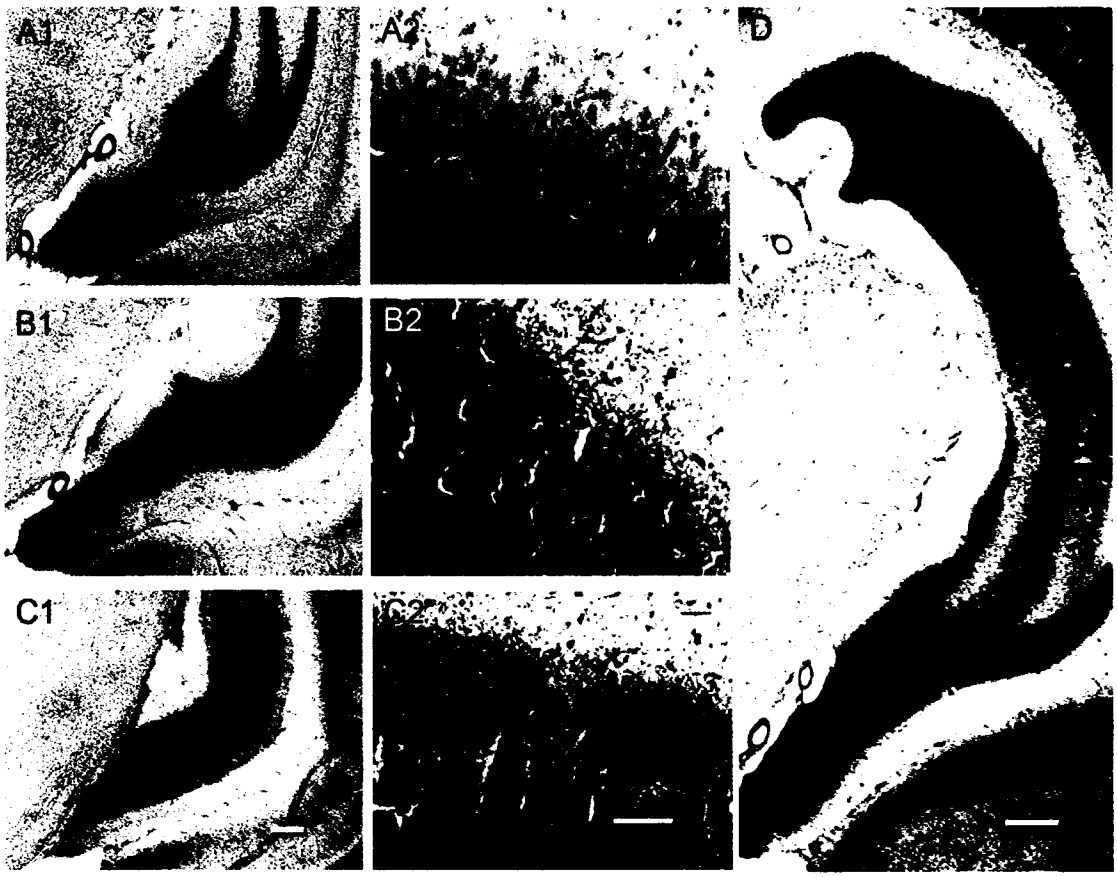

Fig. 4.10 Representative coronal Timm-stained-sections focusing on the ipsi- and contralateral ventral hippocampi. Top and bottom panels show ipsilateral Timm stained sections (A1 and C1) and magnified views of the inner molecular layer of the dentate gyrus (A2 and C2) from a control and HI-treated epileptic rat respectively. Middle panel shows the corresponding contralateral sections from the same HI-treated epileptic rat as shown in panel C (B1 and B2). The ventral hippocampus from a control rat (**A1**) shows Timm staining in the dentate hilus and Grade 0-1 stain product in the dentate inner molecular layer. A more robust stain product is seen in both B and C panels with grade 3 staining in the dentate inner molecular layer bilaterally (**C2** more than **B2**). Contralateral Timm stain showed a differential grade of stain in the dorsal vs. ventral hippocampus of epileptic rats. A representative coronal section from an epileptic rat (**D**) showing grade 1 compared to grade 3 of Timm stain in the dentate inner molecular of the dorsal hippocampus at the top of the panel and the ventral hippocampus in the bottom of the panel respectively. Scale bars = 250 μm in C1 (applies to A1 and B1); 50 μm in C2 (applies to A2 and B2); 500 μm in D.

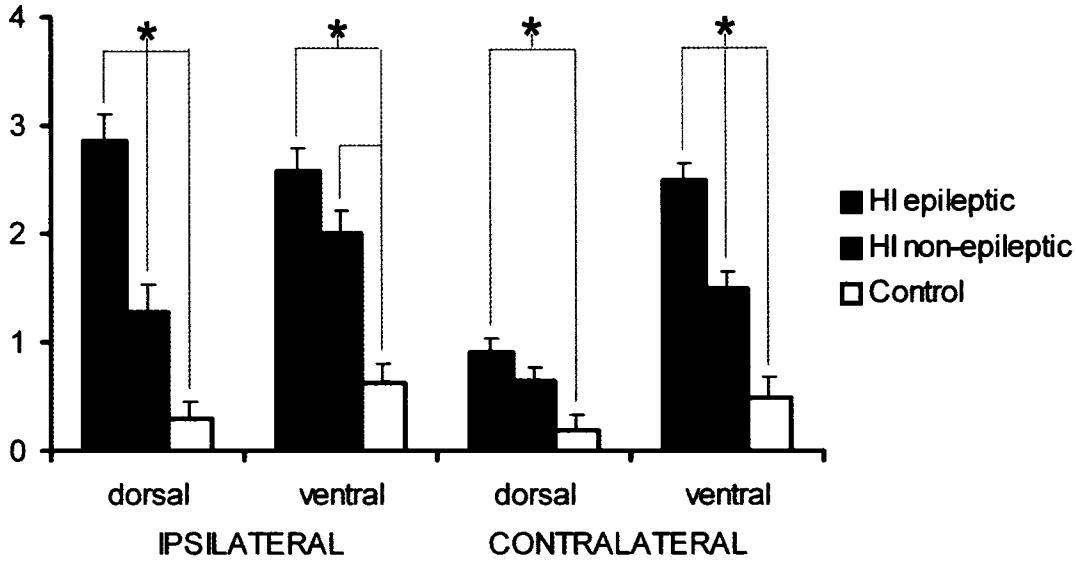

Fig. 4.11 Comparison of Timm stain grades in the dentate inner molecular layer of ipsi- and contralateral dorsal and ventral hippocampi of i) HI-treated rats that were detected to be epileptic (n=11). ii) HI-treated rats that were not detected to be epileptic (n=14) iii) sham control rats (n=12). Significant differences between groups for each anatomical location are indicated by asterisks.

non-epileptic and control rats (P=0.001 and P=0.0001 respectively) contralaterally but ipsilaterally they were only significantly different from control (P<0.0001). Average grades for HI-treated non-epileptic rats as a group were significantly different from average grades for control rats on both counts. These data suggest that HI-treated epileptic rats have significantly greater mossy fiber sprouting ipsilaterally both in the severely atrophied dorsal and non-atrophied ventral hippocampus, but more importantly also in the contralateral hippocampus, in significantly greater grades in the ventral hippocampus than the dorsal. This contralateral sprouting in the ventral hippocampus of the HI-treated epileptic and non-epileptic rats, which anatomically is representative of the anterior head of the human hippocampus, suggests chronic inter-hemispheric diachisis associated with this perinatal insult that was significantly different for rats with seizures

versus rats without detectable seizures. Similar significance was not found for the contralateral dorsal hippocampus in this study.

CHAPTER 5

INVESTIGATION OF TEMPORAL FEATURES OF EPILEPTOGENESIS WITH PERINATAL HI INSULT USING CHRONIC VIDEO-TELEMETRIC MONITORING OF EEG

This study used long-term continuous cortical electroencephalograms (EEG) recordings with an aim to account for every ictal event during the period of monitoring occurring in rats that developed epilepsy after an HI insult at P7. Implanting 2 groups of rats at an early (2 months) and later (>6 months) time point provided a data sets that spanned ~12 months after the perinatal insult accounting for 556 ictal episodes in 10 epileptic rats. The hypothesis for the long-term monitoring of cortical EEG that was initiated as soon as possible (see methods) after the postnatal day 7 HI insult was that similar to human epilepsy, interictal spikes would be the first EEG events detected in epileptic rats. Based on the histopathological features noted in epileptic rats described in chapter 4, it was also hypothesized that inter-ictal and ictal EEG's in this animal model would be representative of the progressive nature of the post-infarct epileptogenesis. The study found a time-dependant increase in seizure frequency as a function of time that showed the epilepsy to be progressive in nature. The concomitant synchronous video-monitoring was used to classify every ictal episode on the Racine (1971) scale. This helped detect the non-convulsive and partial seizures from the generalized motor

seizures. We found that the progression also related to the seizure severity as the non-convulsive ictal discharges and partial seizures (P1-3) were predominant in the initial months of monitoring. Clustering of seizures was a predominant feature of the resultant epilepsy. The increase in the episodes of such clusters and the increase in seizure numbers within each subsequent cluster contributed to the data fitting the exponential growth phase of a sigmoid curve. The equation for the best fit sigmoid curve predicted a half maximal seizure rate of ~111.5 seizures/month at 18 months of age.

5.1 Seizure semiology - partial vs. generalized seizures

Modified Racine scale was used as described above to grade the seizures and differentiate partial vs. generalized seizures. There was another small group of ictal events that can only be described as non-convulsive (they had none of the behavioral features described in the classification). The behavioral correlates for these events were either an inactive state or an active state with a hunkering down posture with stretching out of the torso followed by wet dog shakes. They were classified as P0 for this study. All the ictal events recorded on EEG that were graded as P0-P3 were classified as partial electrographic seizures. Behavioral monitoring for these events revealed frozen posturing, waking up from sleep and head bobbing followed by frozen posturing. Almost all such events ended in wet dog shakes. Behaviorally the period of post-ictal inactivity was minimal to absent. P3 seizures that according to the modified scale indicate lordotic posturing and forelimb clonus in this model was usually limited to a left forelimb clonus or forelimb clonus initiated in the left forelimb followed by progression to the right forelimb. A large number of the generalized seizures (P4 & P5) also started the tonic clonic phase with a left forelimb clonus. This consistent seizure semiology supports an

ipsilateral (right hemisphere) onset of ictal activity. Another significant observation was the presence of versive posturing at the onset of an ictal episode (Fig. 5.1). Unambiguous and predominantly ispsiversive head and neck posturing sometimes also involved the torso while a few were contraversive.

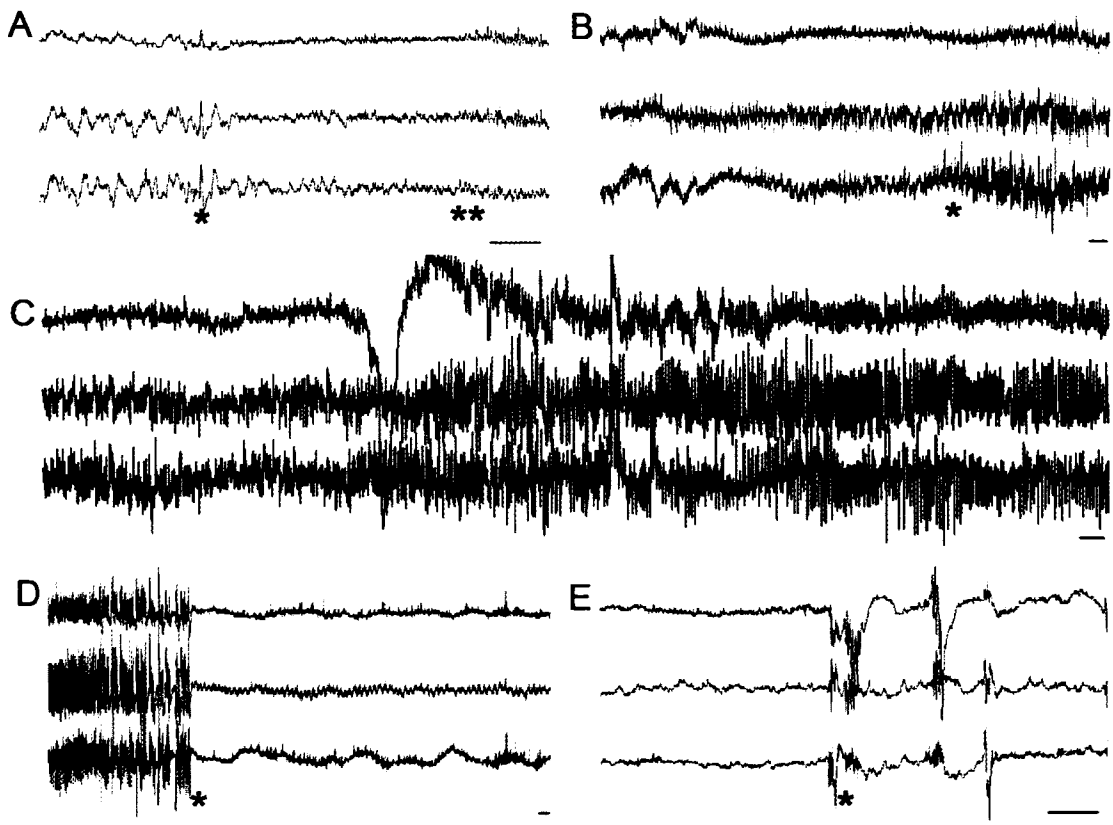

Fig. 5.1 Representative electrographic P5 seizure as recorded on Ch 1, 2 & 3; top to bottom on each panel respectively. Generalized EEG discharge starting in all three channels at the same time leading to a tonic-clonic convulsive seizure. A. * Initial spike in EEG/ rat sleeping ** rat wakes up and head slowly tilts to the right; B.* Rat rears on hind limbs with tonic forelimb posturing; C. * Forelimb tonic-clonic movements begin; D. * Abrupt cessation of forelimb tonic/clonic movements coincides with disappearance of cortical spikes in all three leads followed behaviorally by immobile frozen posturing with facial convulsions seen as post-ictal depression electrographically; E. * Post ictal EEG discharges coincide with wet dog shakes. Scale bar - 1 sec, Asterisks - EEG time point as related to synchronized behavior during ictus.

5.2 24 h EEG monitoring

In this study the 3 bio-potential telemetry units lasted a maximum of 166 days in this study. Animals in this study were monitored in the system for an average of 118.7 ± 7.7 days (minimum of 33 days and maximum of 166 days). Only 4 out of 27 animals had < 60 days of monitoring that were taken out of the system due loss of/noisy recordings due to dislodged recording electrodes. Every animal had a 24 h D-clamp EEG file for every day it was in the system. The total number of files recorded in this study was 3277

Rat identity	Age (months)	Sex	Time recorded (days)	Reason for end of recording
A1	2	Male	158	Battery
A2	2	Female	155	Battery
A3	2	Male	155	Battery
A4	2	Male	166	Battery
A5	2	Female	33	Rat died
B1	6	Male	152	Battery
B2	6	Male	150	Battery
B3	8	Female	143	Battery
B4	8	Female	51	Lost recording
B5	6	Female	53	Lost recording

Table 5.1 Characteristics of epileptic rats and EEG recordings. Two groups of rats were implanted with telemetry units for continuous EEG recording at 2 and ≥6 months of age (group A and B respectively). Ten HI-treated rats (5 from each group) were detected to be epileptic in this study from the two age groups.

(1216 – HI-epileptic; 821 – HI non-epileptic; 1240 – sham control). Some of these files were lost/ incomplete due to computer related technical issues. This loss amounted to 2.75 % of the total. Even for this loss of EEG data we had concomitant video recordings which were analyzed by viewing the tapes in their entirety. We had 24/7 synchronous video monitoring for all the above mentioned files (except for 0.24% loss due to power failure) and these were viewed concomitantly over specific time durations as determined by the analysis of the EEG files. Out of the 28 implanted rats monitored in the telemetry system 10 were randomly selected male and female sham control rats (5 of each gender) from 6 different litters. 18 were randomly selected male and female rats (9 of each gender) HI-treated rats from 8 different litters. The 10 rats that were found to be epileptic (5 of each gender) were monitored for 121.6 ± 16.8 days (for details of monitoring for individual epileptic rat refer to table 5.1). HI-treated non-epileptic and sham control rats were monitored for 102.6 ± 13.8 and 124 ± 8.2 days respectively.

5.3 Lateralization of ictal and interictal spike activity and their spatio-temporal relationship.

An isolated spike or wave that is apart from the seizure itself and is the most prominent feature of EEG's of epileptic patients. The EEG's recorded from freely moving rats in this study detected interictal spikes as spikes or sharp waves. The distinction between these 2 patterns has been described to have no etiologic significance, the only difference being one of EEG pattern morphology. A spike is defined as being less than 70 milliseconds in duration, and a sharp wave has duration of 70-200 ms. Seen as a paroxysmal depolarization in form of a negative deflection they had durations that

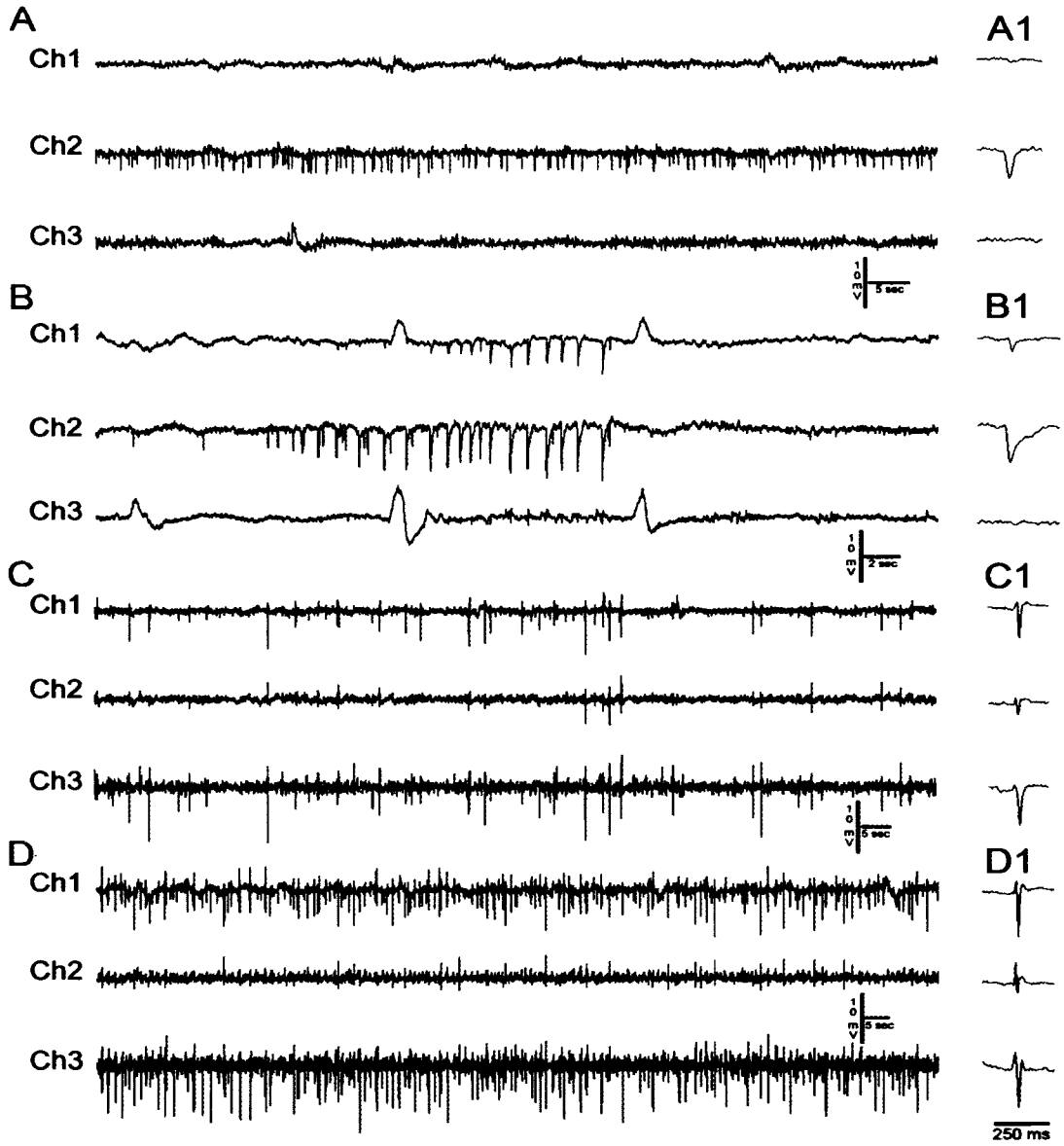

Fig. 5.2 Variability of interictal spike activity and spike durations. Lateralization of interictal activity in early recordings from the young group (A). Interictal spikes recorded on Ch 2 only; Interictal spikes recorded on Ch 1 & 2 with clear primary onset in Ch 2 (B); Variable frequency of inter-ictal activity was seen in chronically epileptic rats - C. Interictal spikes recorded on all three channels with a lower frequency in Ch2 compared to Ch1 and Ch3; D. robust interictal spikes seen between a cluster of seizures with a frequency ~ 1 Hz. A1, B1, C1 and D1 show individual spikes from approximate center of respective traces showing spikes and sharp waves (see results).

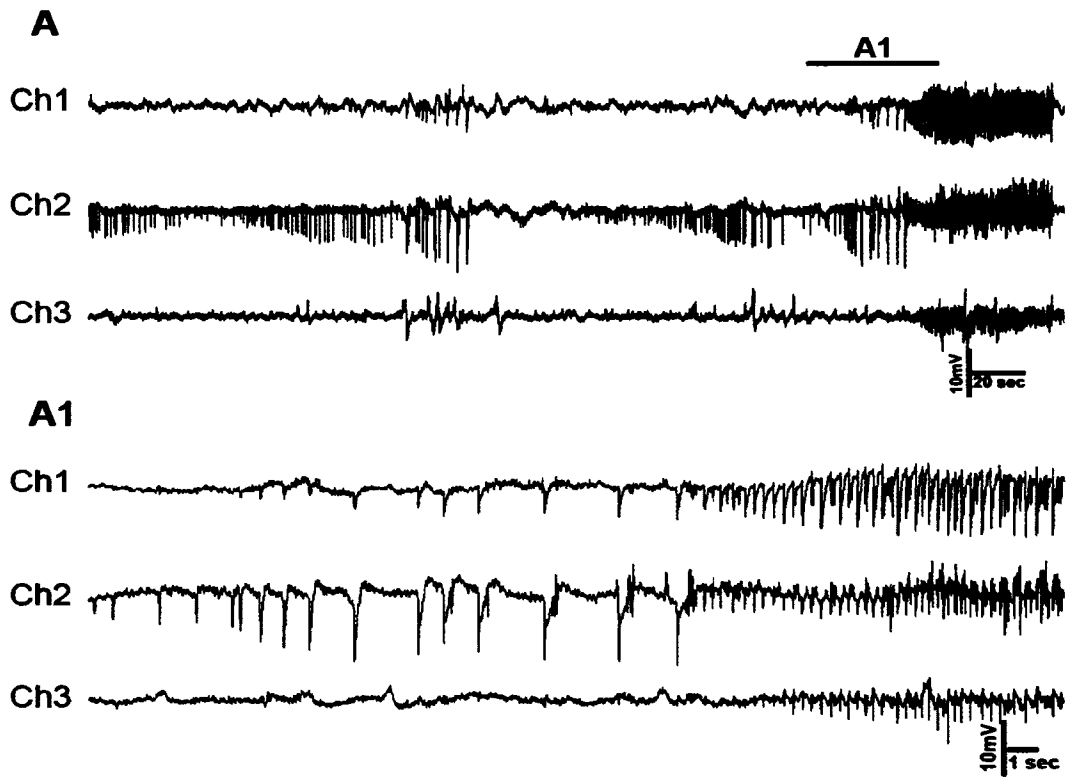

Fig. 5.3 Lateralization of onset of electrographic activity. A. Early seizure in 2-month-old - Three EEG channels (labeled 1, 2 & 3), representing locations described in Fig. 1, recorded ictal activity that was initiated in Ch 2 (para-infarct zone) seconds before spiking activity occurred in Ch 1 (core of infarct), followed by Ch3 (contralateral motor cortex). A1 is an expansion of the EEG trace marked by solid black line in A.

ranged from a few 10's of milliseconds (spikes) to couple 100 milliseconds (sharp waves). They were variable in amplitude but always distinct from baseline. Early interictal discharges showed ipsilateral lateralization with the very first detected EEG spikes were recorded on Ch2 that overlay the ipsilateral parainfarct neocortex (Fig. 5.2, A) of the younger group of implanted rats. Even when they were recorded on both the ipsilateral leads (Ch1 and Ch2) clear initiation was discernable on Ch2 (Fig. 5.2, B). Most of the lateralized interictal spikes were recorded before the first behavioral ictal events

were detected and confirmed on synchronized video footage. In the following months most of the interictal activity was seen preceding and following an ictal event (Fig. 5.2, C) and markedly between ictal events that occurred as clusters. This spike activity sometimes was as high as 1 Hz in frequency (fig 5.2, D). Most ictal events that ranged from P1-5 were recorded simultaneously on all three leads but when there was evidence for lateralization it was similarly detected over Ch2 (Fig.5.3 and 5.4).

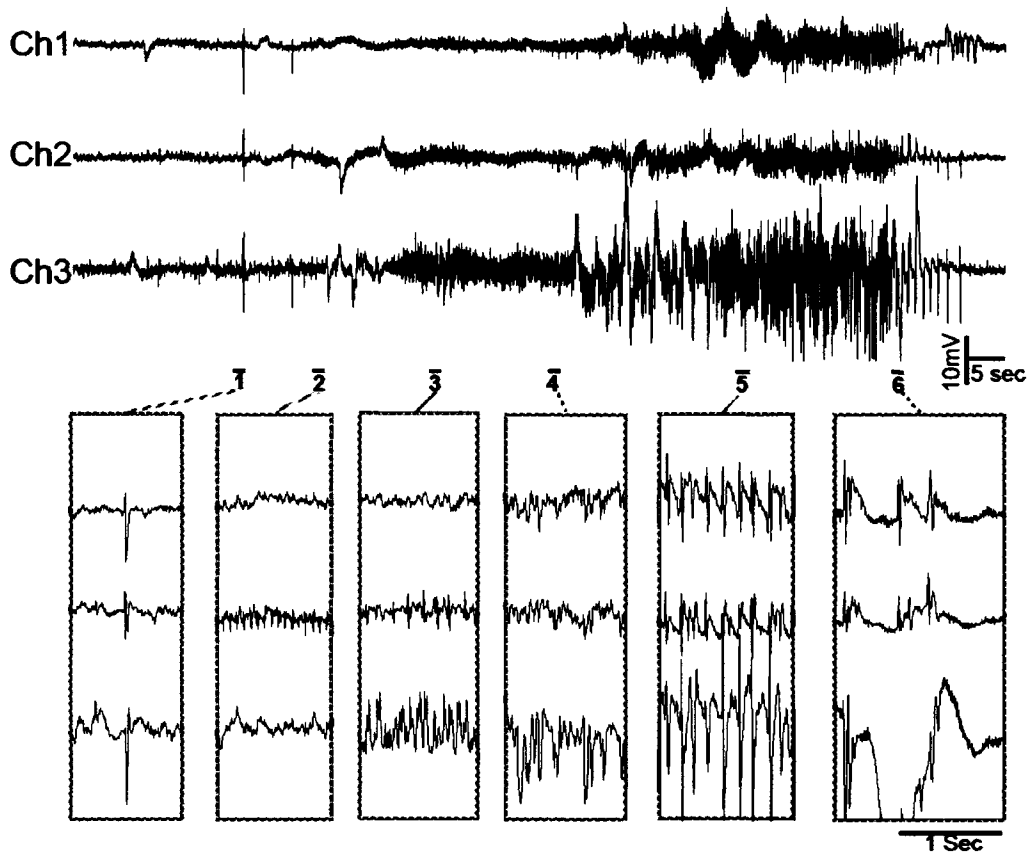

Fig. 5.4 Representative P5 tonic-clonic generalized seizure in a 6-month-old rat. Expansions in lower panel show: 1) onset of seizure heralded by the initial large-amplitude spike; 2) followed by rhythmic spiking activity first seen in Ch2; 3) spiking activity seen on Ch2 and Ch3; 4) low-amplitude high-frequency spiking activity seen in all three channels; 5) rhythmic 6-7 Hz large-amplitude synchronous spike-wave activity in all three channels; 6) termination of seizure with large-amplitude low-frequency spike-wave forms with intervening silent periods.

5.4 Progressive increase in seizure frequency and severity

Rats that were implanted at 2 months of age yielded data for the first five months (age 3 to 7 months) and the older age group (>6 months) yielded data for the next 6

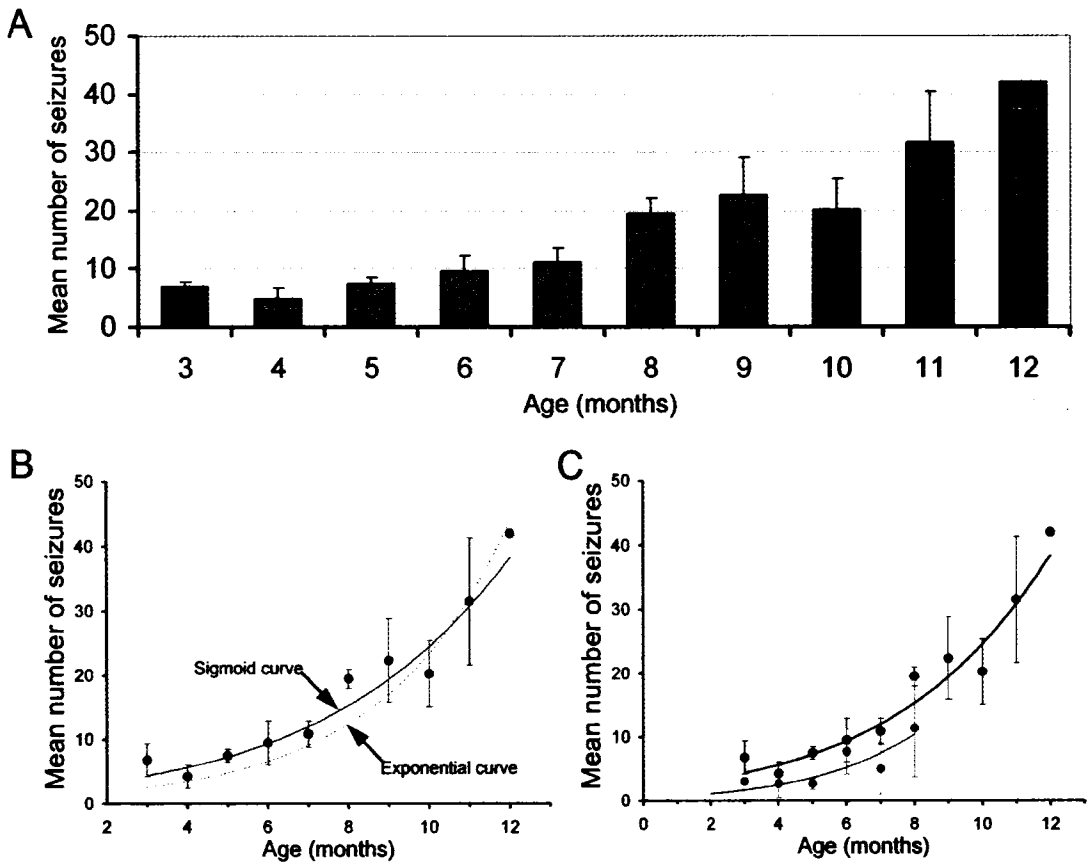

Fig. 5.5 Increase in seizure frequency and severity as a function of time. A. Chronic video-EEG monitoring detected an increase in seizure frequency and severity (Racine scale) over time in HI rats implanted at 2 months and at > 6 months. Bar graph shows a stacked column analysis for partial (P1 2 &3) and generalized (P4 & 5) seizure distribution over time for 10 HI-treated epileptic rats averaged over 11 months. B. Best fit for the data in A. with an exponential growth curve represented by the dotted line and a sigmoid curve that was the better fit represented by the solid red line. C. Data in A with best fit sigmoid curve from B shown here together with 7-month data acquired from a separate group of HI-treated epileptic rats that were behaviorally video-monitored (non-invasive) for 1 week every month (1/4 of the monitoring time compared to data in A). Best fit sigmoid curve for behavioral data (red) mirrors sigmoid curve for telemetry data (black) with lower mean values representative of the shorter monitoring duration.

months (age 7 to 12 months). The data from these two groups were coalesced to get information for epileptogenesis for this HI model over the duration of a year after the initial P7 insult. Analysis of the EEG's revealed 10 out of 18 implanted HI-treated rats were to be epileptic. The protocol detected a progression of the seizure frequencies for these rats (Fig. 5.5, A) that increased from a mean rate of 0.2 seizures per day at 3 months to 1.4 seizures per day at 12 months age. This 10 fold increase over the duration of 10 months during which every ictal event was accounted for, fit the exponential growth phase of a sigmoid curve with the equation $f = 223.7620/(1+\exp(-(x - 18.1221)/3.8785)$ where x represents the advancing age of the rat in months (fig 5.5,B). Seizure severity represented by the Racine scale indicated a lower seizure severity in the initial month of monitoring (Fig. 5.5, A). Seizure frequencies from the present 24/7 protocol when plotted with 25% continuous monitoring time protocol (1 week per month for 7 months) previously described in chapter 3 showed parallel trends (Fig. 5.5,C).

5.5 Seizure duration and severity (Racine scale)

Seizure durations detected in this protocol ranged from 10 sec to 240 sec for the total of 556 ictal events detected with the present protocol in the 10 HI-treated epileptic rats. Average seizure durations for P5 seizures (n=483) were 95.3 ± 1.4 sec and that for <P5 seizures were 47 ± 3.479 sec (n=73). This association between seizure severity and duration can be visualized in the polar plot depicted in figure 5.6A. The seizure durations for P5 ictal events ranged from 25 to 240 seconds and 10 to 120 sec for the <P5 ictal events. Average durations for the partial seizures (P0 - P3) were 39.5 ±3.6 sec and thus

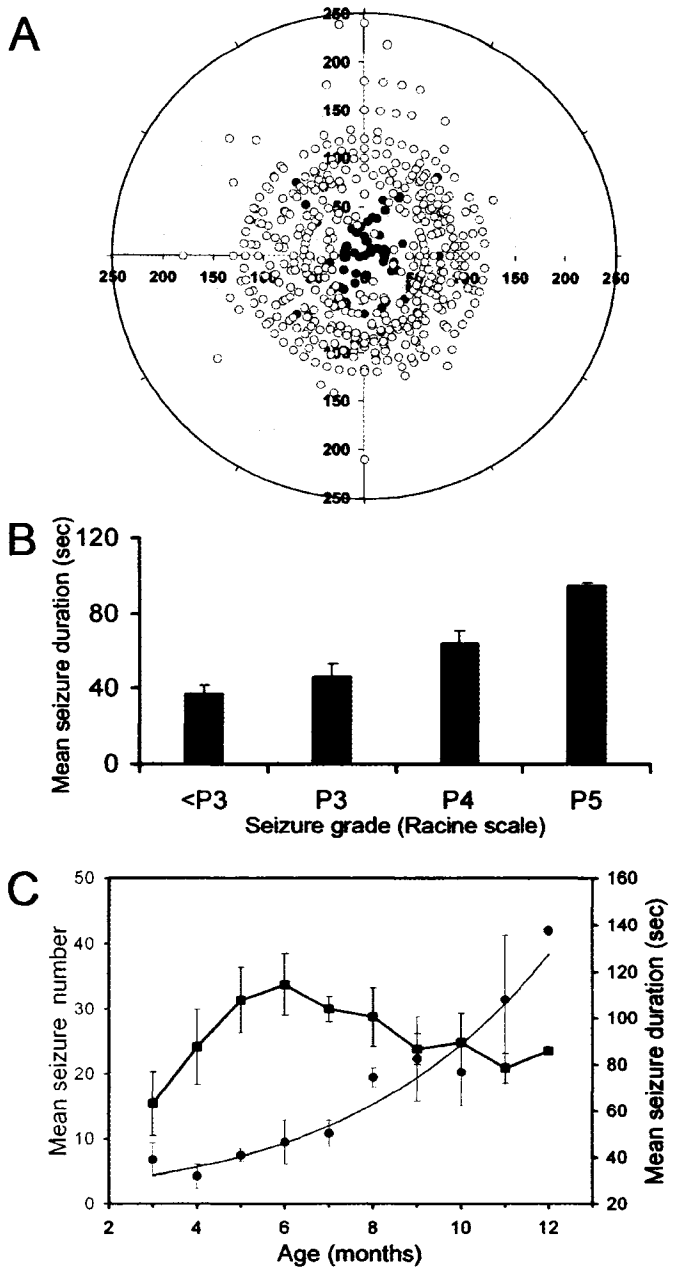

Fig. 5.6 Analysis of seizure durations by severity and as a function of time. A. Polar plot depicting the time durations for total number of electrographic seizures detected in this study (556) , 483 P5 seizures (open circles) compared to 73 <P5 seizures (closed circles) with time in seconds on the X and Y axes. The plot shows the centrifugally distributed P5 seizures representing longer ictal durations as compared to the centripetal distribution of the <P5 seizures indicating shorter ictal durations. B. Bar graph of mean seizure durations for grades of seizure severity classified according to the Racine's scale. C. Mean seizure durations plotted as a function of time after HI insult shows that mean seizure duration in the first recorded month (3rd month after P7 insult) was ~60 sec, progressively increased in durations over the next 3 months, and then decreased to a plateau of 80+ sec. The

superimposed mean seizure frequencies for those same times show that the gradual decline in the mean seizure durations after the 6th month coincides with the exponential growth phase of the sigmoid curve for seizure progression as a function of time.

lower than the <P5 averages (Fig. 5.6, B). Therefore a direct correlation between seizure severity and duration was found that was statistically significant (P=0.01). Average seizure durations of seizures occurring in the 30 day time bins (seizures per month) were calculated for every HI-treated epileptic rat individually (n=10). Means for all the animals were then compared over the 10 months of data to assess the relationship of increasing seizure rates over time to the associated seizure durations. We found that seizure durations progressively increased from the 3rd month after the HI-insult up to the 6th month *pari passu* with the gradual increase in seizure frequency. After the 6th month average seizure durations declined with increasing seizure frequencies which coincided with the exponential growth phase of the best fit sigmoid curve.

5.6 Seizure clusters

Chronic continuous electrographic monitoring of the HI-treated epileptic rats revealed that seizure clustering was a distinct feature of the seizure semiology of the post HI-epilepsy in this model (Fig. 5.7). Clustering was dominant feature seen both in the young (Fig. 5.7, A) and older group (Fig. 5.7, B) of epileptic rats. 3 out of 5 rats from the young age group rats had their first detected seizures present as clusters of partial or partial and generalized seizures. Even with the low initial seizure frequencies reported here the rats had couple of seizures within a 24 h period and then remain seizure free for the next week or more. Increase in seizure frequency over time resulted by decrease in

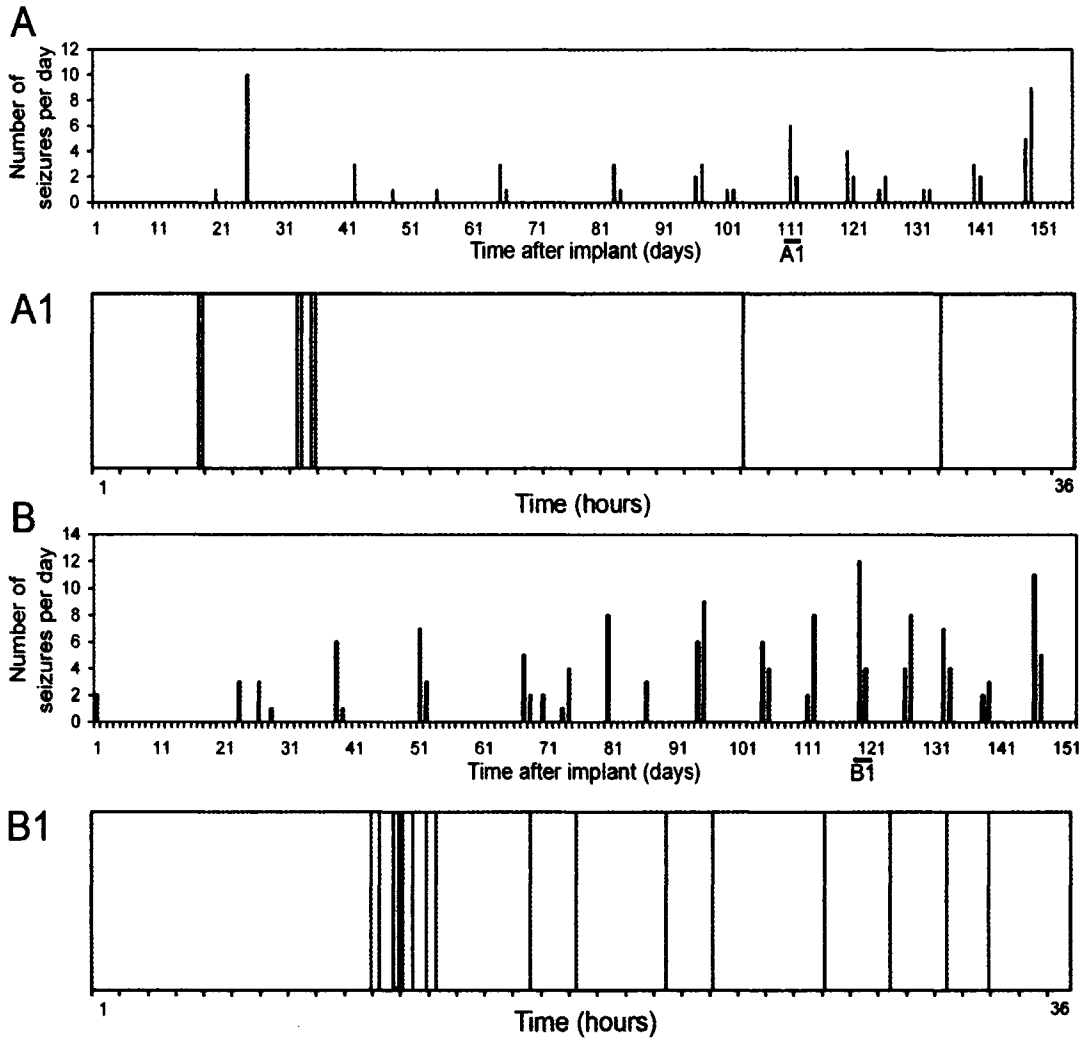

Fig. 5.7 Raster plots showing seizure clusters. Chronic EEG monitoring recorded every ictal event, which revealed clusters of ictal events within a 24-48 h period followed by seizure-free periods of several days. A. Seizure clusters seen in a rat implanted at 2 months of age with an expansion of seizure distribution within one of these clusters spread over 36 h (a). B. Seizure clusters seen in a rat implanted at 6 months of age with an expansion of seizure distribution within one of these clusters spread over 36 hr (b).

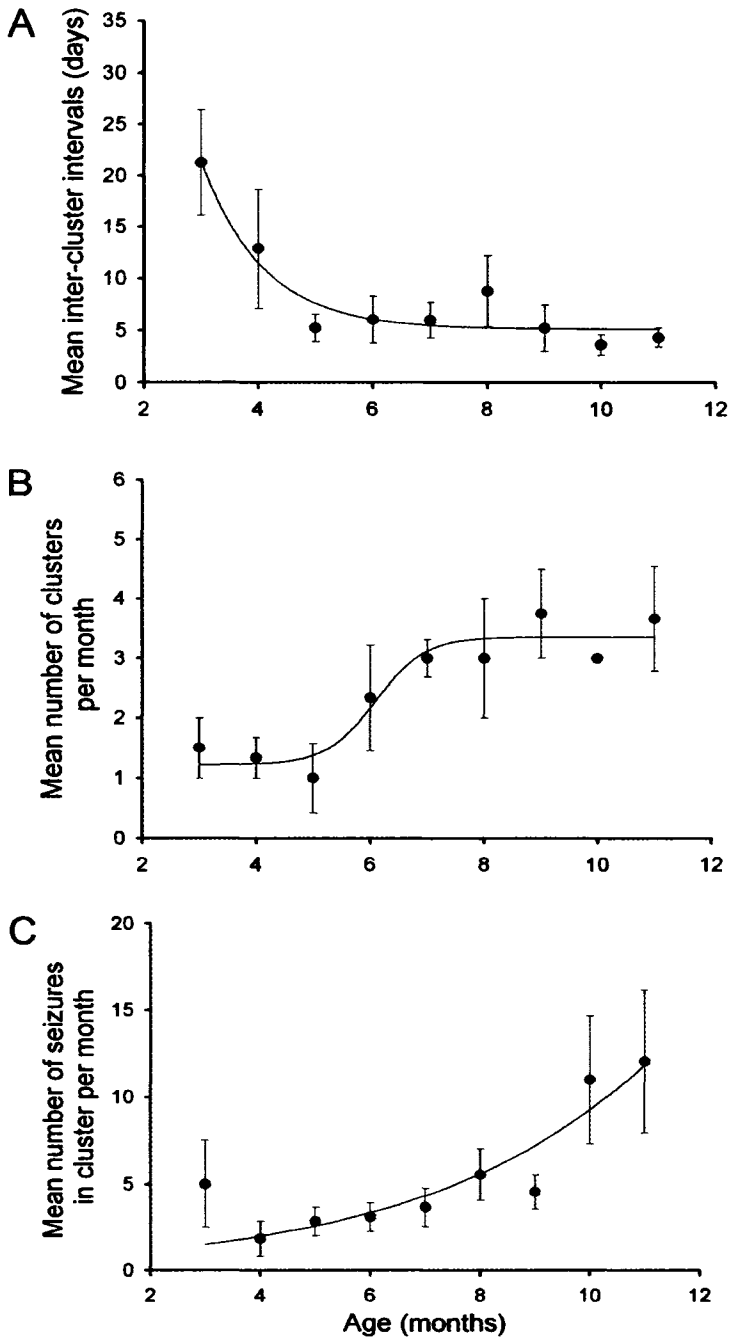

Fig. 5.8 Seizure clusters as a function of time after HI. A. Inter-cluster intervals plotted as a function time showed sharp decrease in the time period between the 1st and 3rd month of monitoring (age 2 to 5 months), after which the inter-cluster interval remained relatively stable with a steady state value of 5.11 ± 1.36 days for the best fit exponential decay curve, B. Mean number of clusters plotted against time a sigmoid curve with half maximal increase at 6.1 ± 0.49 months of age, C. Mean number of seizures within in a cluster normalized to cluster frequency plotted as a function of time also showed a progressive increase that was best fit by the exponential growth phase of a sigmoid curve.

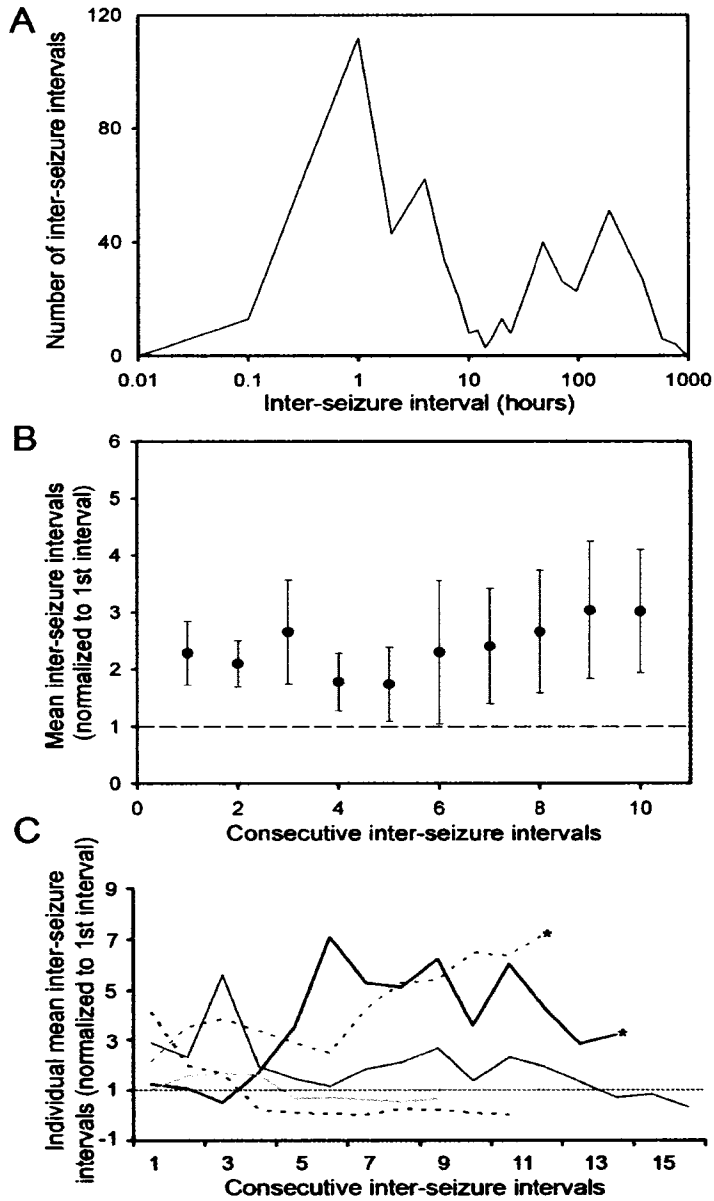

Figure 5.9 Inter-seizure intervals. A. Inter-seizure intervals for every epileptic rat plotted as a function of interval durations on the log scale to better visualize the variability that ranged from a few minutes to a few weeks. Plot shows two prominent groups in the distribution: 1) shorter intervals between seizures within clusters and 2) longer intervals between clusters (i.e. last seizure in first cluster and first seizure in second cluster) B. Inter-seizure intervals for seizures within a cluster were analyzed for all clusters (inter-seizure interval $\leq$ 24 h) with at least 4 seizures so that there were three inter-seizure intervals and the 2^{nd} and 3^{rd} interval could be normalized to the 1st interval to nullify the variability of the duration of the 1st inter-seizure intervals between animals and between clusters and a trend could be discerned. This analysis was conducted in 5 HI-treated epileptic rats such that they each had at least a one cluster with $\geq$4 seizures. Data averaged between animals did not show any specific trends between consecutive inter-

seizure intervals C. Individual trends for the HI-epileptic rats showed variability with 3 rats having a reduction in their inter-seizure intervals over increasing consecutive intervals and 2 rats showed the exact opposite trend (asterisk).

inter-cluster intervals as a function of time (Fig. 5.8, A) associated with gradual increase in the number of clusters occurring per month (Fig. 5.8, B). The exponential growth phase of the increase in seizure frequency over time was a result of an exponential growth in the number of seizures within clusters as a function of time (Fig. 5.8, C). When testing for non-randomness of the entire group of ictal events detected in this study (556), every interictal interval was plotted on a log scale to accommodate variability that ranged from a few minutes to a few weeks. The frequency distribution was not only non-random but showed two possible Gaussian distributions for the entire data. The first peak represented the ictal events within clusters while the second peak represented inter-cluster intervals (Fig. 5.9, A). Inter-seizure intervals for seizures occurring within a cluster showed variable trends for the different epileptic animals in this study. Thus the overall mean, statistically did not show either an increasing or decreasing progression of inter-seizure intervals within a cluster (Fig. 5.9, B). Closer inspection showed that this was due to individual rats showing trends that were exact opposites of each other (Fig. 5.9, C). Two rats showed a clear pattern within their clusters such that the cluster onset was heralded by a flurry of seizures occurring in rapid succession followed by gradual waning of their seizure frequency. Three rats showed the opposite format wherein the seizures had larger inter-seizure intervals to begin with that reduced over the increasing size of a cluster with an abrupt termination. The epileptic rats that were excluded from the above analysis (n=5) were from the 2 month old group that had a lower individual

seizure rate, showed clustering that that fewer than 4 seizures within such episodes therefore a definite trend could not be ascertained.

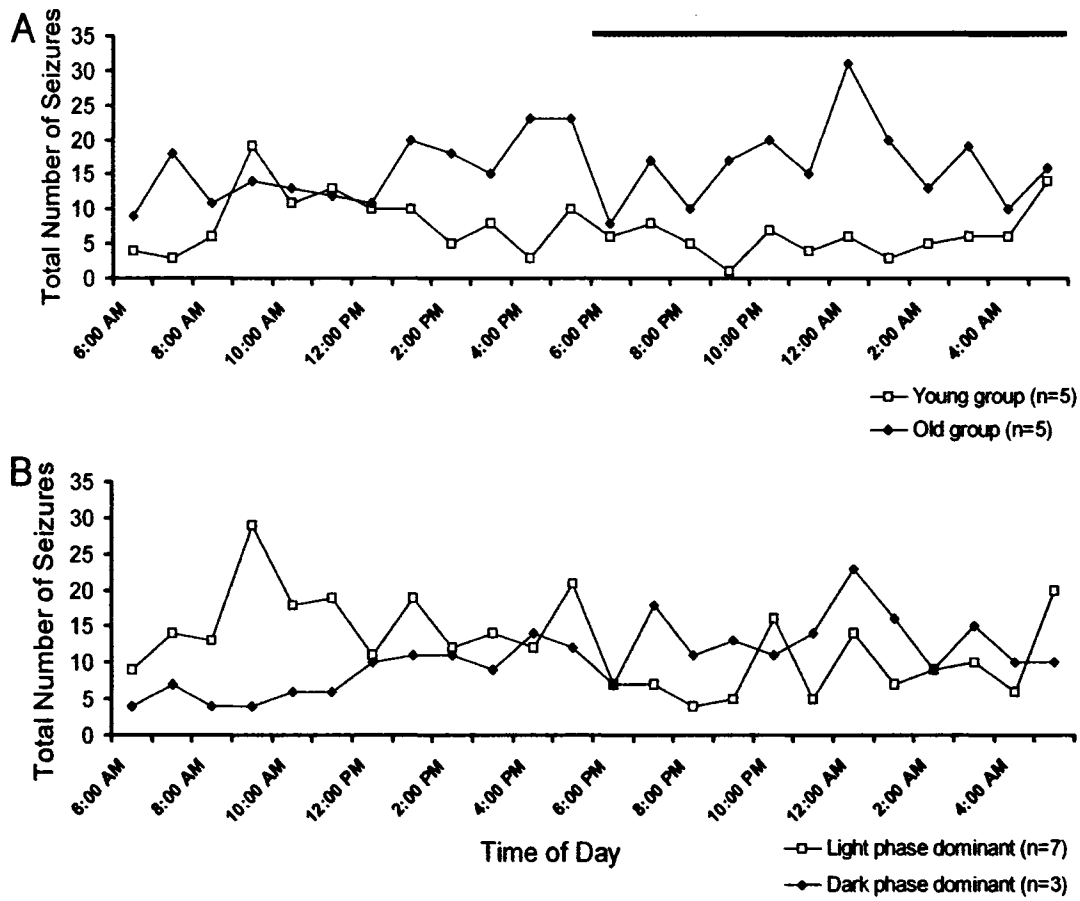

Fig. 5.10 Diurnal distribution of ictal events. A. Distribution of ictal events for the two groups (young and old) over the 24 h light/dark phase. The older group showed a peak at midnight whereas the younger group showed a peak at 9 am. Pair wise T test failed to show significance for overall light vs. dark phase variation for both groups separately and combined. Notice the overall lower seizure counts for the younger age group compared to the older; B. When the data was differentially analyzed by grouping rats with light or dark phase preponderance of ictal events irrespective of age group, 7 (4 young, 3 old) out of 10 rats were found to have light phase preponderance. Statistical significance was found for diurnal variation in this group for individual pair wise comparisons for light and dark phase variations of ictal events (P=0.005). A similar comparison for the dark cycle preponderant group did not show significance (P> 0.05).

5.7 Diurnal seizure variation

24 h monitoring yielded specific times for ictal events that were first detected on the EEG and then confirmed and graded with the synchronous video-monitoring tapes. The diurnal distribution of ictal events was assessed in the HI-treated epileptic rats (Fig. 5.10). Statistical analysis of number of light cycle and dark cycle seizures for 10 epileptic rats did not show significant diurnal variation for the entire group ($P>0.05$). When the group was split into rats implanted at 2 months age (n=5) and rats implanted at 6 months (n=5) the line graphs depicting their diurnal distributions showed maximum peaks at 9 am and 12 am for the young and older rats respectively (Fig. 5.10, A). No significance was found for either group for light/dark phase seizure frequencies ($P>0.05$). When individual rats were grouped according to light phase or dark phase dominance (i.e. preponderance to seize in the light or dark phase), 7 out of the 10 rats were found to have light cycle dominance (Fig. 5.10, B) in their diurnal variations which was also statistically significant ($P= 0.005$) as opposed to the dark cycle dominant group (n=3) which was not statistically significant ($P>0.05$).

5.8 Reflex seizures

Two out the 5 HI-treated epileptic rats from the young group (implanted at 2 months) were detected to have initial reflex seizures as their 1st generalized behavioral seizures. These were seizures which occurred only and right after being handled for a cage change. First one of these rats later went on to have one spontaneous generalized seizure followed by more reflex seizures but the second one progressed to develop spontaneous seizures unrelated to handling with no further reflex seizures. These reflex

seizures did not occur with every cage change (alternate weekdays). We are unable to pinpoint whether the reflex seizures were due to a startle or tactile stimulus with the handling by the animal care personnel.

5.9 7-12 Hz spike wave discharges (SWD) in 2 HI-treated rats associated with freeze posturing.

Two rats (female littermates) from the young group (implanted at 2 months) that were grouped with the HI-treated non-epileptic rats developed episodes of 7-12 Hz SWD detected on all three leads (Fig. 5.11, A). Behaviorally these were associated with freeze posturing and twitching of vibrissae. Over time the frequency of these episodes grew in number for one rat and for the other they remained random occurrences. For the rat that they increased in frequency, they were detected predominantly during the dark phase of diurnal cycle (Fig. 5.11, B). These episodes usually were clusters of short (few seconds) episodes (Fig. 5.11, C). Histologically the animals did not have an ipsilateral infarct or distinct hypoxia related cortical or sub-cortical lesions. The rats did not have a single ictal event throughout the period they were monitored. The study also implanted 3 other litter mates (1 HI-treated and 2 controls) and similar episodes were not recorded in any of them. Electrographically these episodes always remained the 7-12 SWD format (Wiest and Nicolelis, 2003). Considering both rats were litter mates and showed no infarcts this finding may be strain related (Kelly, 2005).

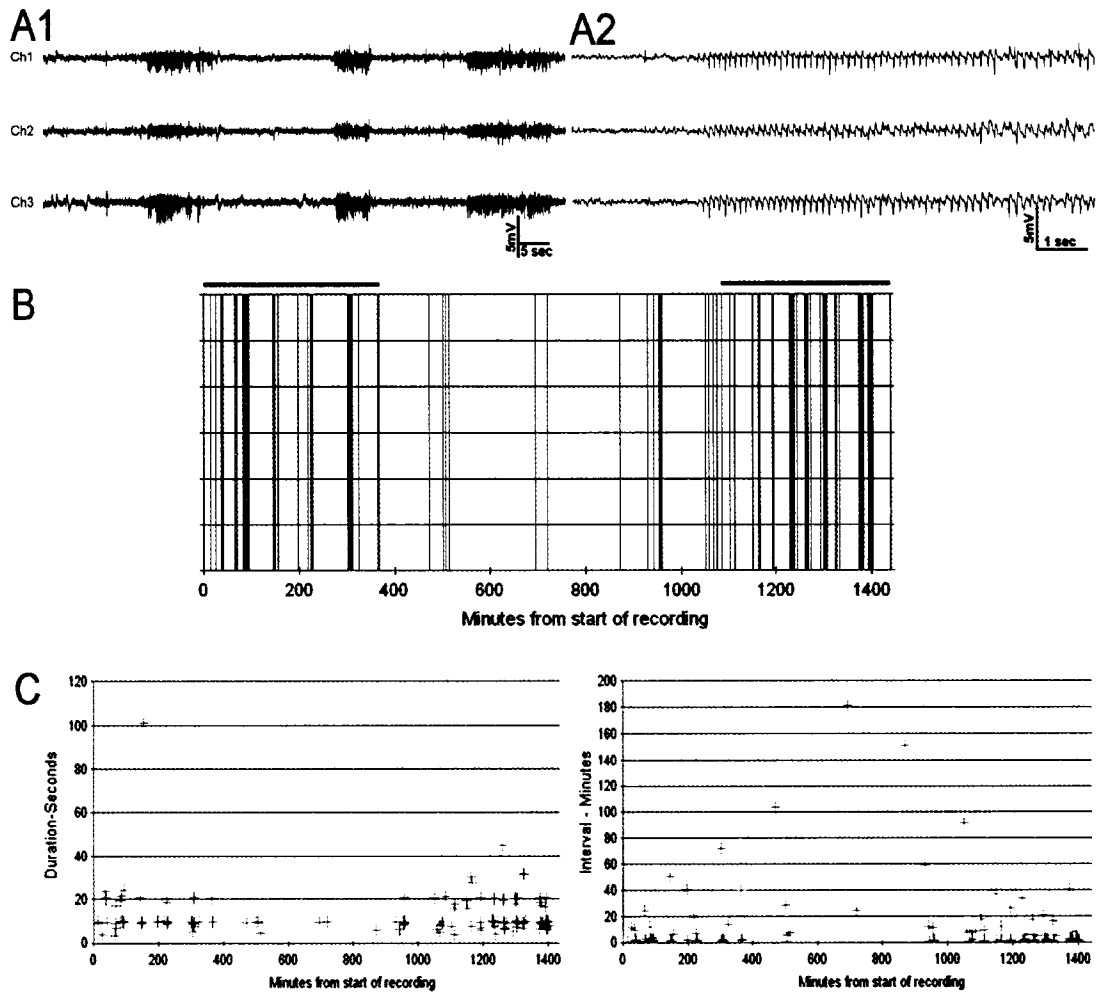

Fig. 5.11 7-12 Hz spike-wave discharges (SWDs) in 2 HI-treated non-lesioned rats associated with freeze posturing. A. EEG trace that shows multiple short episodes of 7-12 Hz spike-wake discharges distinct in amplitude from base line in a HI-treated rat that was associated with freeze posturing. B. same trace at slower time scale shows the 7-12 Hz SWDs seen in all three leads simultaneously. C. Sample diurnal distribution of these multiple events that showed a predominantly nocturnal occurrence over the 1440 minutes (24h) of EEG recording starting at midnight. Black bars represent the dark phase. D. These events were all of short durations (10-20 seconds). On the EEG they presented as clusters with short inter-event intervals (few sec) that the automated detection program reported as a single event. The total time involving such discharges for this 24 h file was ~31 minutes. It was not possible to discern from the in-sync video whether the animal had altered behavior for the intervening few seconds assuming the freeze behavior represents any kind of altered epileptiform syndrome (see discussion). E. Inter-cluster intervals during the dark phase were variable lasting from two to tens of minutes during the dark phase.

5.10 Histological findings

Every rat that was implanted in this study was euthanized after they were taken off the telemetry system and the brains fixed and stained with cresyl violet and Timm stain. All the HI-treated rats that were detected to be epileptic by this protocol also had cystic HI lesions in their ipsilateral hemispheres. Therefore there was a positive correlation between occurrence of infarction and the genesis of epilepsy. We have previously reported the neuropathology related to HI-epileptic rats (Kadam et al., 2003).

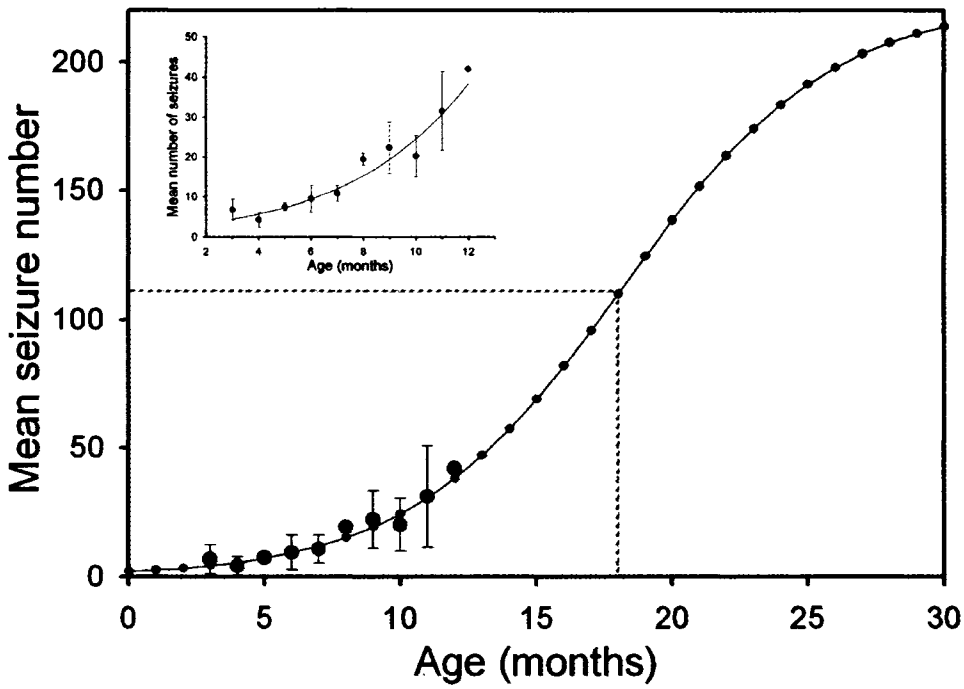

Fig. 5.12 Predictions of seizure progression with chronic telemetry protocol. Seizure progression over extended period of time using predictive coordinates (green) by using parameters obtained from the equation of the best fit sigmoid curve predict a half maximal seizure rate of ~111.5 seizures per month at the age of 18 months for HI-treated epileptic rats in this study. The estimated maximal seizure rate was ~223 seizures per month.

5.11 Predictions for seizure progression

The time-dependant increase in seizure frequency detected in this study shows the P7 HI insult resultant injury to be progressive in nature. This progression also relates to the seizure severity as most of the partial seizures (P1-3) were detected in the first months of monitoring. This onset was detected with an apparent latency of 68 days. Clustering of seizures was a predominant feature of the resultant epilepsy. The increase in the episodes of such clusters and the increase in seizure numbers within each consequent cluster within the period of monitoring (1 yr) contributed to the data fitting the exponential growth phase of a sigmoid curve. The equation for the best fit sigmoid curve predicted a half maximal seizure rate of ~111.5 seizures/month at 18 months of age (Fig. 5.12)

CHAPTER 6

IN VITRO NEOCORTICAL STUDIES IN A RAT MODEL OF PERINATAL HYPOXIA-ISCHEMIA WITH SPONTANEOUS CONVULSIVE SEIZURES

Cortical lesions like acquired dysplasias and infarcts have a strong association with intractable epilepsy in humans. Little is known about the physiologic abnormalities that are present in these conditions. Acquired cortical dysplasias are often associated with focal perfusion failures in the immature brain. When postnatal day 7 Sprague Dawley rats were exposed to unilateral carotid ligation followed by a 2h exposure to hypoxia with 8% oxygen they suffered ipsilateral infarcts in the parasagittal neocortex that extends into middle cerebral artery perfusion territories in severe forms (chapter 4). Importantly they developed a progressive form of epilepsy with the presence of multiple forms of cortical dysplasias in the spared ipsilateral neocortex and over time in the contralateral mirror foci. These dysplasias include columnar neuronal death with cytomegaly in isolated groups of dysmorphic neurons. Cortical dysgenesis in the forms of deep laminar gliosis, microgyri, white matter hypercellularity, and blurring of the white and grey matter junction. In vitro brain slices from resected brain tissues with similar cortical dysplasias have been shown to be capable of epileptiform activity in the presence of chemo-convulsant 4-aminopyridine (Avoli et al., 1999; Mattia et al., 1995). It has been

shown that strong disinhibition in the neocortex of normal rats show all-or-none epileptiform extracellular field potentials that represent network bursts (Chervin et al., 1988). Such network bursts have been demonstrated as representative of focal epileptogenesis in the freeze-lesion induced dysplastic cortex of rodents (Jacobs et al., 1996; Peters et al., 2004). In photochemically-induced infarctions, significant reduction in paired-pulse inhibition has been demonstrated in para-lesion neocortices that represent the post-infarct alteration in electrophysiological properties (Domann et al., 1993). The current study was performed to examine if in vitro brain slices from perinatally induced HI infarcts revealed epileptiform activity in the spared ipsi- and contra-lateral somatosensory cortices. Cortical spontaneous and evoked field potentials were recorded in two groups of HI-treated rats: one was at an acute time point (i.e., a couple of weeks after the insult) and the other was months after (i.e., $\geq$6 months) the initial perinatal HI. Activity was recorded in normal medium and after near complete antagonism of the $GABA_A$ receptor by high dose bicuculline methiodide (BMI).

6.1 Experimental design and data presentation

All experiments were carried out on Sprague-Dawley rats in accordance with protocols approved by Colorado State University and the University of Utah School of Medicine animal research review boards. In vitro brain slices were obtained from 34 HI-treated and 19 control rats at the two time points. Experimental animals came from 9 litters and both male and female rats were used. We opted to randomly select animals for ligation and the sham-control procedure at age 7 days because determination of the sex of rats is unreliable at that age. The rats were later used for in vitro slice experiments at $\leq$1

month and ≥6 months of age when the sex was easily determined. Out of the total 53 rats used for this in vitro study, there were 20 male and 33 female rats.

HI insult at postnatal day 7, produced lesions at the opposite ends of the spectrum i.e. there was either a distinct ipsilateral infarct lesion or no visibly discernable lesion. This phenomenon has been reported previously for this model. It most probably results due to insufficient drop in perfusion pressure during hypoxia due to a sufficiently patent carotid. This was further verified by the EFPs recorded from HI non-cystic brain tissue in the adult group of rats which did not show spontaneous or evoked epileptiform bursts and were thus similar to slices from control brains. We have further evidence of the lack of epileptiform plasticity in the somatosensory cortices of HI-treated rats with no discernable infarcts from another study conducted in two age groups (at 2 months and 6 months after the postnatal 7 HI-insult) done with chronic and continuous recording of cortical electroencephalograms using telemetry. The HI-treated rats that were implanted and their brains later histologically processed to show absence of a HI-related infarct did not have a single electrographic seizure, but every HI-treated rat that had a cystic infarct developed spontaneous recurrent seizures. For analysis of EFPs from the adult group the HI-treated rats were classified as HI-cystic and HI non-cystic respectively. Slices from HI-cystic rat brains showed similar properties for evoked field potentials ipsi- and contralaterally after analysis; therefore they were grouped together for data presentation. From the acute group of rats HI non-cystic data are not presented because the data from the long-term group was not statistically different from control in their demonstrable epileptiform activity therefore we did not expect the acute group would be any different from control either. On the other hand there was a marked difference in EFPs from the

ipsi- and contralateral somatosensory cortices and therefore they have been analyzed and presented separately. In summary the older rat group data are presented as comparisons between EFPs in three groups, namely HI-treated rats with cystic infarcts (HI-cystic), HI-treated rats with no discernable infarct (HI non-cystic) and control; whereas the young rat group data are presented as comparisons between EFPs recorded from HI-treated rats with a cystic infarct: 1) in the ipsilateral somatosensory cortex (HI cystic ipsi); 2) in the contralateral cortex (HI cystic contra) and in control.

6.2 In vitro evoked field potentials in adult (≥ 6 month old) rats.

The older group of rats was the first to undergo the in vitro slice experiments because the chronic cortical encephalographic study had shown that the progressive epilepsy that develops in these rats has a seizure frequency rate that reaches the exponential growth phase of a sigmoid curve at the age of 6 months. We hypothesized that the post-infarct plasticity of the immature brain was responsible for the epileptogenesis therefore, considering the very low seizure rate we recorded at 2 months in the EEG study we chose to start the in vitro studies for the acute stage at postnatal day 21, where we expected the adaptive plasticity of sensorimotor cortex after the perinatal HI-insult to be in its initial phases compared to the 6 month time point. Some consideration was given to the idea of starting the study of EFP among the acute group at an earlier stage after the postnatal day 7 insults. We decided against it to avoid the developmental window period of the first 2 postnatal weeks wherein massive physiological changes in the properties of the inhibitory circuits have been shown to occur which we thought would make the acute data set less comparable to the data from

the older group of HI-treated rats (Dzhala et al., 2005). In normal medium all-or-none long-and-variable latency EFPs were recorded in HI-cystic slices both ipsi- and contralaterally (Fig. 6.2, B1 and C1) compared to graded responses in control slices to increasing stimulus intensities (Fig. 6.2, A1). When normalized to threshold responses, the all-or-none response trend for the HI-cystic brains in normal medium became evident for amplitude, duration and overall areas of the EFPs (Fig. 6.3, A, B and C). Mean peak amplitude of EFPs for HI cystic brains in normal medium was 1.584 ±0.03 mV and significantly higher compared to 0.722±0.09 and 0.829±0.08 mV for control and HI non-cystic rats respectively (Fig. 6.4, A; P=0.009 in both cases). In all preparations from HI

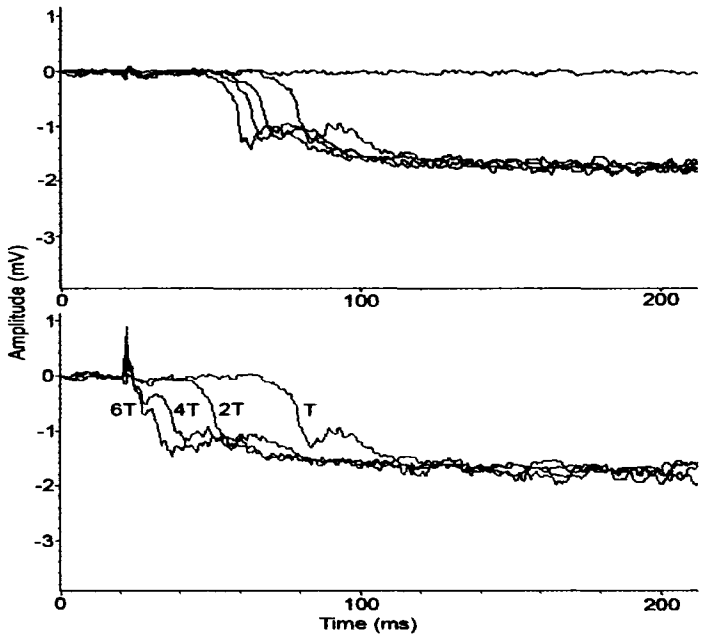

Fig. 6.1 Representative traces of EFPs at threshold (top traces) and increasing stimulus intensities (bottom traces) in ipsilateral somatosensory cortex. Top traces show long-variable latency all-or-none EFPs recorded at threshold in the ipsilateral somatosensory cortex of a HI-treated rat with a cystic infarct. Bottom traces show that standard increments in threshold stimulus (T) intensities reduced latency of EFP onset as seen here with the 4 traces at T, 2T, 4T and 6T.

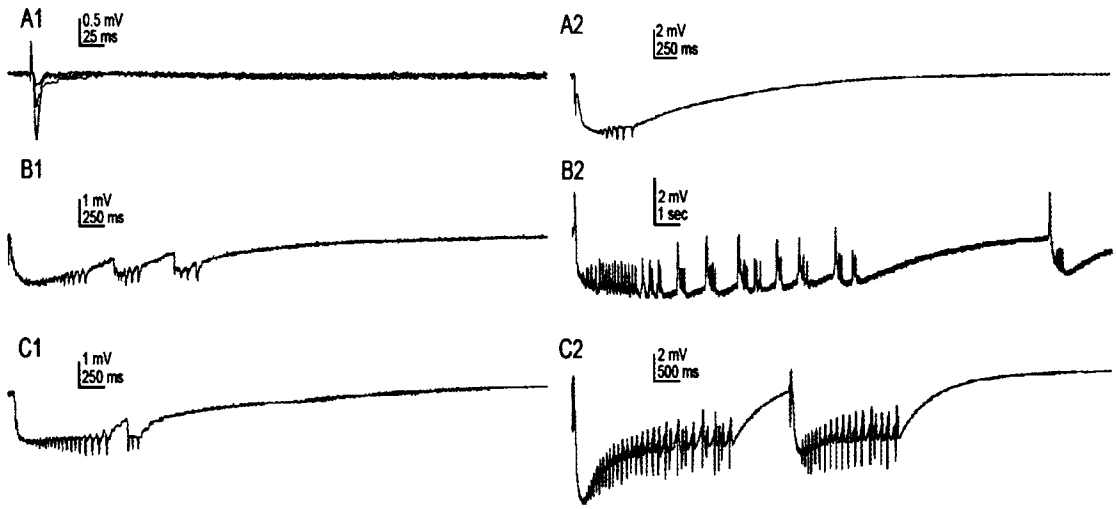

Fig. 6.2 EFPs recorded in layer II/III of sensorimotor cortex by stimulation at the layer VI/white matter junction of adult (>6 months old) control and HI-treated rats in normal medium (left column) and 30μM BMI (right column). A1. Graded responses to increments of threshold (200μsec duration at 0.1 Hz) stimuli (1X, 2X, 4X and 6X) in normal medium and all-or-none threshold response in 30μM BMI (A2) in control slices. B1. All-or-none prolonged spiking responses at threshold in normal medium and complex/variable responses in BMI (B2) from ipsilateral spared somatosensory cortex of HI-treated rats with cystic infarcts. C1. All-or-none prolonged spiking responses at threshold in normal medium and complex/variable responses in BMI (C2) from contra-lateral somatosensory cortex of HI-treated rats with cystic infarcts.

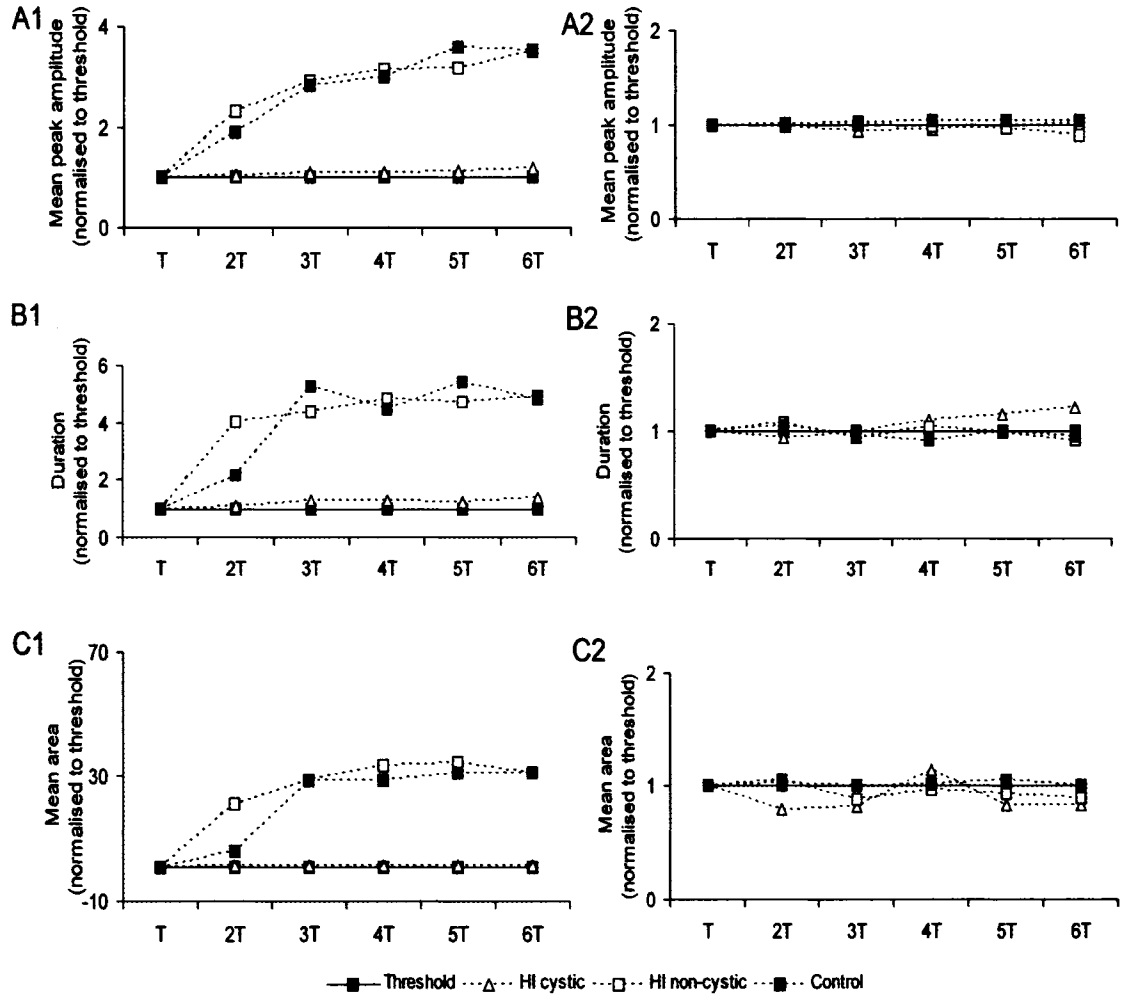

Fig 6.3 Mean parameters of EFPs at standard increments (1 to 6 times) of threshold stimulus intensity (T) normalized to threshold in adult (≥6 month) rats in normal medium (left column) and 30μM BMI (right column). A1. Mean amplitudes revealed the all-or-none peak response of the HI-cystic somatosensory EFP (ipsi- and contralateral) at threshold compared to the graded responses of both control and HI-treated non-lesioned (non-cystic) brain slices with increasing stimulus intensities. Similar findings were seen for both parameters of EFP duration (B1) and areas (C1) respectively, for the three groups of rats. After blocking $GABA_A$ receptor mediated inhibition with 30μM BMI all the above mentioned parameters became all-or-none responses as seen in A2, B2 and C2 respectively.

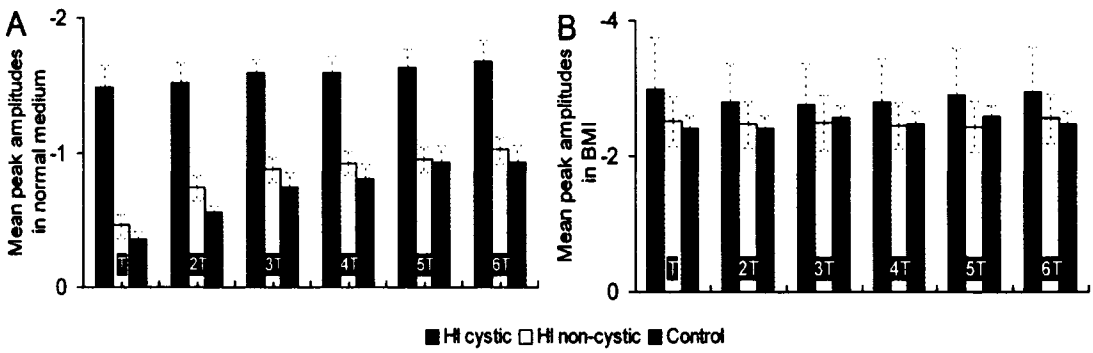

Fig. 6.4 Histograms comparing mean peak amplitudes (mV) of EFPs at increasing standard increments of stimulus intensity in adult rats (≥6 month) compared between slices with an obvious infarct related cystic lesion, slices with no discernable infarct lesion and controls in normal medium (left) and 30μM BMI (right). The HI-cystic slices demonstrated large amplitude all-or-none EFPs in normal medium (A) bilaterally in significant contrast to the smaller amplitude graded responses seen in HI non-cystic and control brains. In BMI responses in all three groups became all-or-none and comparable in amplitudes.

rats with a visible infarcts, EFPs in ipsi- and contralateral somatosensory cortices at threshold lasted much longer (i.e., seconds) compared to the tens of milliseconds in the control slices. Overall average amplitudes and durations (Fig. 6.5, A and B respectively) of HI-cystic EFPs were significantly larger than both control and HI non-cystic averages. Average areas (Fig. 6.5, C) of the negatively going field potential traces were significantly different for HI-cystic rats compared to both control and HI non-cystic rats (i.e., P= 0.00001 in both cases) whereas HI non-cystic EFP areas as stated earlier were not significantly different from control (P= 0.45). When $GABA_A$ receptor mediated inhibition was blocked all-or-none long-and-variable latency EFPs were recorded in all three groups with larger amplitudes compared to those seen in normal medium (fig 6.4, A) but now became comparable between three groups and were not significantly different form each other anymore (HI-cystic vs. Control and HI-cystic vs. HI non-cystic; P= 0.09 and HI non-cystic vs. control, P= 0.07). They were however significantly different in the

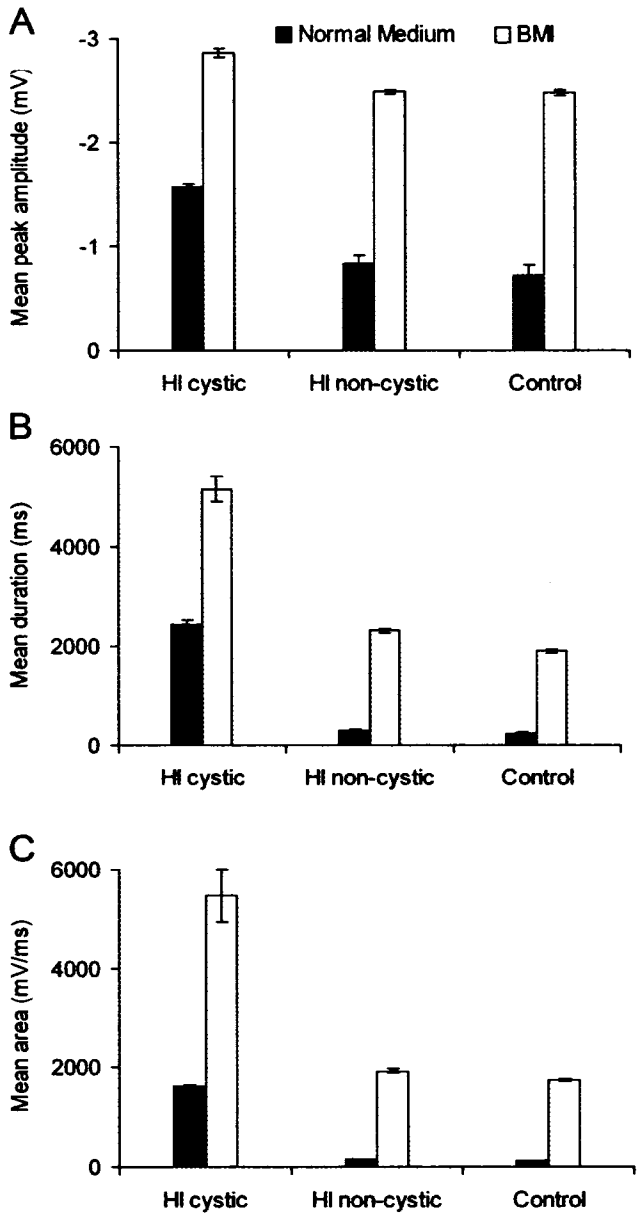

Fig. 6.5 Histograms comparing the mean values of parameters for EFPs (amplitude, duration and area) averaged over all stimulus intensities (T to 6T) from adult rats (≥6 month) in normal medium and 30μM BMI. Although amplitudes of EFP responses lost their significance for differences in BMI medium (A) for amplitude as described in detail in Fig. 5, significance for duration and therefore areas of EFPs that was seen in normal medium persisted after BMI application for HI-cystic slices compared to HI non-cystic and control slices that remained similar for both parameters in both mediums.

kind of multiphasic epileptiform events lasting ~7 or 8 seconds that were recorded only in slices from HI-cystic brains both ipsi- and contralaterally (Fig. 6.1, A2, B2 and C2). The epileptiform events seen in HI-cystic slices were more complex, asynchronous and less stereotypical with increasing stimulus intensities and within the multiple traces recorded per stimulus intensity compared to similar paradigms used in a control and HI non-cystic slices treated with 30 μm BMI. The average areas of these responses therefore was statistically different from both control and HI non-cystic brains (P= 0.00003 for both) whereas HI non-cystic responses were not significantly different from control (P= 0.08). Average threshold stimulus intensities for HI-cystic slices were lower than those required for both control and HI non-cystic slices but significantly different only from control (P=0.007). Average threshold stimulus intensities for HI non-cystic brains were lower than control but with a smaller significance (P= 0.01). With increasing stimulus intensities, the onset latencies of these epileptiform events shortened (Fig. 6.1, B and 6.10, A). Latency for the EFP was defined as delay between the time of applied threshold stimulus and the time of the wave onset. The mean for the long-latency EFPs recorded from HI-cystic brains in normal medium was 31.4 ± 5.8 ms and significantly different from both control and HI non-cystic brains (11.3 ± 2.5ms and 11.7 ± 3.4ms respectively, P=0.001 for both). HI-cystic preparations with no visible cystic/gliotic lesion had latencies similar to control slices. With increasing stimulus intensities the onset latencies shortened in both groups with the maximum shortening seen between threshold (T) and 2 times threshold (2T) for all groups (Fig. 6.11, A). In presence of BMI latencies shortened for HI-cystic and became longer in both control and HI non-cystic slices (Fig. 6.11, A).

6.3 In vitro evoked field potentials in young (P21-P32) rats.

In normal medium EFPs in both ipsi- and contralateral somatosensory cortices of HI-cystic rats were graded and thus similar to control (Fig. 6.6, A1, B1 and C1). When normalized to threshold stimulus amplitudes from ipsilateral HI-cystic although not all-or-none as observed in the older group of rats, were the least graded (Fig. 6.7, A; open triangles) compared to the other two groups of data. Their durations increased

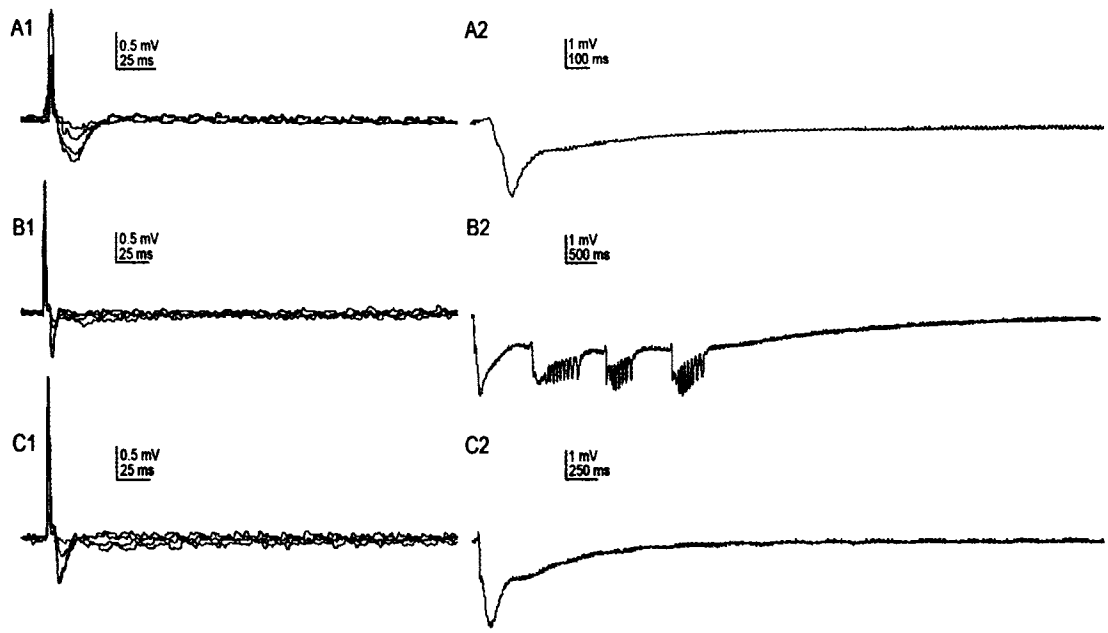

Fig. 6.6 EFPs recorded in layer II/III of sensorimotor cortex by stimulation at the layer VI/white matter junction of young (P21-P32) control and HI-treated rats in normal medium (left column) and 30μM BMI (right column). A1. Graded responses to standard increments of threshold (200μsec duration at 0.1 Hz) stimuli (1X, 2X, 4X and 6X) in normal medium and all-or-none threshold response in 30μM BMI (A2) in control rat slices. B1. Graded responses in normal medium and all-or-none complex/variable latency epileptiform responses in BMI (B2) from ipsilateral somatosensory cortex of HI-treated rats with cystic infarcts. C1. Graded responses in normal medium and all-or-none responses in BMI (C2) from contralateral somatosensory cortex of HI-treated rats with cystic infarcts were similar to control.

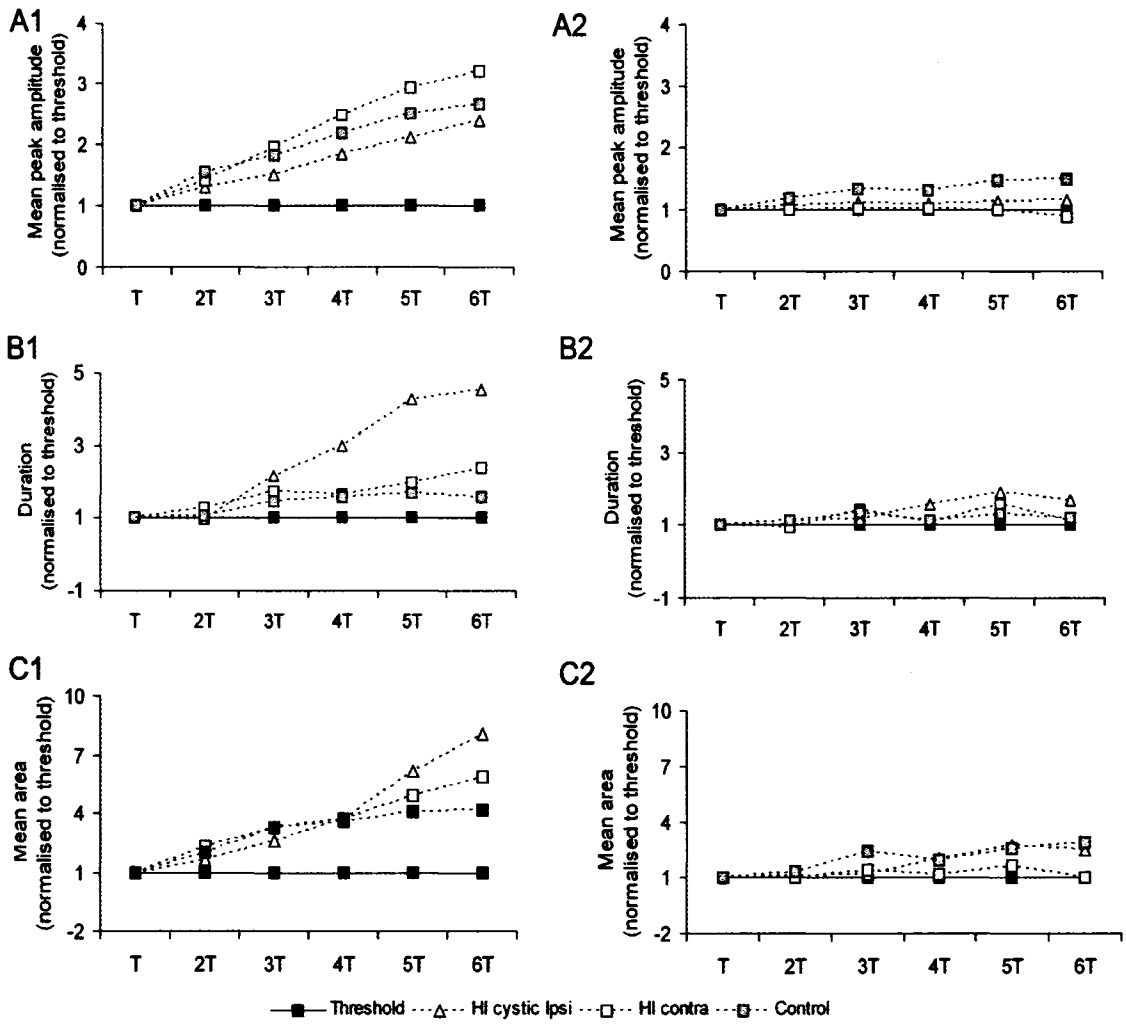

Fig. 6.7 Mean parameters of EFPs at standard increments (1 to 6 times) of threshold stimulus intensity (T) normalized to threshold in young (P21-P32) rats in normal medium (left column) and 30μM BMI (right column). A1. Mean amplitudes revealed graded responses of the HI-cystic somatosensory EFP (ipsi- and contralateral) at threshold similar to the graded responses of control brain slices with increasing stimulus intensities. Similar findings were seen for both parameters of EFP duration (B1) and areas (C1) respectively, for the three groups of rats. After blocking $GABA_A$ receptor mediated inhibition with 30μM BMI all the above mentioned parameters became all-or-none responses as seen in A2, B2 and C2 respectively.

substantially from normalized levels beginning at 4 times threshold (4T) that separated those responses from trends observed in control and HI cystic contralateral responses.

Overall EFPs from ipsilateral HI-cystic somatosensory cortices distinguished themselves from those evoked in the contralateral hemisphere and control by being marginally larger in average amplitude (Fig. 6.8, A; HI cystic ipsi vs. control, P= 0.01; HI cystic ipsi vs. HI cystic contra, P= 0.02) and durations, therefore average areas (Fig. 6.9, A, B and C) but still remained graded to increasing stimulus intensities. Areas of the EFPs from HI-cystic ipsilateral cortices, averaged over the responses from T to 6T was 27.8 ± 7.9 mV/ms and significantly different from similarly averaged control and HI-cystic contralateral responses (P= 0.02 for both; Fig. 6.9, C). When $GABA_A$ receptor mediated inhibition was blocked responses in all three groups analyzed became all-or-none (Fig. 6.7) but only the ipsilateral HI-cystic cortex elicited multiphasic epileptiform events (Fig.6.6, A2, B2 and

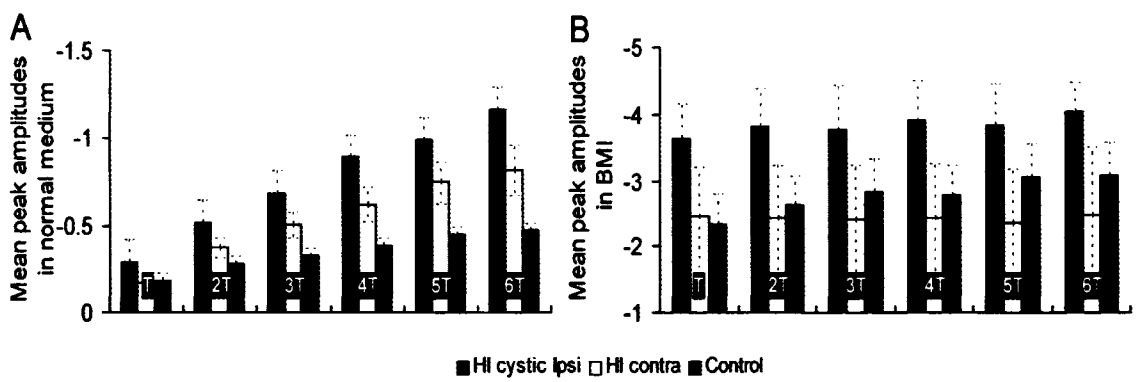

Fig. 6.8 Histograms comparing mean peak amplitudes (mV) of EFPs at increasing standard increments of stimulus intensity in young rats (P21-P32) between ipsilateral somatosensory cortex of slices with an cystic parasagittal infarct, contra-lateral somatosensory cortex of the same brains and controls in normal medium (left) and 30μM BMI (right). Responses in all three groups of EFPs remained graded (A) but HI cystic responses were still significantly larger in amplitude compared to the contralateral responses that were not significantly different from control (P=0.149). In BMI all three responses became all-or-none in their amplitudes with increasing stimulus intensities but HI cystic responses ipsilaterally still remained significantly different from both contralateral and control amplitudes.

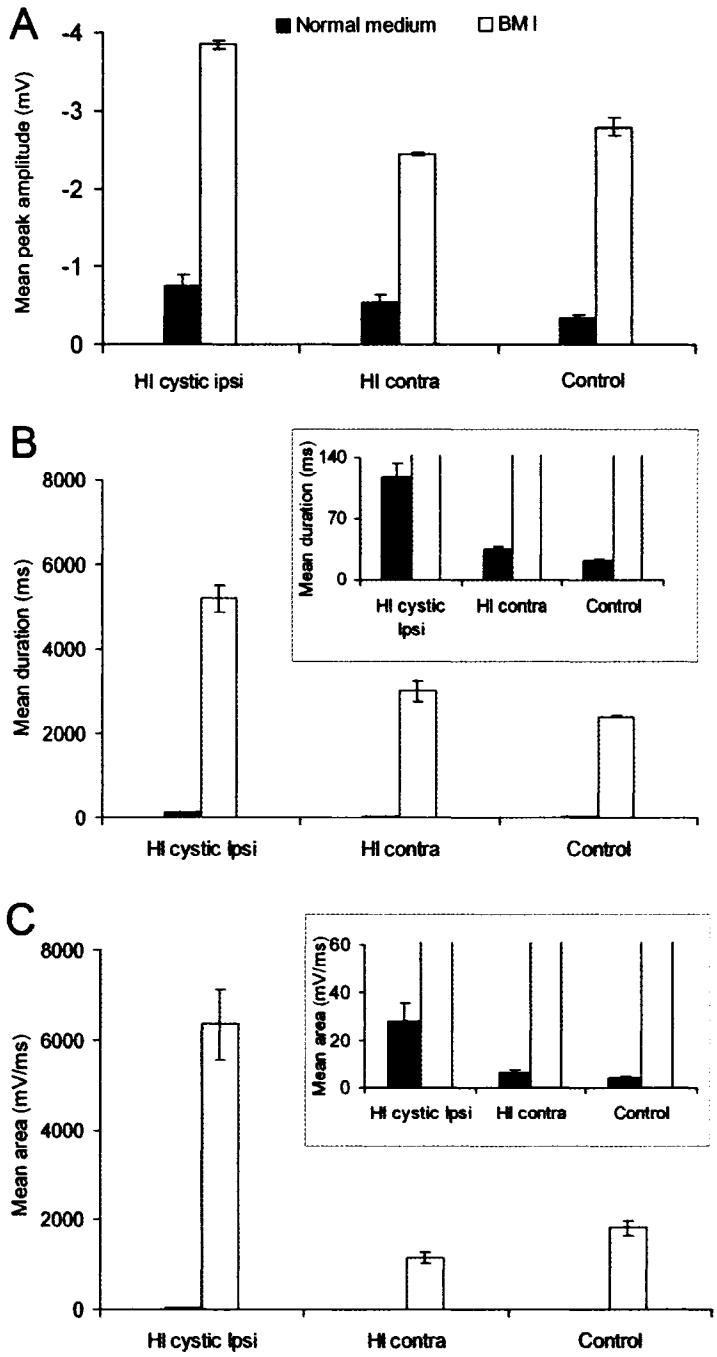

Fig 6.9 Histograms comparing the mean values of parameters for EFPs (amplitude, duration and area) averaged over all stimulus intensities (T to 6T) from young rats (P21-P32) in normal medium and 30μM BMI. Amplitudes (A), duration (B) and overall areas (C) of EFPs in HI cystic slices from ipsi-lateral spared somatosensory cortices were significantly different from both the contralateral hemisphere and control, both in normal and BMI medium.

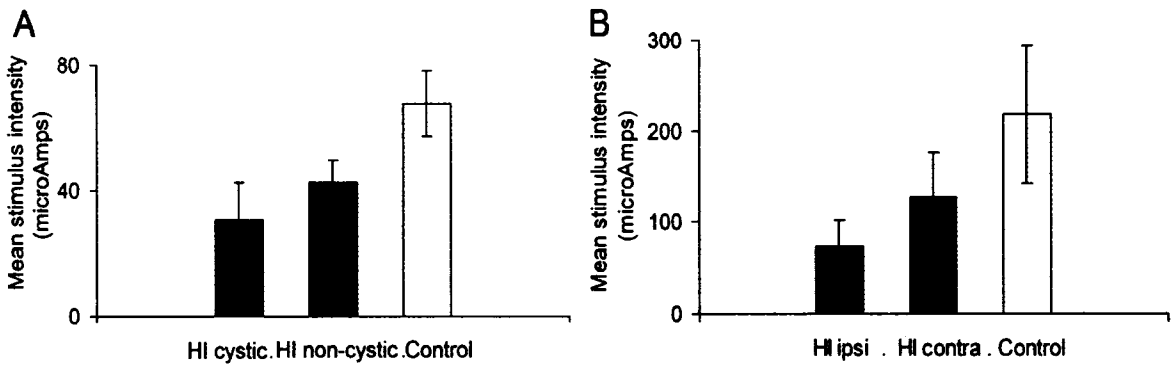

Fig. 6.10 Average threshold stimulus intensities (μAmps) required to generate a minimum 0.3 ± 0.04 mV evoked field potential in control slices or the all-or-none responses recorded in slices from HI-treated rats in normal medium. Overall average threshold stimulus intensities required to evoke responses in the older group of rats (A) were smaller compared to those required in the younger group of rats (B). This difference may reflect the developmental differences in overall superficial grey matter myelination and synaptogenesis at those two time points. But in both groups average stimulus intensities required at threshold were smallest in HI-cystic brains and always significantly different form control.

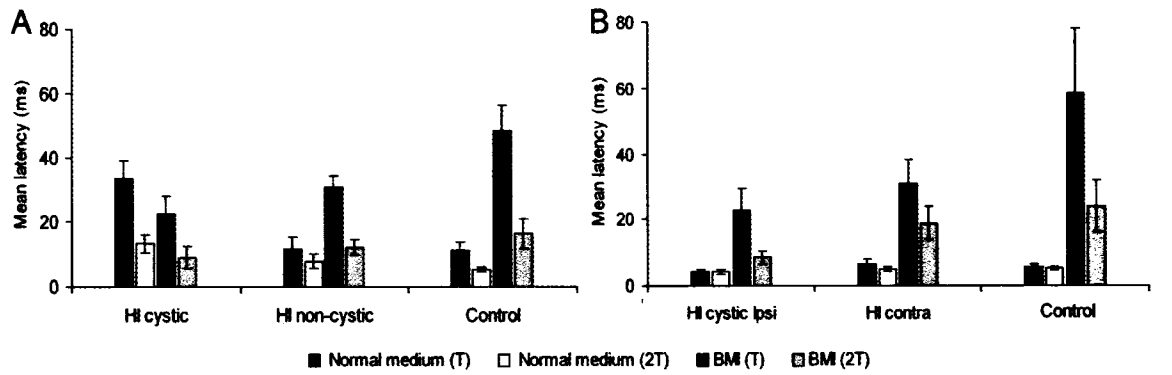

Fig. 6.11 Histogram of latency to EFP wave onset evoked at threshold (T) or twice-threshold (2T) stimuli in normal medium and in 30 μM BMI for adult rats (≥6 month) in left panel and young rats (P21-P32) in right panel. Long-latency EFP responses seen in HI-cystic brains in the older group of rats (A) may indicate network responses with a dominant excitatory transmission compared to both HI non-cystic and control responses. After disinhibition both control and HI non-cystic responses had long-latencies indicating conversion of the focal response in normal medium to a network response after blocking $GABA_A$ receptor mediated inhibition. In contrast the younger group of rats all had comparatively shorter latencies (B) compared to the older group probably indicating focal responses along with age specific weaker synaptogenesis and myelination.

C2) in sharp contrast to the epileptiform evoked discharges recorded in the bilateral somatosensory cortices of the adult group of rats (Fig. 6.2, B2 and C2). In BMI amplitudes of EFPs increased for all three groups with a large variability but HI-cystic ipsilateral EFP amplitudes still remained significantly larger than contralateral and control responses ($P< 0.0005$) and although contralateral responses were slightly smaller than control slices at all the stimulus increments recorded (Fig. 6.8, B) they were not significantly different ($P=0.14$). Average threshold stimulus intensities for HI-cystic ipsilateral cortices were lower than those required for both control and HI-cystic contralateral cortices but significantly different only from control ($P=0.03$). Average threshold stimulus intensities for HI non-cystic brains were lower than control but with no significance ($P= 0.1$). Overall latencies of EFPs in all three groups in normal medium were short indicating a very focal response and much shorter (<7ms) compared to those seen in the older group of rats (>10ms) in normal medium at threshold (Fig. 6.11, B). They were also not significantly different from each other (HI-cystic ipsi vs. control, $P= 0.12$; HI-cystic ipsi vs. HI-cystic contra, $P=0.27$; HI cystic contra vs. control, $P= 0.73$). With increasing stimulus intensities, the onset latencies of EFPs epileptiform events did not change substantially (Fig. 6.11, B; <6ms). In presence of BMI, latencies for EFPs became longer for all groups indicating network responses, compared to the focal responses seen in normal medium. In BMI HI-cystic latencies were the shortest ipsilaterally and significantly different from control ($P= 0.04$) but not from contralateral values ($P= 0.18$). In BMI increasing stimulus intensities shortened the onset latencies with the maximum shortening seen between threshold (T) and 2 times threshold (2T) for all groups (Fig. 6.11, B).

CHAPTER 7

DISCUSSION

The objectives of this study were to investigate the progression and temporal distribution of spontaneous seizures occurring in the epilepsy detected in this rodent model for perinatal HI damage. It addresses the histopathological features of the resultant lesion in the neocortex and hippocampus and their possible pathognomonic significance to the epilepsy. The results indicate that the perinatal HI insult resulted in a progressive type of epilepsy with an apparent latency of ~2 months (Fig. 7.1). The epilepsy was progressive, with an increase in the frequency of spontaneous seizures, which predominantly occurred in clusters. The histopathological features studied at an early (postnatal day 30) and a late time point (≥6 months of age) after the perinatal HI insult revealed multiple cortical dysplasias. The presence of porencephalic cysts, microgyri, neocortical dislamination, deep laminar gliosis and dysmorphic neurons in the ipsilateral neocortices of the epileptic rats suggests this is a relevant model to study the equivalent human condition. Dysplastic features were observed in the spared ipsilateral cortex, and more importantly in the contralateral hemisphere, in the form of cortical dysplasia, white matter hypercellularity and mossy fiber sprouting without the concomitant massive cell loss and atrophy seen on the ipsilateral side. The in vitro slice study indicates significant changes in electrophysiological properties of the neocortex

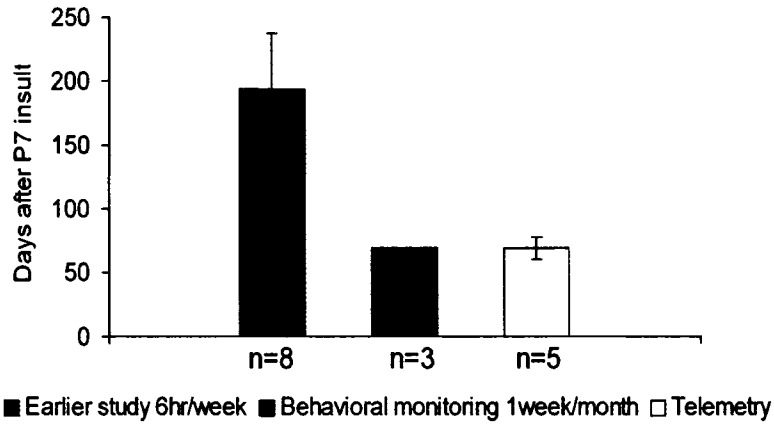

Fig. 7.1 Apparent latencies to first detected seizures comparing 3 different monitoring protocols. Studies reported here had significantly shorter but comparable apparent latencies (68.3 ± 0.3 and 68.8 ± 8.3 days for the grey and white bars respectively) in contrast to those previously reported (194 ± 43 days; solid black bar; Williams et al., 2004).

that is progressive in the form of involvement of the contralateral neocortex. This finding along with the histology suggests diaschisis due to the unilateral lesion or unilateral epileptic zone or both. It presents the model as that of "dual pathology" by having histopathological features both in the neocortex and hippocampus that have been linked to epileptogenic lesions both in humans and multiple animal models of epilepsy.

7.1 Spontaneous motor seizures detected in behavioral monitoring protocol

Focal onset. The postnatal day 7 rat model for perinatal HI with the modified Levine's method develops spontaneous motor seizures that behaviorally represent a right-sided lesion. All 3 epileptic rats (100%) in the video-monitoring study showed left forelimb clonus as their first detected behavioral seizure; this may indicate a focal ipsilateral brain involvement, at least initially. Even in the generalized forms of the motor seizures detected, a left forelimb onset was noted in animals with gross middle cerebral arterial territory infarcts with no obvious left-sided motor disability.

Latency and progression. The 25% monitoring protocol (chapter 3) used in this study lead to the detection of shorter latent periods (68.3 ± 0.3 days). The previously reported latency of 194 ± 43 days (Williams et al., 2004) used a 6 h (random) per week monitoring protocol (~4% monitoring time). If seizure occurrence was random, the mean seizure rate (0.66 ± 0.35 seizures per day) suggests these rats have one seizure every two days, on average. However we found only 16% of the total detected seizures to have occurred in isolation at the rate of ≤1 seizure/24 h whereas 63% of the total detected seizures occurred at the rate of ≥3 seizures/24h. The continuous video-monitoring over the 1-week duration revealed that the seizures occurred in close proximity to each other. Seizure clustering has been defined clinically as a number of seizures per unit time and, statistically, as a deviation from a random distribution and is commonly seen in human epilepsies (Haut et al., 2005). With 25% continuous monitoring time, this study detected a gradual progression of increasing seizure frequency as a function of time due to an increase in the number of seizure clusters and seizures within each cluster. The preponderance of clustering of spontaneous seizures could explain why the above-mentioned trends were not evident with the random 6h per week monitoring protocol (Williams et al., 2004). The low seizure rate and the lack of a continuous monitoring protocol, suggests that we may have failed to detect all of the epileptic rats with this protocol. The seizure rate of the epileptic rats at 7 months after HI (maximum time studied after HI) compared to kainate-treated rats (Hellier et al., 1998) at 6 months after treatment (estimated period of peak seizure frequency in kainate-treated rats) was approximately ten times lower (1.62 seizures per day to 16.3 seizures per day, respectively). Thus, the apparent latent period was about 2 months with 25% monitoring

(i.e., the actual latent period is presumably much shorter) and the mean behavioral seizure frequency was about 0.66 seizures/day; however, because most seizures occurred in clusters, many seizures could occur in one day and most days had no motor seizures.

Diurnal distribution. Seizure frequencies for the light and dark phase of the diurnal cycle were not significantly different. However, significantly more seizures occurred during inactive states during the light phase. These data suggest that the activity state rather than the light-dark cycle influences seizure occurrence. Activity state did not appear to affect seizure occurrence in the dark phase possibly because the rats had fewer episodes of non-active states during the dark phase. These data are similar those with kainate-induced epilepsy (Hellier et al. 1998).

7.2 The neocortical lesion and its implications for progressive epilepsy

Every HI-treated rat detected to have spontaneous recurrent seizures had ipsilateral cystic infarcts. Surviving frontal, paracingulate (anterior cerebral artery perfusion) and entorhinal cortices (posterior cerebral artery perfusion) that were spared from the liquifactive necrosis involved in formation of a porencephalic cyst showed multiple forms of cortical dysplasias. Analogous human HI insults show different combinations of similar post-lesion histopathology, although the neurological loss of function in form of prominent motor disabilities, a common clinical feature of the human HI syndrome, was not obvious in these rats. The histological findings at the early time point (postnatal day 30) were similar in their "watershed zone" distribution and cortical and sub-cortical involvement, to those of human neonatal encephalopathies due to HI. At the later ($\geq$6 months of age) time point, histopathological data suggest progressive shrinking of gliotic

bands in the neocortex causing the collapse of the columnar and laminar gliosis, distinctly seen at 1 month of age, to form microgyri and islands of isolated neurons with altered orientation and morphology. This progressive transformation may be associated with the progressive epilepsy. Commonalities of these findings (above) and the extensive histopathological reporting on the human fetal brain (Marin-Padilla, 1999, 2000; Norman, 1981), suggest this is a useful model for investigations of epileptogenesis after a perinatal HI insult.

Hippocampal histopathology has been a major focus of studies of epileptogenesis. The field of epilepsy is unsettled on whether the hippocampus generates or propagates seizures or both. Clinical data suggest that non-hippocampal sources of epileptiform discharges are common even in patients diagnosed with TLE (dual pathology). Dual pathology has been commonly reported in human cases with porencephalic cysts and reactive gliosis (Cendes et al., 1995; Ho et al., 1998). Clinically, cortical dysplasias are now commonly detected in resected temporal lobe tissues associated with refractory temporal lobe epilepsy (Kasper et al., 1999; Porter et al., 2003). Disrupted cortical lamination, dystrophic and maloriented neurons are characteristic findings of the cortical dysplasia found in the temporal neocortex. The multiple cortical dysplasias detected in conjunction with the robust mossy fiber sprouting in the dentate gyrus emphasize the need to investigate the electrophysiology of these dysmorphisms in this model. Microgyral malformations in the parasagittal cortex of the HI-treated epileptic rats from the late group are analogous with numerous human resective and autopsy studies of ulegyric/polymicrogyric tissue. Similarly located in watershed zones in neonates and children, they are thought to have a common pathogenic mechanism related to perfusion

failure in that area (Villani et al., 2003). To our knowledge, this finding has never been reported for this model. Conditions like polymicrogyri are also thought to result from ischemic insults in the perinatal period (Dvorak et al., 1993). Golgi preparations from resected human tissue demonstrate that neurons of the mid-cortical layers are replaced by a tangential band of fibrous astrocytes, variably layers II--V, in the microgyric cortex. These findings confirm impressions from general cell and fiber stains that acquired microgyria are the result of a destructive process striking predominantly in mid-cortical regions. It must occur after migration is complete but before the development of secondary and tertiary gyri (Williams et.al, 1976). With the HI insult at postnatal day 7, we saw similar mid-cortical gliosis that eventually collapsed into the four-layered acquired microgyral structure. Rat neocortex migration is thought to be complete at postnatal day 7 (Hagberg et al., 2002). Microgyral-like structures were noted for their absence in a previous study in this model by Towfighi et al. (1991). Since these dysmorphisms are commonly found in the human fetal brain, it was concurred that the animal model was different from the human condition in this matter. However, all of the histological data presented in that publication were from postnatal day 30 rats. The present study also failed to detect classical microgyral structures in the postnatal day 30 sections, but they were found in sections from older HI-treated rats ($\geq$6 months of age) documented to be epileptic (45%). The gray and white matter anomalies detected in this study months after initial injury suggest that it would not be advisable to use the contralateral hemisphere as "control cortex" in this model, as previously reported with histological studies done at early (postnatal day 30) time points (Towfighi et al., 1994).

7.3 Mossy fiber sprouting

Detection of Timm stain product in the dentate inner molecular layer is thought to represent mossy fiber sprouting, which has been detected in children with extra-hippocampal seizures (Mathern et al., 1994). Previous studies have not found a correlation between sprouting and severity of the epilepsy. This study also found no such correlation. The animals with spontaneous motor seizures (chronic group $\geq$ 6 months) demonstrated mossy fiber sprouting in both the ipsi- and contralateral dorsal and ventral hippocampi. The Timm stain scores were comparable ipsilaterally in the dorsal and ventral hippocampi (2.86 $\pm$ 0.14 & 2.57 $\pm$ 0.20, respectively), but significantly different in the contralateral hippocampi at those two anatomical locations (0.91$\pm$ 0.16 & 2.5 $\pm$ 0.22, respectively). In every instance, the grade for Timm stain in the contralateral ventral hippocampus was higher than the contralateral dorsal hippocampus. The ventral hippocampus in the rodent is thought to represent the human anterior temporal hippocampal lobe, which is often surgically resected in patients with refractory temporal lobe epilepsy. This robust sprouting in the ipsi- and contralateral ventral hippocampi is evidence of distant neuroplasticity of apparently non-injured cortical structures, and represents one of the possible effects of trans-hemispherical diaschisis in this model. The animals that were not detected to have spontaneous motor seizures also had mossy fiber sprouting in the ipsi- and contralateral hippocampus that was significantly lower in grade from the rats with spontaneous seizures, dorsally but not ventrally in the ipsilateral hippocampi and the opposite was true for the contralateral hippocampus. Timm stain was not done in the early (postnatal day 30) group of animals because at that time point we had no behavioral data to determine the epileptic status of that group of HI-treated

animals. Understanding the significance of the robust mossy fiber sprouting in trans-hemispheric ventral hippocampus of HI-treated epileptic rats may help shed light on the mechanisms of epileptogenesis for this model.

7.4 Seizure semiology in rats implanted with sub-dural electrodes and telemetry units.

The profile of the seizure semiology detected in the prior study conducted with behavioral monitoring alone (chapter 3) pointed to the ipsilateral somatosensory cortex as an important initiator of the ictal events. This behavioral profile was not altered by the invasive monitoring with chronically implanted sub-dural electrodes for this study. The cortical EEG data lent strong support to the possibility of an ipsilateral focus in the spared paracingulate neocortex in the form if lateralized channel specific recordings of interictal and ictal initiation of spiking. Subsequent histological protocols found that all epileptic HI-treated animals had ipsilateral cystic cortical infarcts and the non-epileptic HI animals did not have any discernable cortical or sub-cortical infarcts. No correlation between the severity of the infarct and the severity of the resultant epilepsy was obvious.

7.5 Temporal distribution of seizures in telemetry study

Seizure clustering has been reported to be a possible marker for intractable and poorly controlled epilepsy (Haut et al., 2005a and b). Clusters associated with short interictal intervals in humans have been linked to events originating from the same side as the previous seizure compared to those with longer interictal intervals (Haut et al., 1997). This would then implicate the ipsilateral hemisphere (given the left-sided onset of

the motor seizures) to be a possible source of the seizure clusters detected in this study. The two possible Gaussian distributions were seen for the total population of interictal events for the seizures within clusters and inter-cluster-intervals. The exponential decay of the inter-cluster-interval over time may be suggestive of a positive feedback mechanism. Thus clustering itself may be responsible for secondary alterations that facilitate the occurrence of the subsequent attack that is graded in severity over time. On the other hand the clustering may be responsible for negative feedback in the form of acute substantiation of inhibition that is responsible for the intervening seizure free period that is the inter-cluster-interval. More realistically both these phenomenon may occur simultaneously and play modulating roles that define the composite picture. This non-random distribution of seizures will be of importance when evaluating the effect of antiepileptic drugs. In this study clustering was seen in both male and female epileptic rats, more clearly detected in the rats with longer monitoring durations in the telemetry system. Seizures within clusters showed opposing sets of trends with individual animals but were fairly consistent for the animal between subsequent clusters. Few rats showed a decrease in inter-seizure interval over time within a cluster indicating a possible facilitation by the first few seizures. While other rats showed gradual increase in inter-seizure intervals within a cluster, ultimately terminating followed by a long inter-cluster interval.

7.6 Reflex seizures

Reflex seizures result from neuronal circuits that are hyperexcitable to specific afferent stimuli. Genetic and lesional mechanisms that facilitate the recruitment and

synchronization of larger neuronal pools by incoming sensory volleys have been implicated in the process (Palmini et al., 2005). Cortical malformations are known clinically and experimentally to be highly epileptogenic. This hyperexcitability clinically is often reflected by the occurrence of reflex seizures. It is thought that these malformations not only have intrinsic epileptogenic properties but establish abnormal intra and sub-cortical circuitry that enables fast recruitment and synchronization of hyperexcitable signals. In this model we know from previous studies that the ipsilateral somatosensory cortex displays a multitude of known epileptogenic malformations. The detection of seizures brought on exclusively by handling in 2 out the 10 HI-treated rats that were detected to be epileptic probably represent reflex seizures brought on by either a tactile or startle stimuli.

7.7 Continuous monitoring and antiepileptic drug (AED) testing

Studies designed to investigate the efficacy of commonly used AEDs on seizure syndromes of animal models using intermittent or non-continuous monitoring rely on fairly stable seizure frequencies for extended periods of time. The goal of every AED therapy is to prevent the occurrence of all seizures. The overall low seizure frequency and long inter-cluster intervals detected with continuous monitoring in this particular model of perinatal HI- related epilepsy has the potential of false positive results for AED efficacy if intermittent monitoring were to be used. Intermittent monitoring would potentially give erroneous seizure rates for individual rats to begin with. Although the battery life of implanted telemetry transmitters is limited (~5 months) they can be easily turned on and off using a non-invasive method. Therefore an initial phase of continuous

monitoring could be used to assess epileptic status and seizure rates, followed by a later continuous phase of monitoring in the same animals on an AED therapy of choice. More ambitiously availability of smaller implantable transmitters will help assess antiepileptogenic properties of AEDs when started with or soon after the acute perinatal insult.

7.8 Epilepsy as related to sex of rat

This study used both male and female rats. We opted to randomly select animals for ligation and the sham-control procedure at age 7 days because determination of the sex of rats is unreliable at that age. The rats were later implanted at 2 and ≥6 months of age when the sex was easily determined, therefore equal numbers of male and female HI-treated and control rats were implanted for each age group monitored. Eighteen randomly selected HI treated rats (9 of each sex) were implanted and monitored, to detect 10 epileptic rats that turned out to be 5 of each sex for the 2 age groups combined. Monitoring of both sexes in this study helped model the human condition. A correlation between individual seizure severity and sex of the rats could not be statistically determined because 3 out of the 4 rats that had less than 60 days of continuous monitoring were female HI-treated epileptic rats. This could be attributed to the fact that adult female rats are smaller in size and weight compared to males and the post-surgical complications like pressure necrosis occurred more frequently in this group. Clustering of seizures has been reported as a feature of catamenial epilepsy (Tauboll et al., 1990). Although we cannot rule out cyclical variations to be one of the underlying causes for clustering in the female rats, clustering was robust in the male epileptic rats as well.

7.9 In vitro slice electrophysiology and cortical epileptogenesis

Acquired cortical dysplasias found in this model of perinatal HI have been strongly associated with intractable epilepsy in humans. Data presented in chapter 4 and 5 showed that there was an increased propensity for epilepsy in rats with HI-induced cystic lesions that was not seen in HI-treated but non-lesioned rats. It was also demonstrated that the resultant epilepsy was not only progressive in terms of seizure frequencies but also severity. Early electrographic seizures recorded in rats implanted at 2 months of age were non-convulsive or partial and focal originating in ipsilaterally placed cortical leads on the cortical EEGs. Behaviorally they were associated with contralateral motor seizures which over time became generalized both electrographically and behaviorally. The contribution of these dysplasias and the spared somatosensory cortex to the resultant epileptic condition in this model of post-stroke epilepsy will help understand the ongoing epileptogenic process after insults to an immature brain. This study is the first to demonstrate for this model, the increased propensity of epileptiform activity in the ipsilateral spared somatosensory cortex that in a slice preparation that is isolated from other brain structures. The EFPs at the two time points revealed the progression of the epileptogenic properties of the spared cortex and the distinct involvement of the contralateral mirror cortex at the later time point that was not seen initially. These findings encourage the detailed study of the cortical malformations in the spared cortex and will help address the therapeutic long term effects of putative preventative interventional therapies.

Although the present data cannot address the mechanistic possibilities of the detected hyperexcitability it adds to the information derived from the electrographic data recorded from this model wherein lateralization of paroxysmal epileptiform discharges and seizure onsets were seen ipsilaterally over the spared paracingulate cortices in HI-treated epileptic rats. It also demonstrates that the ipsilateral spared cortex may act as the initial epileptic foci but over time the contralateral mirror focus becomes equally hyperexcitable. Although a tenuous question to answer, it may prove interesting to tease apart the role of further seizures playing a pivotal role in the strengthening of the epileptic pathways that lead to generalization of the seizures or just reflecting an underlying ongoing process of epileptogenesis. Clarification of the importance of these factors in the pathogenesis of the disease may have diagnostic and therapeutic implications.

In the present study the hyperexcitability of the ipsilateral somatosensory cortex in the acute stage was masked by an effective inhibitory circuitry. Only strong disinhibition of the slice elicited epileptiform discharges in ipsi-lateral neocortices that were not seen in normal medium. This would indicate that initially although there is an alteration in the excitatory transmission of the spared cortex, the inhibitory mechanisms mediated by $GABA_A$ receptors effectively mask those changes. This however changes over time when in the slices from older lesioned rats, epileptiform discharges could be evoked even in normal medium. This may indicate a few possibilities, one being that at this point in time the local inhibitory circuit is compromised to some extent or that the slice preparation has isolated the somatosensory cortex from its new compensatory inhibitory circuit. An overall uncompensated increase in excitatory transmission alone cannot explain the long

interictal periods of seizure free days observed in this model with preponderance for clustering of seizures.

Hyperexcitability in post-stroke sensorimotor cortices have been documented in human patients. It has been proposed that hyperexcitability in the spared motor cortex that has been studied in adult post-stroke rehabilitation studies is integral to the functional recovery (Cicinelli P. et al., 2005; Johansen-Berg H. et al., 2002). Explanations put forth for post-stroke cortical reorganization leading to hyperexcitability are not restricted to, but include adaptive changes that increase the output "gain" of the weakened motor cortex to match the unaffected sensory feedback. Another possibility is the shift of motor function to the less excitatory supplementary motor areas during post-stroke plasticity, that now have to adjust to generating efficient outputs to the to spinal motor neurons. Also one cannot rule out deregulation of the injured cortex by loss of inhibitory reciprocal circuits through inter- and intra-hemispheric connections in the intact brain. Alterations in the connectivity of cortical circuits may occur due axonal sprouting within pyramidal cell intracortical arbors. These enhanced excitatory connections may increase recurrent excitatory loops within the epileptogenic zones (Jacobs et al., 2000 and 2005; Luhmann et al., 1998). Hyperinnervation attributable to reorganization of thalamocortical, callosal, and intracortical circuitry, and failure to prune immature connections, may all be a prominent result of post-stroke plasticity of a developing neocortex. On the cellular level alterations in membrane properties due to differential ion-channel compositions may render principal cells in dysplastic cortical tissue capable of epileptiform discharges. Reduced Mg^{2+} sensitivity associated with decreased NMDA-receptor NR2B subunit mRNA and protein expression in cytomegalic and a dominant

fraction of normal pyramidal-shaped neurons has been demonstrated in cortical dysplasias resected to cure epilepsy in children (Mathern, 2005). Therefore in cases of pediatric epilepsies due to cortical dysplasias, NMDA receptors with altered receptor subunit composition could contribute in the generation and/or propagation of epileptic discharges due to the increased capability of generating long-lasting membrane depolarization. Thus epileptogenesis in the developing brain most probably is not as simplistic as a mere increase in excitation and/or a decrease in inhibition, but a variety of complicated neuronal interactions that may vary at different times in the epileptogenesis (Engel, 1996). The findings reported here warrant the further investigation of these epileptogenic features in this model for perinatal HI-induced epilepsy.

7.10 Models of epilepsy from perinatal insults

Chronic models of pediatric epilepsy related to prenatal and perinatal insults have focused on cortical dysplasias, which are the hypothesized epileptogenic zones, in affected brains. Microgyri-like malformations have been induced with the freeze-lesion model and cortical dysplasias by prenatal exposure to irradiation and the neuroteratogen methylazoxymethanol (MAM) (Chevassus-Au-Louis et al., 1999; Kondo et al., 2001; Schwartzkroin et al., 2004; Smith et al., 1999). Animal models using perinatal rats have induced acute seizures using hyperthermia, hypoxia and Flurothyl (Jensen, 2006) to mimic relevant clinical conditions that present as seizures during the neonatal period. Neonatal seizures caused by poorly understood, known or unknown causes are predictors of adverse neurological outcomes, one of which is chronic epilepsy (Lombroso, 1996). Until recently, the acute insult or the resulting lesions in these models have not been

shown to result in spontaneous recurrent motor seizures. There is no consensus on the controversy of neonatal seizures simply reflecting an existing underlying brain injury or a de-novo causative factor for further damage causing chronic epilepsy (Scher, 2003). Animal models have been designed to address this issue by combining a hyperthermia insult to a postnatal rat with a perinatally induced cortical malformation created either by the freeze lesion or MAM exposure. The MAM-treated rat with hyperthermia-induced seizures showed a lower threshold to the hyperthermia-induced behavioral seizures (Germano et al., 1996), but the high mortality (~90%) and low yield after the second insult made it difficult to test for recurrent spontaneous seizures in these animals. The rat model with the freeze-lesion-induced microgyral cortical malformations, when subjected to hyperthermia at postnatal age of 10 days, has recently been shown to have abnormal EEG recordings in the amygdala associated with freeze behaviors (Scantlebury et al., 2005). This monitoring protocol was conducted ~2 months after the second insult and did not detect any generalized motor seizures. Another animal model designed to mimic early-life prolonged seizures that result in chronic epilepsy is the lithium-pilocarpine model of status epilepticus (Raol et al., 2003). This model has shown a 67% incidence of chronic epilepsy in rats with the chemotoxin-induced status at postnatal age of 20 days, but it is not clear that an insult at that age can be classified as a model for developmental epileptogenesis. Immature rodents below the age of 3 weeks have been shown to be resistant to chemoconvulsant-induced status paradigms in terms of neuronal death in the hippocampus and resultant spontaneous seizures (Priel, 1996; Haas et al., 2001).

This study reports the cortical and hippocampal histopathological features of a model of perinatal HI with spontaneous recurrent motor seizures. Similar

histopathological alterations have been reported in a variety of multi–causal human perinatal injuries and insults (Rorke, 1992; Villani et al., 2003). Evidence is presented for a progressive transformation of the damaged neocortex with the possibility of surviving cortical neurons adapting by transforming their structure and connectivity to compensate for the massive laminar and columnar neuronal loss. The ongoing structural plasticity in this model coincides with the progressive nature of the resultant epilepsy. Whether this structural plasticity also functions as the pathological mechanism contributing to the epileptogenesis in this model with an apparent latency of 2 months requires further studies. The diachisis seen in the form of histological and electrophysiological alterations in the contralateral somatosensory cortex are relevant to alterations noted in human non-affected cortices (Andrews, 1991; Kraemer et al., 2004; Nakashima et al., 1985). Finally the presence of the dual pathology present in this model in the form of neocortical and hippocampal histological aberrations provides the means to study the interrelationship of these features with the porencephalic lesion morphology similar to the one found in humans and provide insights into the epileptogenesis in patients with congenital porencephaly (Cusmai et al., 1993; Ho et al., 1998).

CHAPTER 8

SUMMARY

8.1 Summary

This work describes the progressive histopathological and electrophysiological features associated with the epilepsy that results after a perinatal HI injury in a rat model for HI encephalopathy. The data presented here help better understand the animal model as related to its epilepsy and the possible benefits for further studies using it, in relation to understanding the human condition it has been designed to model. The analysis of the data explores the chronic progression of the neuropathogy associated with a severe excitotoxic episode in the developmental window period. Although we have addressed one kind of insult (i.e., perfusion failure) that leads to an excitotoxic insult, the study of the chronic progression in general represents features of the adaptive plasticity after a developmental paroxysmal episode. Plasticity peaks during the developmental phase due to the on going neurogenesis in certain brain regions, deletion of neurons by programmed cell death and formation and pruning of synapses that leads to strengthening of certain pathways. Although most plasticity refers to the ability of the brain to recover from injury by reorganization, adaptive plasticity that is excessive may result in neurologic disorders by forming new maladaptive circuits. Chronic animal model studies such as the one done here, help understand the features of such impaired plasticity after specific developmental insults. The results (chapter 7) for the first aim indicate that there is an increased

susceptibility for developing epilepsy in adulthood after a perinatal HI insult. For the animal model this increased susceptibility was directly related to severity of the HI-induced infarct but no correlation was found between the size of the infarct and severity of the resultant epilepsy. Data from the second aim indicate that this rodent model has neuropathological features commonly seen in human cases of perinatal HI and therefore represents a good model to study the pathogenesis of such lesions. The study is the first to report the use of telemetric EEG monitoring in this model that allowed the chronic and continuous analysis of the post-stroke epilepsy in "freely behaving" rats. The ictal and inter-ictal data derived from the third aim in this study strengthens the idea that the para-infarct spared cortex has the potential to act as the initial seizure focus that over time shows progression in the form of generalized EEG activity. The behavioral data shows progression in the severity of seizure semiology by generalization of the initial non-convulsive and partial seizures. Analysis of data acquired from the fourth and final aim indicate that epileptiform plasticity occurring in sensorimotor cortices also show progression as a function of time. Epileptiform discharges could only be evoked ipsilateral to the infarct after blocking inhibition at the early time point. However such discharges could be evoked bilaterally in normal medium at later time points. The results reported here for both the long term EEG analysis and the in vitro slice studies will help to design future studies that address the mechanistic questions related to epileptogenesis for this model.

8.2 Future Work

This work has a lot of potential for future expansions. The findings of multiple cortical dysplasias associated with the epileptic rats beg the detailed study of their

epileptogenic properties. The distinctive features of the seizure progression determined by the chronic telemetric EEG monitoring warrant designing novel drug delivery protocols to study the efficacy of widely used AEDS in this model. The strong association of the severe infarcts with the development of epilepsy encourages the further study of neuroprotective methods to reduce ischemic loss after an insult.

REFERENCES

Alonso-Nanclares,L., Garbelli,R., Sola,R.G., Pastor,J., Tassi,L., Spreafico,R., DeFelipe,J., 2005. Microanatomy of the dysplastic neocortex from epileptic patients. Brain 128, 158-173.

Andres,M., Andre,V.M., Nguyen,S., Salamon,N., Cepeda,C., Levine,M.S., Leite,J.P., Neder,L., Vinters,H.V., Mathern,G.W., 2005. Human cortical dysplasia and epilepsy: an ontogenetic hypothesis based on volumetric MRI and NeuN neuronal density and size measurements. Cereb Cortex 15, 194-210.

Andrews,R.J., 1991. Transhemispheric diaschisis. A review and comment. Stroke 22, 943-949.

Aneja,S., Ahuja,B., Taluja,V., Bhatia,V.K., 2001. Epilepsy in children with cerebral palsy. Indian J Pediatr 68, 111-115.

Ansari,M.Q., Chincanchan,C.A., Armstrong,D.L., 1990. Brain calcification in hypoxic-ischemic lesions: an autopsy review. Pediatr Neurol 6, 94-101.

Armstrong,D.D., Mizrahi,E.M., 1998. Pathologic basis of the symptomatic epilepsies in childhood. J Child Neurol 13, 361-371.

Aso,K., Scher,M.S., Barmada,M.A., 1990. Cerebral infarcts and seizures in the neonate. J Child Neurol 5, 224-228.

Avoli,M., Bernasconi,A., Mattia,D., Olivier,A., Hwa,G.G., 1999. Epileptiform discharges in the human dysplastic neocortex: in vitro physiology and pharmacology. Ann Neurol 46, 816-826.

Back,S.A., Han,B.H., Luo,N.L., Chricton,C.A., Xanthoudakis,S., Tam,J., Arvin,K.L., Holtzman,D.M., 2002. Selective vulnerability of late oligodendrocyte progenitors to hypoxia-ischemia. J Neurosci 22, 455-463.

Bastlund,J.F., Jennum,P., Mohapel,P., Vogel,V., Watson,W.P., 2004. Measurement of cortical and hippocampal epileptiform activity in freely moving rats by means of implantable radiotelemetry. J Neurosci Methods 138, 65-72.

Bastlund,J.F., Jennum,P., Mohapel,P., Penschuck,S., Watson,W.P., 2005. Spontaneous epileptic rats show changes in sleep architecture and hypothalamic pathology. Epilepsia 46, 934-938.

Ben Ari,Y., 1985. Limbic seizure and brain damage produced by kainic acid: mechanisms and relevance to human temporal lobe epilepsy. Neuroscience 14, 375-403.

Bergamasco,B., Benna,P., Ferrero,P., Gavinelli,R., 1984. Neonatal hypoxia and epileptic risk: a clinical prospective study. Epilepsia 25, 131-136.

Buchkremer-Ratzmann,I., August,M., Hagemann,G., Witte,O.W., 1996. Electrophysiological transcortical diaschisis after cortical photothrombosis in rat brain. Stroke 27, 1105-1109.

Burneo,J.G., Bebin,M., Kuzniecky,R.I., Knowlton,R.C., 2004. Electroclinical and magnetoencephalographic studies in epilepsy patients with polymicrogyria. Epilepsy Res 62, 125-133.

Calcagnotto,M.E., Paredes,M.F., Tihan,T., Barbaro,N.M., Baraban,S.C., 2005. Dysfunction of synaptic inhibition in epilepsy associated with focal cortical dysplasia. J Neurosci 25, 9649-9657.

Cendes,F., Cook,M.J., Watson,C., Andermann,F., Fish,D.R., Shorvon,S.D., Bergin,P., Free,S., Dubeau,F., Arnold,D.L., 1995. Frequency and characteristics of dual pathology in patients with lesional epilepsy. Neurology 45, 2058-2064.

Cepeda,C., Hurst,R.S., Flores-Hernandez,J., Hernandez-Echeagaray,E., Klapstein,G.J., Boylan,M.K., Calvert,C.R., Jocoy,E.L., Nguyen,O.K., Andre,V.M., Vinters,H.V., Ariano,M.A., Levine,M.S., Mathern,G.W., 2003. Morphological and electrophysiological

characterization of abnormal cell types in pediatric cortical dysplasia. J Neurosci Res 72, 472-486.

Cepeda,C., Andre,V.M., Flores-Hernandez,J., Nguyen,O.K., Wu,N., Klapstein,G.J., Nguyen,S., Koh,S., Vinters,H.V., Levine,M.S., Mathern,G.W., 2005. Pediatric cortical dysplasia: correlations between neuroimaging, electrophysiology and location of cytomegalic neurons and balloon cells and glutamate/GABA synaptic circuits. Dev Neurosci 27, 59-76.

Chagnac-Amitai,Y., Connors,B.W., 1989. Horizontal spread of synchronized activity in neocortex and its control by GABA-mediated inhibition. J Neurophysiol 61, 747-758.

Chagnac-Amitai,Y., Connors,B.W., 1989. Synchronized excitation and inhibition driven by intrinsically bursting neurons in neocortex. J Neurophysiol 62, 1149-1162.

Chervin,R.D., Pierce,P.A., Connors,B.W., 1988. Periodicity and directionality in the propagation of epileptiform discharges across neocortex. J Neurophysiol 60, 1695-1713.

Chevassus-Au-Louis,N., Jorquera,I., Ben Ari,Y., Represa,A., 1999. Abnormal connections in the malformed cortex of rats with prenatal treatment with methylazoxymethanol may support hyperexcitability. Dev Neurosci 21, 385-392.

Chevassus-Au-Louis,N., Baraban,S.C., Gaiarsa,J.L., Ben Ari,Y., 1999. Cortical malformations and epilepsy: new insights from animal models. Epilepsia 40, 811-821.

Cicinelli,P., Marconi,B., Zaccagnini,M., Pasqualetti,P., Filippi,M.M., Rossini,P.M., 2006. Imagery-induced cortical excitability changes in stroke: a transcranial magnetic stimulation study. Cereb Cortex 16, 247-253.

Connell,J., Oozeer,R., de Vries,L., Dubowitz,L.M., Dubowitz,V., 1989. Clinical and EEG response to anticonvulsants in neonatal seizures. Arch Dis Child 64, 459-464.

Courville,C.B., 1958. Etiology and pathogenesis of laminar cortical necrosis; its significance in evaluation of uniform cortical atrophies of early life. AMA Arch Neurol Psychiatry 79, 7-30.

Courville,C.B., 1959. Antenatal and paranatal circulatory disorders as a cause of cerebral damage in early life. J Neuropathol Exp Neurol 18, 115-140.

Cowan,F., Rutherford,M., Groenendaal,F., Eken,P., Mercuri,E., Bydder,G.M., Meiners,L.C., Dubowitz,L.M., de Vries,L.S., 2003. Origin and timing of brain lesions in term infants with neonatal encephalopathy. The Lancet 361, 736-742.

Cusmai R, Ricci S, Pinard J.M, Plouin P, Fariello G, Dulac O., 1993. West syndrome due to perinatal insults. Epilepsia 34, 738-742.

Dijkhuizen,R.M., Ren,J., Mandeville,J.B., Wu,O., Ozdag,F.M., Moskowitz,M.A., Rosen,B.R., Finklestein,S.P., 2001. Functional magnetic resonance imaging of reorganization in rat brain after stroke. 98, 12766-12771.

Domann,R., Hagemann,G., Kraemer,M., Freund,H.J., Witte,O.W., 1993. Electrophysiological changes in the surrounding brain tissue of photochemically induced cortical infarcts in the rat. Neurosci Lett 155, 69-72.

du Plessis,A.J., Volpe,J.J., 2002. Perinatal brain injury in the preterm and term newborn. Curr Opin Neurol 15, 151-157.

Dudek,F.E., Wuarin,J.P., Tasker,J.G., Kim,Y.I., Peacock,W.J., 1995. Neurophysiology of neocortical slices resected from children undergoing surgical treatment for epilepsy. J Neurosci Methods 59, 49-58.

Dvorak,K., Feit,J., 1993. [Pathogenesis of micropolygyria]. Cesk Patol 29, 125-133.

Dzhala,V.I., Talos,D.M., Sdrulla,D.A., Brumback,A.C., Mathews,G.C., Benke,T.A., Delpire,E., Jensen,F.E., Staley,K.J., 2005. NKCC1 transporter facilitates seizures in the developing brain. Nat Med 11, 1205-1213.

Engel J. Jr., 1996 Excitation and inhibition in epilepsy. Can J Neurol Sci. 23, 167-174.

Estan, J., Hope, P., 1997. Unilateral neonatal cerebral infarction in full term infants. Arch Dis Child Fetal Neonatal Ed 76, 88-93.

Feeney,D.M., Baron,J.C., 1986. Diaschisis. Stroke 17, 817-830.

Ferrer,I., Pineda,M., Tallada,M., Oliver,B., Russi,A., Oller,L., Noboa,R., Zujar,M.J., Alcantara,S., 1992. Abnormal local-circuit neurons in epilepsia partialis continua associated with focal cortical dysplasia. Acta Neuropathol (Berl) 83, 647-652.

Frahm,C., Haupt,C., Witte,O.W., 2004. GABA neurons survive focal ischemic injury. Neuroscience 127, 341-346.

Germano,I.M., Zhang,Y.F., Sperber,E.F., Moshe,S.L., 1996. Neuronal migration disorders increase susceptibility to hyperthermia-induced seizures in developing rats. Epilepsia 37, 902-910.

Golomb M.R, MacGregor D.L, Domi T, Armstrong D.C, McCrindle B.W, Mayank S,deVeber G.A., 2001. Presumed pre- or perinatal arterial ischemic stroke: risk factors and outcomes. Ann Neurol 50, 163-168.

Gotman,J., Marciani,M.G., 1985. Electroencephalographic spiking activity, drug levels, and seizure occurrence in epileptic patients. Ann Neurol 17, 597-603.

Gotman,J., 1991. Relationships between interictal spiking and seizures: human and experimental evidence. Can J Neurol Sci 18, 573-576.

Gutnick,M.J., Connors,B.W., Prince,D.A., 1982. Mechanisms of neocortical epileptogenesis in vitro. J Neurophysiol 48, 1321-1335.

Haas,K.Z., Sperber,E.F., Opanashuk,L.A., Stanton,P.K., Moshe,S.L., 2001. Resistance of immature hippocampus to morphologic and physiologic alterations following status epilepticus or kindling. Hippocampus 11, 615-625.

Hadjipanayis,A., Hadjichristodoulou,C., Youroukos,S., 1997. Epilepsy in patients with cerebral palsy. Dev Med Child Neurol 39, 659-663.

Hagberg,H., Ichord,R., Palmer,C., Yager,J.Y., Vannucci,S.J., 2002. Animal models of developmental brain injury: relevance to human disease. A summary of the panel

discussion from the Third Hershey Conference on Developmental Cerebral Blood Flow and Metabolism. Dev Neurosci 24, 364-366.

Haut,S.R., Legatt,A.D., O'Dell,C., Moshe,S.L., Shinnar,S., 1997. Seizure lateralization during EEG monitoring in patients with bilateral foci: the cluster effect. Epilepsia 38, 937-940.

Haut,S.R., 2005. Seizure clustering. Epilepsy Behav. 8, 50-5.

Haut,S.R., Shinnar,S., Moshe,S.L., 2005. Seizure clustering: risks and outcomes. Epilepsia 46, 146-149.

Hellier,J.L., Patrylo,P.R., Buckmaster,P.S., Dudek,F.E., 1998. Recurrent spontaneous motor seizures after repeated low-dose systemic treatment with kainate: assessment of a rat model of temporal lobe epilepsy. Epilepsy Res 31, 73-84.

Hellier,J.L., Dudek,F.E., 1999. Spontaneous motor seizures of rats with kainate-induced epilepsy: effect of time of day and activity state. Epilepsy Res 35, 47-57.

Hill,A., Volpe,J.J., 1982. Hypoxic-ischemic brain injury in the newborn. Semin Perinatol 6, 25-41.

Ho,S.S., Kuzniecky,R.I., Gilliam,F., Faught,E., Bebin,M., Morawetz,R., 1998. Congenital porencephaly: MR features and relationship to hippocampal sclerosis. Am J Neuroradiol 19, 135-141.

Hufnagel,A., Dumpelmann,M., Zentner,J., Schijns,O., Elger,C.E., 2000. Clinical relevance of quantified intracranial interictal spike activity in presurgical evaluation of epilepsy. Epilepsia 41, 467-478.

Inder,T.E., Volpe,J.J., 2000. Mechanisms of perinatal brain injury. Semin Neonatol 5, 3-16.

Jacobs,K.M., Graber,K.D., Kharazia,V.N., Parada,I., Prince,D.A., 2000. Postlesional epilepsy: the ultimate brain plasticity. Epilepsia 41 Suppl 6, S153-S161.

Jacobs,K.M., Prince,D.A., 2005. Excitatory and inhibitory postsynaptic currents in a rat model of epileptogenic microgyria. J Neurophysiol 93, 687-696.

Jensen,F.E., Applegate,C., Burchfiel,J., Lombroso,C.T., 1991. Differential effects of perinatal hypoxia and anoxia on long term seizure susceptibility in the rat. Life Sci 49, 399-407.

Jensen,F.E., 1997. Perinatal hypoxic-ischemic brain injury: Maturation-dependent relation to epilepsy. MRDD Research Reviews 3:85-95.

Jensen,F.E., 2006. Pediatric epilepsy models. Epilepsy Res 68, 28-31.

Johansen-Berg,H., Dawes,H., Guy,C., Smith,S.M., Wade,D.T., Matthews,P.M., 2002. Correlation between motor improvements and altered fMRI activity after rehabilitative therapy. Brain 125, 2731-2742.

Johnston,M.V., 2004. Clinical disorders of brain plasticity. Brain Dev 26, 73-80.

Kadam,S.D., Williams,P.A., Dudek,F.E., 2003. Modified Levine's method in the P7 rat pup causes a lesion similar to the hypoxic encephalopathy-induced parasagittal injury of human neonates. Soc. Neurosci. Abstr. 29: 211.5

Kasper,B.S., Stefan,H., Buchfelder,M., Paulus,W., 1999. Temporal lobe microdysgenesis in epilepsy versus control brains. J Neuropathol Exp Neurol 58, 22-28.

Kelly,K.M., 2004. Spike–wave discharges: absence or not, a common finding in common laboratory rats. Epilepsy Curr 4,176-177.

Kelly,K.M., 2002. Poststroke seizures and epilepsy: clinical studies and animal models. Epilepsy currents 2, 173-177.

Kerfoot,C., Vinters,H.V., Mathern,G.W., 1999. Cerebral cortical dysplasia: giant neurons show potential for increased excitation and axonal plasticity. Dev Neurosci 21, 260-270.

Kobayashi,M., Wen,X., Buckmaster,P.S., 2003. Reduced inhibition and increased output of layer II neurons in the medial entorhinal cortex in a model of temporal lobe epilepsy. J Neurosci 23, 8471-8479.

Kondo,S., Najm,I., Kunieda,T., Perryman,S., Yacubova,K., Luders,H.O., 2001. Electroencephalographic characterization of an adult rat model of radiation-induced cortical dysplasia. Epilepsia 42, 1221-1227.

Kraemer,M., Schormann,T., Hagemann,G., Qi,B., Witte,O.W., Seitz,R.J., 2004. Delayed shrinkage of the brain after ischemic stroke: preliminary observations with voxel-guided morphometry. J Neuroimaging 14, 265-272.

Lanska,M.J., Lanska,D.J., Horwitz,S.J., Aram,D.M., 1991. Presentation, clinical course, and outcome of childhood stroke. Pediatr Neurol 7, 333-341.

Lesser,R.P., Kaplan,P.W., 1994. Long-term monitoring with digital technology for epilepsy. J Child Neurol 9 Suppl 1, S64-S70.

Levine,S., 1960. Anoxic-ischemic encephalopathy in rats. The American Journal of Pathology 36, 1-17.

Levine,D.N., Fisher,M.A., Caviness,V.S., Jr., 1974. Porencephaly with microgyria: a pathologic study. Acta Neuropathol (Berl) 29, 99-113.

Lombroso,C.T., 1996. Neonatal seizures: historic note and present controversies. Epilepsia 37 Suppl 3, 5-13.

Luhmann,H.J., Mudrick-Donnon,L.A., Mittmann,T., Heinemann,U., 1995. Ischaemia-induced long-term hyperexcitability in rat neocortex. Eur J Neurosci 7, 180-191.

Luhmann,H.J., Raabe,K., Qu,M., Zilles,K., 1998. Characterization of neuronal migration disorders in neocortical structures: extracellular in vitro recordings. Eur J Neurosci 10, 3085-3094.

Lye,R.H., Clough,P.H., 1989. The applicability of brain slice methodology to the study of focal cerebral ischaemia in the rat: an evaluation. J Neurosci Methods 28, 1-6.

Lynch,J.K., Hirtz,D.G., DeVeber,G., Nelson,K.B., 2002. Report of the National Institute of Neurological Disorders and Stroke Workshop on Perinatal and Childhood Stroke. Pediatrics 109, 116-123.
Marin-Padilla,M., 1999. Developmental neuropathology and impact of perinatal brain damage. III: gray matter lesions of the neocortex. J Neuropathol Exp Neurol 58, 407-429.

Marin-Padilla,M., 2000a. Perinatal brain damage, cortical reorganization (acquired cortical dysplasias), and epilepsy. Neocortical Epilepsies. Lippincott Williams & Wilkins; 1st edition (November 15, 2000), pp. 153-172.

Marín-Padilla,M., 2000b. Neuropathologic correlates of perinatal asphyxia. International Pediatrics 15, 221-228.

Marin-Padilla,M., Tsai,R.J., King,M.A., Roper,S.N., 2003. Altered corticogenesis and neuronal morphology in irradiation-induced cortical dysplasia: a Golgi-Cox study. J Neuropathol Exp Neurol 62, 1129-1143.

Mathern,G.W., Leite,J.P., Pretorius,J.K., Quinn,B., Peacock,W.J., Babb,T.L., 1994. Children with severe epilepsy: evidence of hippocampal neuron losses and aberrant mossy fiber sprouting during postnatal granule cell migration and differentiation. Brain Res Dev Brain Res 78, 70-80.

Mathern,G.W., 2005. Development and post insult plasticity. Epilepsia 46, 199-201.

Matsumoto,R., Kinoshita,M., Taki,J., Hitomi,T., Mikuni,N., Shibasaki,H., Fukuyama,H., Hashimoto,N., Ikeda,A., 2005. In vivo epileptogenicity of focal cortical dysplasia: A direct cortical paired stimulation study. Epilepsia 46, 1744-1749.

Mattia,D., Olivier,A., Avoli,M., 1995. Seizure-like discharges recorded in human dysplastic neocortex maintained in vitro. Neurology 45, 1391-1395.

McCormick,D.A., Prince,D.A., 1987. Post-natal development of electrophysiological properties of rat cerebral cortical pyramidal neurones. J Physiol 393, 743-762.

Meencke,H.J., Janz,D., 1985. The significance of microdysgenesia in primary generalized epilepsy: an answer to the considerations of Lyon and Gastaut. Epilepsia 26, 368-371.

Mischel,P.S., Nguyen,L.P., Vinters,H.V., 1995. Cerebral cortical dysplasia associated with pediatric epilepsy. Review of neuropathologic features and proposal for a grading system. J Neuropathol Exp Neurol 54, 137-153.

Najm,I., Ying,Z., Babb,T., Crino,P.B., Macdonald,R., Mathern,G.W., Spreafico,R., 2004. Mechanisms of epileptogenicity in cortical dysplasias. Neurology 62, S9-13.

Nakashima,K., Kanba,M., Fujimoto,K., Sato,T., Takahashi,K., 1985. Somatosensory evoked potentials over the non-affected hemisphere in patients with unilateral cerebrovascular lesions. J Neurol Sci 70, 117-127.

Nelson,K.B., Lynch,J.K., 2004. Stroke in newborn infants. The Lancet Neurology 3, 150-158.

Neumann-Haefelin,T., Witte,O.W., 2000. Periinfarct and remote excitability changes after transient middle cerebral artery occlusion. J Cereb Blood Flow Metab 20, 45-52.
Norman M.G., 1981. On the morphogenesis of ulegyria. Acta Neuropathol (Berl) 53, 331-332.

Palmer,C., 1995. Hypoxic-ischemic encephalopathy. Therapeutic approaches against microvascular injury, and role of neutrophils, PAF, and free radicals. Clin Perinatol 22, 481-517.

Palmini,A., Halasz,P., Scheffer,I.E., Takahashi,Y., Jimenez,P.A., Dubeau,F., Andermann,F., Paglioli-Neto,E., Costa da Costa,J., Rosenow,F., Fritsch,B., 2005. Reflex Seizures in Patients with Malformations of Cortical Development and Refractory Epilepsy. Epilepsia 46, 1224-1234.

Palmini,A., Gambardella,A., Andermann,F., Dubeau,F., da Costa,J.C., Olivier,A., Tampieri,D., Robitaille,Y., Paglioli,E., Paglioli,N.E.,1994. Operative strategies for patients with cortical dysplastic lesions and intractable epilepsy. Epilepsia 35 Suppl 6, S57-S71.

Paxinos,G., Watson,C., 1998. The rat brain in stereotaxic coordinates, 4th edition Ed. Academic Press, New York.

Peters,O., Redecker,C., Hagemann,G., Bruehl,C., Luhmann,H.J., Witte,O.W., 2004. Impaired synaptic plasticity in the surround of perinatally acquired dysplasia in rat cerebral cortex. Cereb Cortex 14, 1081-1087.

Porter,B.E., Brooks-Kayal,A., Golden,J.A., 2002. Disorders of cortical development and epilepsy. Arch Neurol 59, 361-365.

Porter,B.E., Judkins,A.R., Clancy,R.R., Duhaime,A., Dlugos,D.J., Golden,J.A., 2003. Dysplasia: a common finding in intractable pediatric temporal lobe epilepsy. Neurology 61, 365-368.

Priel,M.R., dos Santos,N.F., Cavalheiro,E.A., 1996. Developmental aspects of the pilocarpine model of epilepsy. Epilepsy Res 26, 115-121.

Prince,D.A., Tseng,G.F., 1993. Epileptogenesis in chronically injured cortex: in vitro studies. J Neurophysiol 69, 1276-1291.

Prince,D.A., Jacobs,K.M., Salin,P.A., Hoffman,S., Parada,I., 1997. Chronic focal neocortical epileptogenesis: does disinhibition play a role? Can J Physiol Pharmacol 75, 500-507.

Pulsinelli,W.A., Brierley,J.B., Plum,F., 1982. Temporal profile of neuronal damage in a model of transient forebrain ischemia. Ann Neurol 11, 491-498.

Purpura,D.P., Housepian,E.M., 1961. Morphological and physiological properties of chronically isolated immature neocortex. Exp Neurol 4, 377-401.

Racine,R.J., 1972. Modification of seizure activity by electrical stimulation. II. Motor seizure. Electroencephalogr Clin Neurophysiol 32, 281-294.

Ramaswamy,V., Miller,S.P., Barkovich,A.J., Partridge,J.C., Ferriero,D.M., 2004. Perinatal stroke in term infants with neonatal encephalopathy. Neurology 62, 2088-2091.

Raol,Y.S., Budreck,E.C., Brooks-Kayal,A.R., 2003. Epilepsy after early-life seizures can be independent of hippocampal injury. Ann Neurol 53, 503-511.

Reinecke,S., Lutzenburg,M., Hagemann,G., Bruehl,C., Neumann-Haefelin,T., Witte,O.W., 1999. Electrophysiological transcortical diaschisis after middle cerebral artery occlusion (MCAO) in rats. Neurosci Lett 261, 85-88.

Rice,J.E., Vannucci,R.C., Brierley,J.B., 1981. The influence of immaturity on hypoxic-ischemic brain damage in the rat. Ann Neurol 9, 131-141.

Rodin,E.A., Rhodes,R.J., Velarde,N.N., 1965. The prognosis for patients with epilepsy. J Occup Med 7, 560-563.

Romijn,H.J., Voskuyl,R.A., Coenen,A.M., 1994. Hypoxic-ischemic encephalopathy sustained in early postnatal life may result in permanent epileptic activity and an altered cortical convulsive threshold in rat. Epilepsy Res 17, 31-42.

Roper,S.N., King,M.A., Abraham,L.A., Boillot,M.A., 1997. Disinhibited in vitro neocortical slices containing experimentally induced cortical dysplasia demonstrate hyperexcitability. Epilepsy Res 26, 443-449.

Rorke,L.B., 1992. Anatomical features of the developing brain implicated in pathogenesis of hypoxic-ischemic injury. Brain Pathol 2, 211-221.

Rosati,A., Aghakhani,Y., Bernasconi,A., Olivier,A., Andermann,F., Gotman,J., Dubeau,F., 2003. Intractable temporal lobe epilepsy with rare spikes is less severe than with frequent spikes. Neurology 60, 1290-1295.

Scantlebury,M.H., Ouellet,P.L., Psarropoulou,C., Carmant,L., 2004. Freeze lesion-induced focal cortical dysplasia predisposes to atypical hyperthermic seizures in the immature rat. Epilepsia 45, 592-600.

Scher,M.S., Wiznitzer,M., Bangert,B.A., 2002. Cerebral infarctions in the fetus and neonate: maternal-placental-fetal considerations. Clin Perinatol 29, 693-724.

Scher,M.S., 2003. Neonatal seizures and brain damage. Pediatr Neurol 29, 381-390.

Schwartzkroin,P.A., Roper,S.N., Wenzel,H.J., 2004. Cortical dysplasia and epilepsy: animal models. Adv Exp Med Biol 548, 145-174.

Silverstein,F., Buchanan,K., Johnston,M.V., 1984. Pathogenesis of hypoxic-ischemic brain injury in a perinatal rodent model. Neurosci Lett 49, 271-277.

Sizonenko,S.V., Sirimanne,E., Mayall,Y., Gluckaman,P.D., Inder,T., Williams,C., 2003. Selective cortical alteration after hypoxic-ischemic injury in the very immature rat brain. Pediatr Res 54, 263-269.

Smith,B.N., Dudek,F.E., Roper,S.N., 1999. Synaptic responses of neurons in heterotopic gray matter in an animal model of cortical dysgenesis. Dev Neurosci 21, 365-373.

Somogyi,P., Tamas,G., Lujan,R., Buhl,E.H., 1998. Salient features of synaptic organisation in the cerebral cortex. Brain Res Brain Res Rev 26, 113-135.

Spreafico,R., Battaglia,G., Arcelli,P., Andermann,F., Dubeau,F., Palmini,A., Olivier,A., Villemure,J.G., Tampieri,D., Avanzini,G., Avoli,M., 1998. Cortical dysplasia: an immunocytochemical study of three patients. Neurology 50, 27-36.

Stein,V., Hermans-Borgmeyer,I., Jentsch,T.J., Hubner,C.A., 2004. Expression of the KCl cotransporter KCC2 parallels neuronal maturation and the emergence of low intracellular chloride. J Comp Neurol 468, 57-64.

Stevens,J.R., Kodama,H., Lonsbury,B., Mills,L., 1971. Ultradian characteristics of spontaneous seizure discharges recorded by radio telemetry in man. Electroencephalogr Clin Neurophysiol 31, 313-325.

Sussova,J., Seidl,Z., Faber,J., 1990. Hemiparetic forms of cerebral palsy in relation to epilepsy and mental retardation. Dev Med Child Neurol 32, 792-795.

Swann,J.W., 2004. The effects of seizures on the connectivity and circuitry of the developing brain. Ment Retard Dev Disabil Res Rev 10, 96-100.

Talos,D.M., Follett,P.L., Folkerth,R.D., Fishman,R.E., Trachtenberg,F.L., Volpe,J.J., Jensen,F.E., 2006. Developmental regulation of alpha-amino-3-hydroxy-5-methyl-4-isoxazole-propionic acid receptor subunit expression in forebrain and relationship to regional susceptibility to hypoxic/ischemic injury. II. Human cerebral white matter and cortex. J Comp Neurol 497, 61-77.

Tauboll,E., Lundervold,A., Gjerstad,L., 1991. Temporal distribution of seizures in epilepsy. Epilepsy Res 8, 153-165.

Telfeian,A.E., Connors,B.W., 1998. Layer-specific pathways for the horizontal propagation of epileptiform discharges in neocortex. Epilepsia 39, 700-708.

Towfighi,J., Yager,J.Y., Housman,C., Vannucci,R.C., 1991. Neuropathology of remote hypoxic-ischemic damage in the immature rat. Acta Neuropathol (Berl) 81, 578-587.

Towfighi,J., Housman,C., Vannucci,R.C., Heitjan,D.F., 1994. Effect of unilateral perinatal hypoxic-ischemic brain damage on the gross development of opposite cerebral hemisphere. Biol Neonate 65, 108-118.

Vannucci,R.C., Vannucci,S.J., 1997. A model of perinatal hypoxic-ischemic brain damage. Ann N Y Acad Sci 835, 234-249.

Vannucci,R.C., Vannucci,S.J., 2005. Perinatal hypoxic-ischemic brain damage: Evolution of an animal model. Developmental Neuroscience 27, 81-86.

Villani,F., D'Incerti,L., Granata,T., Battaglia,G., Vitali,P., Chiapparini,L., Avanzini,G., 2003. Epileptic and imaging findings in perinatal hypoxic-ischemic encephalopathy with ulegyria. Epilepsy Res 55, 235-243.

Volpe,J.J., 2001. Neurology of the newborn. Philadelphia: WB Saunders: 217-331.

White,A.M, Williams,P.A, Ferraro,D., Clark,S., Kadam,S.D, Dudek,F.E, Staley,K.J., 2006 Efficient unsupervised algorithms for the detection of seizures in continuous EEG recordings from rats after brain injury. J Neurosci Methods 152: 255-266.

Wiest,M.C., Nicolelis,M.A., 2003. Behavioral detection of tactile stimuli during 7-12 Hz cortical oscillations in awake rats. Nat Neurosci 6, 913-914.

Williams,P., White,A., Ferraro,D., Clark,S., Staley,K., Dudek,F.E., 2006. The use of radiotelemetry to evaluate electrographic seizures in rats with kainate-induced epilepsy. J Neurosci Methods 155, 39-48.

Williams,P.A., Dou,P., Dudek,F.E., 2004. Epilepsy and synaptic reorganization in a perinatal rat model of hypoxia-ischemia. Epilepsia 45, 1210-1218.

Williams,R.S., Ferrante,R.J., Caviness,V.S., Jr., 1976. The cellular pathology of microgyria. A Golgi analysis. Acta Neuropathol (Berl) 36, 269-283.